

MODELING, SIMULATION, AND CONTROL OF A QUADROTOR HAVING A
2-DOF ROBOTIC ARM

A THESIS SUBMITTED TO
THE GRADUATE SCHOOL OF NATURAL AND APPLIED SCIENCES
OF
MIDDLE EAST TECHNICAL UNIVERSITY

BY

NEBI BULUT

IN PARTIAL FULFILLMENT OF THE REQUIREMENTS
FOR
THE DEGREE OF MASTER OF SCIENCE
IN
MECHANICAL ENGINEERING

JULY 2019

Approval of the thesis:

**MODELING, SIMULATION, AND CONTROL OF A QUADROTOR
HAVING A 2-DOF ROBOTIC ARM**

submitted by **NEBI BULUT** in partial fulfillment of the requirements for the degree of **Master of Science in Mechanical Engineering Department, Middle East Technical University** by,

Prof. Dr. Halil Kalıpçilar
Dean, Graduate School of **Natural and Applied Sciences** _____

Prof. Dr. M. A. Sahir Arıkan
Head of Department, **Mechanical Engineering** _____

Assist. Prof. Dr. Ali Emre Turgut
Supervisor, **Mechanical Engineering, METU** _____

Assist. Prof. Dr. Kutluk Bilge Arıkan
Co-Supervisor, **Mechanical Engineering, TED University** _____

Examining Committee Members:

Assist. Prof. Dr. Ulaş Yaman
Mechanical Engineering Dept., METU _____

Assist. Prof. Dr. Ali Emre Turgut
Mechanical Engineering, METU _____

Assist. Prof. Dr. Kutluk Bilge Arıkan
Mechanical Engineering Dept., TED University _____

Assist. Prof. Dr. Kıvanç Azgın
Mechanical Engineering Dept., METU _____

Prof. Dr. M. Kemal Özgören
Mechanical Engineering Dept., METU _____

Date: 25.07.2019

I hereby declare that all information in this document has been obtained and presented in accordance with academic rules and ethical conduct. I also declare that, as required by these rules and conduct, I have fully cited and referenced all material and results that are not original to this work.

Name, Surname: Nebi Bulut

Signature:

ABSTRACT

MODELING, SIMULATION, AND CONTROL OF A QUADROTOR HAVING A 2-DOF ROBOTIC ARM

Bulut, Nebi

Master of Science, Mechanical Engineering

Supervisor: Assist. Prof. Dr. Ali Emre Turgut

Co-Supervisor: Assist. Prof. Dr. Kutluk Bilge Arıkan

July 2019, 93 pages

In this thesis, modeling, simulation, and control of a combined system that consists of a quadrotor and a 2-DOF robotic serial manipulator are presented. Firstly, the kinematic and dynamic model of the combined system are obtained. Then, the equation of motion of the combined system is derived by using Lagrange-D'Alembert formulation. Based on these equations, control algorithms are developed to control the combined system. Firstly, the cascaded PID controllers are designed by using the linearized decoupled equations of motion. Then, this controller is tested with the ideal dc and servo motor models with highly nonlinear combined system models. Secondly, the feedback linearizing controller is designed by using the nonlinear equations of motion of the system that is in the form of a standard robot dynamics equation. Then, to avoid instability of the system that can be caused by the unmodeled dynamics, parameter variations, and external disturbances, and to estimate these uncertainties, an extended state observer is added to the feedback linearizing controller. Later, the feedback linearizing controller and the extended state observer based the feedback linearizing controller is tested with the nonideal dc and servo motor models with the nonlinear combined system model. All proposed algorithms and the nonlinear combined system model are coded in MATLAB/Simulink environment. Finally, these

control algorithms are validated with a simulation case study, and their performances are compared.

Keywords: Aerial Manipulation, Extended State Observer, PID Control, Cascaded Control, Quadrotor, Serial Manipulator, Feedback Linearizing Control

ÖZ

2 SERBESTLİK DERECELİ ROBOT KOLU BULUNAN BİR KUADROTORUN MODELLENMESİ, SİMÜLASYONU VE KONTROLÜ

Bulut, Nebi

Yüksek Lisans, Makina Mühendisliği

Tez Danışmanı: Dr. Öğr. Üyesi Ali Emre Turgut

Ortak Tez Danışmanı: Dr. Öğr. Üyesi Kutluk Bilge Arıkan

Temmuz 2019, 93 sayfa

Bu tez çalışmasında, kuadrotor ve 2 serbestlik dereceli bir robotik seri manipülatör içeren bir birleşik sistemin modellenmesi, simülasyonu ve kontrolü sunulmuştur. İlk olarak, birleştirilmiş sistemin kinematik ve dinamik modeli elde edilmektedir. Ardından, birleşik sistemin hareket denklemi Lagrange-D'Alembert formülasyonu kullanılarak elde edilmiştir. Bu denklemelere dayanarak, tüm sistemi kontrol etmek için kontrol algoritmaları geliştirilmiştir. İlk olarak, kademeli PID kontrolörleri, doğrusallaştırılmış ve ayrıtırılmış hareket denklemlerine dayanarak tasarlanmıştır. Ardından, bu kontrolör, doğrusal olmayan birleşik sistem modellerine sahip ideal dc ve servo motor modelleri ile test edilir. İkinci olarak, doğrusallaştırılmış geribildirim kontrolör, standart bir robot dinamiği denklemi formundaki sistemin doğrusal olmayan hareket denklemlerini kullanarak tasarlanmıştır. Ardından, modellenmemiş dinamiklerin, parametre değişikliklerinin ve dış bozucuların neden olabileceği sistem kararsızlığını önlemek ve bu belirsizlikleri tahmin etmek için, doğrusallaştırılmış geribildirim kontrolörüne genişletilmiş bir durum gözlemcisi eklenmiştir. Daha sonra, doğrusallaştırılmış geribildirim denetleyicisi ve genişletilmiş durum gözlemcisi tabanlı doğrusallaştırılmış geribildirim denetleyicisi, doğrusal olmayan birleşik sistem modeliyle ideal olmayan dc ve servo motor modelleriyle test edilmiştir. Önerilen tüm

algoritmalar ve doğrusal olmayan birleşik sistem modeli MATLAB / Simulink ortamında kodlanmıştır. Son olarak, bu kontrol algoritmaları bir simülasyon çalışmasıyla doğrulanmış ve performansları karşılaştırılmıştır.

Anahtar Kelimeler: Hava Aracı Manipülasyonu, Genişletilmiş Durum Gözlemcisi, PID Kontrolü, Basamaklı Kontrol, Kuadrotor, Seri Manipülatör, Doğrusallaştırılmış Geribildirim Kontrolcüsü

To the Farmers

ACKNOWLEDGEMENTS

Firstly, I would like to express my deepest gratitude to my supervisor Assist. Prof. Dr. Ali Emre Turgut and co-supervisor Assist. Prof. Dr. Kutluk Bilge Arkan for their guidance, advice, encouragement, and insight throughout the research. I am also grateful to Prof. Dr. M. Kemal Özgören for his instructive discussions related to my questions. Moreover, I would like to thank my dear friend and colleague Fatih Kırımlıoğlu for his support and sincere friendship.

Teşekkür'ün bu bölümne Türkçe devam ediyorum.

Bugünlere gelmem de büyük katkısı olan tüm aile fertlerime, özellikle anneme ve babama en içten teşekkürlerimi sunuyorum.

Daha 12 yaşındayken tanıdığım, bu günlere kadar desteklerini eksik etmeyen ve ODTU'yu kazanmadaki en büyük etkiye sahip olan, Handan ablam ve Dırahşan teyzeme ve aramızda köprü olan babaanneme sonsuz teşekkür etmek istiyorum.

Bugünleri görmesini çok istediğim, ancak uzun zaman önce aramızdan ayrılan dedemi de bu vesile ile anmak istiyorum.

Hazırlık yıllarından beri tanıdığım, sevgili ev arkadaşım Aykut Aydeniz'e desteklerinden ve hayatı dair tartışmalarından dolayı teşekkür ediyorum.

Adını yazmadığım diğer tüm sevgili arkadaşlarına da çok teşekkür ediyorum.

TABLE OF CONTENTS

ABSTRACT	v
ÖZ	vii
ACKNOWLEDGEMENTS	x
TABLE OF CONTENTS	xi
LIST OF TABLES	xv
LIST OF FIGURES	xvi
LIST OF ABBREVIATIONS	xix
LIST OF SYMBOLS	xx
CHAPTERS	
1. INTRODUCTION	1
1.1. Motivation of the Thesis.....	1
1.2. Aim and Contribution of the Thesis	2
1.3. Outline of the Thesis	2
2. LITERATURE REVIEW	5
2.1. Path from Quadrotor to Its Manipulation	5
2.2. Literature on Contributions	9
2.3. Summary of the Literature Survey and Research Objectives.....	13
3. MATHEMATICAL MODELING.....	15
3.1. Kinematics.....	15
3.1.1. Denavit-Hartenberg Parameters.....	16
3.1.1.1. Twist Angles	16
3.1.1.2. Joint Angles.....	16

3.1.1.3. Offsets.....	17
3.1.2. Transformation Matrices	17
3.1.3. Position Analysis.....	19
3.1.4. Velocity Analysis	21
3.1.4.1. Linear Velocity Analysis	21
3.1.4.2. Angular Velocity Analysis	23
3.2. Dynamics	27
3.2.1. The Kinetic and Potential Energies	27
3.2.2. The Equation of Motion	28
3.2.3. Actuating Forces and Torques.....	29
3.2.4. Generalized Input and Interaction Forces	31
3.2.5. The Moments of Inertia Analysis	34
3.2.6. DC and Servo Motors Transfer Functions	36
4. CONTROLLER DESIGN.....	37
4.1. Cascaded PID Controller	37
4.1.1. Outer Loop Controller Design.....	38
4.1.1.1. Translational x&y Controller.....	38
4.1.1.2. Inner Loop Controller Design	39
4.1.1.2.1. Altitude Controller.....	39
4.1.1.2.2. Attitude Controller.....	40
4.1.1.2.3. Robotic Arm Joints Controller.....	41
4.1.2. Feedback Linearizing Controller	43
4.1.2.1. Background	43
4.1.2.2. Problem Formulation.....	44

4.2.3. Position Control of the Quadrotor	46
4.2.4. Attitude Control of the Quadrotor	49
4.2.5. Joints Angle Control of the Manipulator	50
4.3. Feedback Linearizing Control with Extended State Observer	51
4.3.1. Position Control of the Quadrotor	52
4.3.2. Attitude Control of the Quadrotor	53
4.3.3. Joints Angle Control of the Manipulator	53
4.3.4. Concept of Extended State Observer	55
4.3.5. Problem Formulation	56
5. SIMULATION RESULTS AND DISCUSSION	59
5.1. Simulation Environment Information	59
5.2. Simulation Scenario	60
5.3. Simulation Results.....	62
5.3.1. Cascaded PID Controller	62
5.3.1.1. Position Control of the Quadrotor.....	63
5.3.1.2. Orientation Control of the Quadrotor.....	64
5.3.1.3. Joint Angles Control of the Robotic Arm	66
5.3.2. Feedback Linearizing Controller and Feedback Linearizing Control with Extended State Observer.....	68
5.3.2.1. Position Control of the Quadrotor.....	68
5.3.2.2. Orientation Control of the Quadrotor.....	71
5.3.2.3. Joint Angles Control of the Robotic Arm	74
5.3.3. Performance Comparison of the Feedback Linearizing Controller and Feedback Linearizing Controller with Extended State Observer	78

5.3.3.1. Comparison of Error Terms.....	78
5.3.3.2. Comparison of Energy Consumption	79
6. CONCLUSION	85
6.1. General Conclusion.....	85
6.2. Future Work	87
REFERENCES	89

LIST OF TABLES

TABLES

Table 3.1. Denavit-Hartenberg Parameters	17
Table 4.1. The Gains of the PID Controllers	42
Table 4.2. The Gains of the Extended State Observer for the Generalized Coordinates	58
Table 5.1. Numerical Parameters of the Combined System	59
Table 5.2. The Simulation Scenario.....	60
Table 5.3. The Error Term Values of the Each Generalized Coordinates	79

LIST OF FIGURES

FIGURES

Figure 2.1. Direction of the Roll, Pitch and Yaw Moments [2]	6
Figure 2.2. Parallel Manipulator [10]	7
Figure 2.3. Cable Suspended Manipulator [4].....	8
Figure 2.4. Serial Manipulator [8]	8
Figure 3.1. Side View of the Combined System	16
Figure 3.2. Basic Rotation Matrices	18
Figure 3.3. Actuating Forces and Torques Generated by the Quadrotor's Motors [51]	29
Figure 3.4. Approximate 3-D Link Element.....	35
Figure 4.1. The Control Architecture of the Cascaded PID Controller	38
Figure 4.2. Roll Controller Structure	40
Figure 4.3. Feedback Linearizing Controller Architecture.....	45
Figure 4.4. Norms of the Original and Modified Inertia Matrices	48
Figure 4.5. The Error Between the Norms of the Original and Modified Inertia Matrices	48
Figure 4.6. FLC – ESO Architecture	54
Figure 5.1. Reference Trajectories of the Combined System	61
Figure 5.2. Externally Applied Forces on the End-Effector	62
Figure 5.3. Desired and Achieved Inertial Position of the Quadrotor	63
Figure 5.4. The Absolute Error Between the Commanded and the Achieved Quadrotor Position	63
Figure 5.5. The Reference and Achieved Orientation of the Quadrotor	64
Figure 5.6. The Reference and Achieved Orientation of the Quadrotor Between 0 to 5 Seconds	65

Figure 5.7. The Absolute Error Between the Commanded and the Achieved Quadrotor Orientation.....	65
Figure 5.8. The Reference and Achieved Joint Angles of the Robotic Arm	66
Figure 5.9. The Reference and Achieved Joint Angles of the Robotic Arm Between 0 to 5 Seconds	67
Figure 5.10. The Absolute Error Between the Commanded and the Achieved Joint Angles	67
Figure 5.11. Desired and Achieved Inertial Position of the Quadrotor [FLC]	69
Figure 5.12. The Absolute Error Between the Commanded and the Achieved Quadrotor Position [FLC]	69
Figure 5.13. Desired and Achieved Inertial Position of the Quadrotor [FLC-ESO] .	70
Figure 5.14. The Absolute Error Between the Commanded and the Achieved Quadrotor Position [FLC-ESO]	70
Figure 5.15. The Reference and Achieved Orientation of the Quadrotor [FLC].....	71
Figure 5.16. The Reference and Achieved Orientation of the Quadrotor Between 0 to 5 Seconds [FLC]	72
Figure 5.17. The Absolute Error Between the Commanded and the Achieved Quadrotor Orientation [FLC]	72
Figure 5.18. The Reference and Achieved Orientation of the Quadrotor [FLC-ESO]	
.....	73
Figure 5.19. The Reference and Achieved Orientation of the Quadrotor Between 0 to 5 Seconds [FLC-ESO]	73
Figure 5.20. The Absolute Error Between the Commanded and the Achieved Quadrotor Orientation [FLC-ESO]	74
Figure 5.21. The Reference and Achieved Joint Angles of the Robotic Arm [FLC]	75
Figure 5.22. The Reference and Achieved Joint Angles of the Robotic Arm Between 0 to 5 Seconds [FLC]	75
Figure 5.23. The Absolute Error Between the Commanded and the Achieved Joint Angles [FLC]	76

Figure 5.24. The Reference and Achieved Joint Angles of the Robotic Arm [FLC-ESO]	76
Figure 5.25. The Reference and Achieved Joint Angles of the Robotic Arm Between 0 to 5 Seconds [FLC-ESO]	77
Figure 5.26. The Absolute Error Between the Commanded and the Achieved Joint Angles [FLC-ESO]	77
Figure 5.27. Rotational Speeds of the Each DC Motors of the Quadrotor [FLC]	80
Figure 5.28. Rotational Speeds of the Each DC Motors of the Quadrotor [FLC-ESO]	80
Figure 5.29. Robotic Arm Joint Torques [FLC]	81
Figure 5.30. Robotic Arm Joint Torques [FLC-ESO]	82
Figure 5.31. The Joint Velocities of the Robotic Arm [FLC]	83
Figure 5.32. The Joint Velocities of the Robotic Arm [FLC-ESO].....	83

LIST OF ABBREVIATIONS

ABBREVIATIONS

UAV: Unmanned Aerial Vehicle

3-D: Three Dimensional

DOF: Degree of Freedom

ITAE: Integral Time Absolute Error

ITSE: Integral Time Square Error

SSM: Skew Symmetric Matrix

PID: Proportional Integral Derivative

FLC: Feedback Linearizing Controller

ESO: Extended State Observer

LIST OF SYMBOLS

SYMBOLS

ϕ : Euler roll angle

θ : Euler pitch angle

ψ : Euler yaw angle

O_i : Origin of the inertial reference frame

O_b : Origin of the quadrotor's body fixed reference frame

O_1 : Origin of the link-1 fixed reference frame

O_2 : Origin of the link-2 fixed reference frame

O_e : Origin of the end-effector fixed reference frame

θ_1 : Angle between quadrotor body and link-1

θ_2 : Angle between link-1 and link-2

$\vec{u}_1^{(a)}, \vec{u}_2^{(a)}, \vec{u}_3^{(a)}$: Unit basis vectors of reference frame A, they are oriented along the coordinate axes of reference frame A

$\bar{u}_1, \bar{u}_2, \bar{u}_3$: Basic column matrices

$\tilde{u}_1, \tilde{u}_2, \tilde{u}_3$: SSM of the basic column matrices

$\hat{C}^{(b,1)}$: Transformation matrix from link-1 reference frame to quadrotor's body fixed reference frame

$\hat{C}^{(1,2)}$: Transformation matrix from link-2 reference frame to link-1 reference frame

$\hat{C}^{(b,2)}$: Transformation matrix from link-2 reference frame to quadrotor's body fixed reference frame

$\hat{C}^{(i,b)}$: Transformation matrix from quadrotor's body fixed reference frame to inertial fixed reference frame

$\bar{p}_q^{(i)}$: Position of quadrotor with respect to the inertial frame

$\bar{p}_1^{(b)}$: Position of link-1 with respect to the quadrotor's body-fixed reference frame

$\bar{p}_2^{(b)}$: Position of link-2 with respect to the quadrotor's body-fixed reference frame

$\bar{p}_e^{(b)}$: Position of end-effector with respect to the quadrotor's body-fixed reference frame

\hat{J} : Jacobian matrix

L : Lagrange operator

K : Kinetic energy

U : Potential energy

\bar{u} : Generalized input force column matrix

\bar{u}_{ext} : Externally applied force column matrix on the end-effector

m_b, m_1, m_2 : Masses of the quadrotor, link-1 and link-2

m_t : Total mass of the unified system

g : Gravity constant

$\varpi_1, \varpi_2, \varpi_3, \varpi_4$: Angular velocities of the rotors

c_T : Thrust factor

c_Q : Drag factor

K_p : Proportional gain of PID

K_i : Integral gain of PID

K_d : Derivative gain of PID

X_{des} : Desired state “X”

X_{mes} : Measured state “X”

CHAPTER 1

INTRODUCTION

1.1. Motivation of the Thesis

In the last decade, with the advances in technology, research on aerial vehicles increased a lot. Especially, unmanned aerial vehicles (UAV's) are getting more attention from researchers all over the world. Due to their cost and ease of deployment quadrotors are mostly studied. Quadrotors also have the ability of vertical take-off, landing, the capability of high maneuverability and they can hold their position in hover. UAV's are mostly used for surveillance, rescue operations, and imaging tasks.

Recently, robotic arms are being added to UAV's in order to increase their capabilities such as object manipulation and carrying payload. The challenging problem is mathematical modeling and controlling these highly coupled and nonlinear systems. The difficulty of this problem mainly arises from the underactuated nature of the quadrotor itself. In 3-D space, unique locations of the aerial vehicles are represented by the 3 cartesian coordinates and 3 Euler angles. Hence, there are 6 states that should be controlled. However, quadrotors have 4 control inputs that are the rotational speeds of the dc motors of the vehicle. Therefore, 2 states of the UAV are generally controlled as internal states. In this particular vehicle, 2 linear positions of the vehicle are coupled with 2 angular positions. For example, to control the positions x, and y of the UAV, angular positions, and angles of the UAV should be changed.

In this thesis, a combined system that consists of a quadrotor and a 2-DOF robotic arm that is mounted to its bottom is studied. The main focus of this thesis is the kinematic and dynamic analysis of the combined system, and the controller design of this system.

Briefly, the mathematical model of the combined system that consists of a quadrotor and a 2-DOF robotic arm is obtained. After constructing the mathematical model of

the combined system and controller architecture, these models should be implemented in a suitable simulation environment. In literature, MATLAB/SIMULINK environment is mostly preferred. In this dissertation, developed algorithms are simulated in MATLAB/SIMULINK environment since it is easy to handle the coding and track the errors.

1.2. Aim and Contribution of the Thesis

In literature, generally, the end-effector's interaction with the environment was not modeled, and the designed controllers were tested without external forces that are applied to the combined system. Other than that, the studies that modeled the external forces usually considered only force in one direction. In addition, these applied forces on the system are mostly small in up to now researches. In addition, the simpler controllers were generally designed as well as more complex controller structures.

In this thesis, we aim to push a box with a quadrotor and a 2-DOF serial robotic arm. Therefore, multi-directional and large forces are modeled and used. Complex control strategies such as feedback linearizing controller with extended state observer is utilized. Due to this method, active disturbance rejection capability is gained to the combined system. Also, although there are highly coupled states in the system, we achieved to control all the states of the combined system simultaneously.

1.3. Outline of the Thesis

The thesis is organized as six chapters. The first chapter is the introduction.

Chapter 2 deals with the literature related to the quadrotors and manipulation of the quadrotors. Firstly, brief information about quadrotors are given, then the manipulation of these vehicles is discussed. Also, mathematical approaches that are used to model the unified systems in literature are discussed. In addition to these, control strategies that are used to control the overall system are investigated. These works are used to get inspired and improve different ways of solution to the problem.

Chapter 3 presents details of the kinematic and the dynamic modeling of the combined system. Firstly, kinematics relations are obtained for the combined system. Then, for the 2-DOF robotic manipulator, Denavit–Hartenberg Parameters are written. After that, rotation matrices are acquired to express the orientation of the reference frames with respect to each other. Finally, by using the kinematic relations and the Lagrange–D’Alembert formulation, the equation of the overall system is written in the form of a standard robot dynamics equation. Also, for simulating a more realistic scenario, experimentally identified transfer function for the quadrotor’s dc motors is given.

Chapter 4 is devoted to the controller design. In this chapter, different types of controllers are designed to control all states of the combined system simultaneously. Firstly, decoupled control algorithms are developed by using the linearized equations of motion of each state. The general architecture of this controller is a cascaded type PID controller. Secondly, by using the standard equations of motion of the system, a feedback linearizing controller is designed. However, because it has some drawbacks, more robust and adaptive controller is developed. Therefore, an extended state observer is added to the feedback linearizing controller to estimate the uncertainties, unmodelled dynamics, and externally applied forces.

Chapter 5 focuses on the simulation results and discussion. All developed control algorithms are implemented in highly nonlinear system simulation and tested. Their robustness to the externally applied forces on the tip point of the end-effector are tested. Then, for all these 3 control structures, results are obtained, and they are compared to with each other. While comparing, universal performance indexes like Integral Time Absolute Error (ITAE) and Integral Time Square Error (ITSE) are used. Also, the results are discussed in this chapter.

Chapter 6 summarizes the work done throughout the dissertation. It concludes the achievements of the thesis.

CHAPTER 2

LITERATURE REVIEW

2.1. Path from Quadrotor to Its Manipulation

Last two decades, UAVs, especially, quadrotors, are the focus points of the researchers due to their cost and capabilities such as the ability of vertical take-off and landing, staying still in hover position, high agility and maneuverability. Also, these vehicles have practical uses such as delivering enough payload and observation purposes. There are various studies related to quadrotors. For example, a comprehensive study is done corresponding to the aerodynamical characteristics of the rotors of the quadrotor [1]. In this paper, rotor flapping, blade flapping and induced drag that have significant importance on the stability of the aerial vehicle are discussed and modeled. Also, simple expressions for the drag coefficient and thrust coefficient of the motors are derived from the complex mathematical equations by making some assumptions. Kinematics and dynamics of the quadrotor are derived while paying attention to the direction of rotation of the rotors [2]. This is important to generate roll, pitch and yaw moments.

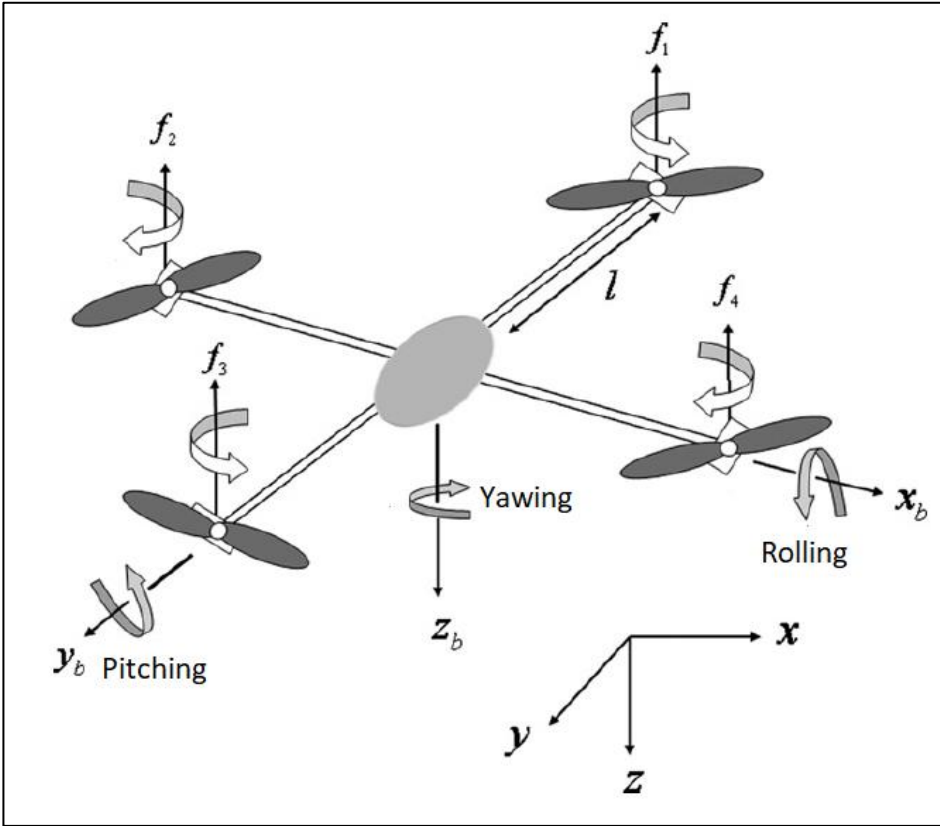


Figure 2.1. Direction of the Roll, Pitch and Yaw Moments [2]

The most challenging part of these flying vehicles is stable and safe trajectory tracking. To achieve this, control algorithms are developed from the equation of motion of the system. To decrease the mathematical complexity of these equations, simplified equations that are obtained by the linearization around some equilibrium points are used [3]. While obtaining control algorithms, underactuated nature of the quadrotor is considered.

In time, the necessity of adding new abilities like manipulating objects to the quadrotors are increased. There are different approaches to achieve this. For instance, cable suspended manipulator was used for manipulation purposes [4], [5], [6]. However, the most common manipulation technique is mounting a robotic arm. There are studies that serial manipulators with various degrees of freedom are used for this

purpose [7], [8], [9]. Also, a parallel manipulator is attached to the bottom of the UAV to increase its capabilities [10].



Figure 2.2. Parallel Manipulator [10]

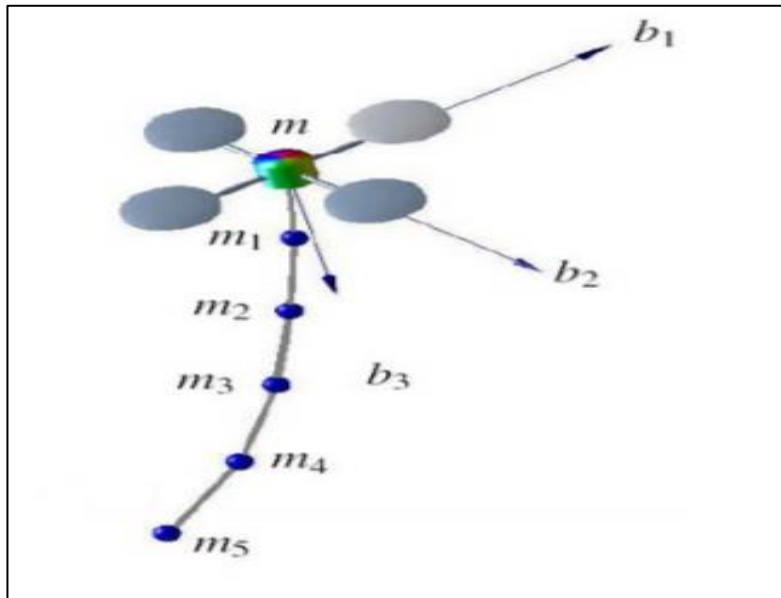


Figure 2.3. Cable Suspended Manipulator [4]

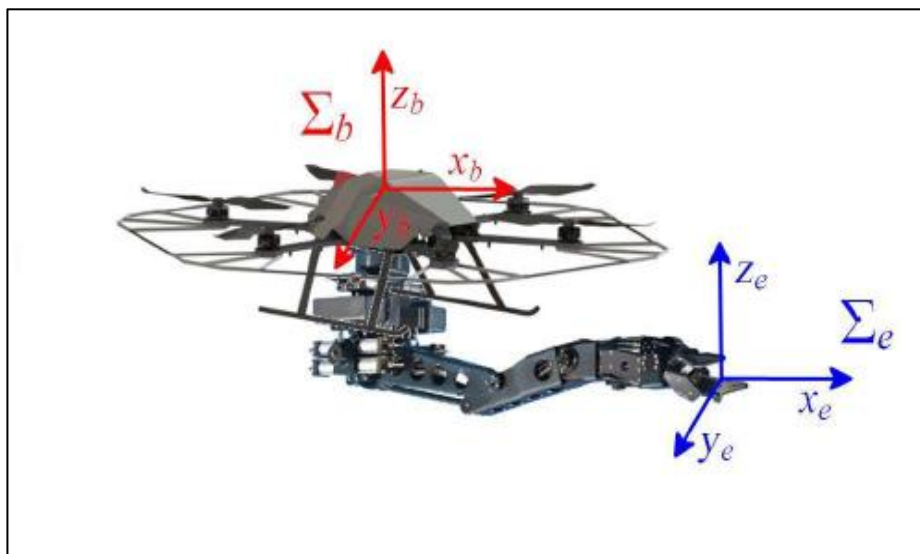


Figure 2.4. Serial Manipulator [8]

In this thesis, a 2-DOF serial robotic arm is used as a manipulator in the quadrotor. Therefore, the literature is limited to serial manipulators and UAV's with serial manipulator.

2.2. Literature on Contributions

To develop control algorithms, the mathematical model of a system has great importance. That's why the kinematic and dynamic model of a system must have high fidelity. In literature, there are diverse approaches both modeling the dynamics of the combined system and controlling the combined system.

A quadrotor with a bottom mounted 2-DOF robotic arm was studied by Kim et al. [7]. Combined system dynamics are derived by using Lagrange-D'Alembert formulation. An adaptive sliding mode controller is designed, and the proposed control algorithms are implemented and tested in a real-life scenario that is moving an object from one location to another. Lee et al. [22] continued to work on aerial robotics, but using a different configuration which is an hexarotor and a 2-DOF serial arm. Equation of motion of the unified system is obtained. An unknown mass is added to the manipulator, and it is estimated by using an online parameter estimator. An augmented passivity-based controller is designed for trajectory tracking of the combined system. Also, unknown mass is estimated by using an adaptive sliding mode controller and results are compared with the proposed algorithms in a simulation environment. In addition to that, proposed algorithms are validated with an experiment. Later, this work was followed by Kim et al. [11] with a slightly different configuration which is a hexarotor combined with a 3-DOF robotic manipulator. In this study, the combined system is guided by using an image-based visual servoing system to drive the end-effector of the manipulator.

A cartesian impedance control scheme was proposed to deal with external contact forces and disturbances by Lippiello and Ruggiero [12]. Proposed algorithms are tested in a simulation environment using a 3-DOF robotic arm mounted to the quadrotor. Two cases are tested. The first case is that a sinusoidal disturbance force is applied in the x direction of the body frame of the quadrotor to simulate wind gust. Then, the system shows a compliant behavior and keep its initial positions for both quadrotor itself and the end-effector. In the second scenario, in addition to the

disturbance force, a force is applied on the end-effector to simulate the contact with the environment. In this case, while the end-effector pose is kept unchanged, quadrotor body's linear and angular positions are chosen to be compliant. Thus, the end-effector position stays around initial conditions with very small error.

In another study, Arleo et al. [13] considered a quadrotor equipped with a 5-DOF serial manipulator. The equations of motion of the unified system are derived using the Euler-Lagrange formulation. Inverse kinematics algorithms are developed to generate reference trajectories for the motion controller. A standard globally linearized control law is selected without any adaptive term to control the combined system in a simulation environment. In a follow up study, Caccavale et al. [8] used the same configuration and added an adaptation law to the controller design for disturbance rejection and unmodeled dynamics. Algorithms are implemented in a simulation environment.

Giglio and Pierri [14] studied a combined system of a quadrotor and a 6-DOF robotic arm. Proposed control architecture consists of three parts. The first part is the inverse kinematics algorithms that compute the motion references for the combined system to bring the end-effector to the desired location. The second part of the control architecture is the impedance filter that brings a compliant behavior to the system in case of interaction with the environment and disturbances. The third part is the motion controller for tracking the reference trajectories. Developed algorithms are tested in a simulation environment. Later, Cataldi et al. [15] studied the same configuration. They improve the impedance, inverse kinematics, and control algorithms, and validate these algorithms with experiments.

In a study by Khalifa et al. [16], a quadrotor with a bottom mounted 2-DOF manipulator was considered. In this work, decoupled equations of motion of the unified system are obtained by using recursive Newton Euler formulation. For each state, feedback linearized controllers are designed, then the trajectory tracking performance of the proposed controllers are tested using simulations. Afterward, in a

follow up study by Khalifa et al. [17], inverse kinematics algorithms were implemented to generate reference inputs for the motion controller for the desired position and orientation of the end-effector. Also, robust internal loop compensator is proposed for controlling the combined system. Developed algorithms are tested in a simulation environment with some tasks such as picking and placing a payload. In a follow up study, Fanni and Khalifa [18] improved results in [17]. A novel inverse kinematics algorithm is presented, and disturbance observer based robust controller is proposed for trajectory tracking. In this study, system parameters such as inertia is determined experimentally. Sensors and actuators are modeled realistically.

Jimenez-Cano et al. [9] investigated the performance of the 2-DOF robotic arm that is attached to a UAV. Different controllers are designed for both quadrotor and the robotic arm. The quadrotor's controller deals with the changes such as inertia caused by the change of the center of gravity of the overall system. The control algorithm is tested by an experiment to show the performance of the controller under the movement of the robotic arm.

In a very recent study by Jones et al. [19], autonomous quadrotor which is equipped by a 2-DOF serial robotic manipulator for indoor tasks is tested in a simulation environment. The purpose of this study is to show the stable performance of the controllers while lifting an unknown mass under the presence of uncertainties such as unmodeled dynamics, and wind gust. The proposed controller consists of a feedforward torque compensation system and L1 adaptive controller. Movement of the arm and delivering a payload are compensated by the controller to ensure a stable flight.

Orsag et al. [20] worked on a quadrotor with a 4-DOF robotic arm. Dynamics of the quadrotor and the serial manipulator are obtained separately by using Newton-Euler formulation. Then, mass, inertia, and movement of the robotic arm are fed to the quadrotor as disturbance input. Lyapunov based model reference adaptive PI-D controller is used. Since the model reference adaptation is sensitive to the

disturbances, a disturbance estimator is also implemented. All these algorithms are tested in a simulation environment with the help of MATLAB/SIMULINK.

In another recent study, Sumathy et al. [21] considered an aerial robot consisting of a UAV and a 2-DOF manipulator that is operating above the workspace of the UAV. Equation of motion of the combined system and the payload attached to the end-effector are derived by using the Euler-Lagrange method. Map of the possible robotic arm trajectories is obtained by considering the physical constraints of the combined system. A gain scheduling PD based feedback linearized controller is designed for trajectory tracking, and the algorithms are tested in MATLAB simulation environment.

In another study, Lee et al. [23], studied the quadrotor system with a bottom-mounted 2-DOF robotic arm. Lyapunov based coordinated controller is applied to the system to achieve zero reference tracking error for both UAV and manipulator.

Villagómez et al. [24] used both the Newton-Euler and Euler-Lagrange methods for determining the equation of motion of the unified system and the couplings between the UAV and 1-DOF robotic manipulator that is used to pose the camera attached to the end of it. Performances of the linear controller, backstepping controller, and the sliding-mode controller are compared in a simulation case study.

A nonlinear model reference control approach is presented by Garimella and Kobilarov [25]. An aerial robot with 2-DOF serial arm experimentally tested by performing pick and place task.

Alvarez-Munoz et al. [26] studied asymptotical stabilization of a quadrotor carrying a robotic arm. The set of nonlinear control laws were proposed. The effectiveness of these control algorithms is tested with simulation study.

Antonelli and Cataldi [27] studied the adaptive control of the quadrotor having a n-DOF robotic arm. The control inputs are generated by considering the physical interaction with the arm. Moreover, the proposed approach is based on the Newton-

Euler formulation, i.e., it is recursive. The stability analysis of the proposed algorithms is also presented.

Ruggiero et al. [28] developed a multi-layer special control architecture in order to effectively control an aerial platform with a 6-DOF serial robotic arm. They proposed a novel mechanism considering a moving battery to counterweight the statics of the robotic arm. Then, in order to overcome the mechanical limitations of the previous layer, the residual of the arm static effects on the UAV is computed and compensated through the given control thrust and torques. The external forces and moments acting on the system were estimated and fed back to the controller.

Heredia et al. [31] studied the design and control of a multirotor-based aerial 7-DOF manipulator for outdoor operation. A stable backstepping-based controller for the multirotor that uses the coupled full dynamic model is proposed, and an admittance controller for the manipulator arm is outlined. Both experiments and simulation results were presented.

2.3. Summary of the Literature Survey and Research Objectives

The first step in studying aerial robotics is the selection of the proper manipulator such as cable-like, parallel or serial manipulator. For instance, for transporting a payload from one location to another, a cable-like manipulator may be sufficient [4]. However, for picking a payload and delivering it to a different place or pushing a box or opening a door, a serial manipulator is the right choice [7]. In this study, a serial manipulator is examined since the task considered in the thesis is box pushing.

The next step is to choose the degree of freedom of the serial manipulator. From 1-DOF [15] to 7-DOF [18] robotic arms are considered in the literature. In this thesis, 2-DOF freedom serial robotic manipulator is studied to keep the system simple.

After selecting the robotic manipulator, the equations of motion of the coupled system should be obtained, then the controller should be designed. In literature, the dynamics of the combined system is obtained either by using Newton-Euler [24] or Euler-

Lagrange [7] methods. There are two main approaches to control the unified system. The first approach is developing different controllers for both the UAV and the robotic manipulator [16]. Then, effects of the robotic arm such as mass, and inertia are fed to quadrotor as a disturbance input, and quadrotor's controller copes with this disturbance. The second approach is designing a common controller by considering the whole system as one system [8]. In this thesis, a single controller is designed to control the overall system. Also, decoupled controllers are developed for comparison purposes.

CHAPTER 3

MATHEMATICAL MODELING

In this chapter, the kinematic (position and velocity analysis) and the dynamic (the equation of motion of the system) of the combined system are presented. Some assumptions are made during mathematical modeling. The aerial vehicle and the links of the robotic arm are assumed to be rigid and symmetric bodies. The rotors and the propellers are also modeled as rigid. Moreover, blade flapping, induced drag, and the rotor flapping are neglected as well as frictions. The generated thrust and the torque are assumed to be proportional to the square of the rotational speed of the rotors. Finally, the robotic arm is assumed to be aligned with the x-axis of the body frame of the UAV.

3.1. Kinematics

Before deriving the dynamical model of the combined system, kinematic modeling should be performed first. Some of the kinematic parameters of the combined system are shown in Figure 3.1.

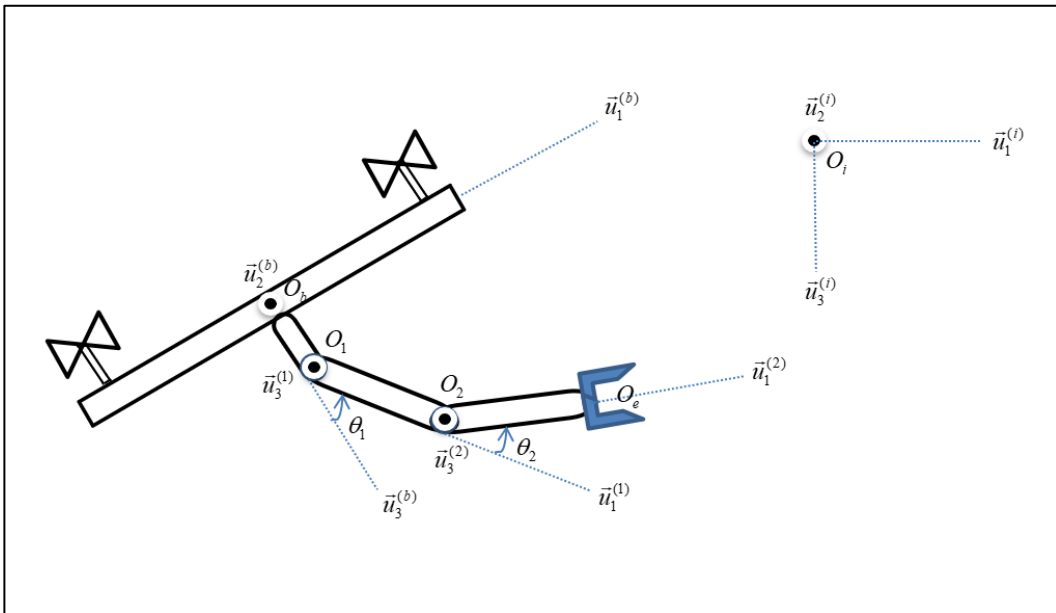


Figure 3.1. Side View of the Combined System

3.1.1. Denavit-Hartenberg Parameters

These parameters are defined for the robotic manipulator [35].

3.1.1.1. Twist Angles

$\beta_1 = -\frac{\pi}{2}$ is the angle between $\vec{u}_3^{(b)}$ and $\vec{u}_3^{(1)}$ about $\vec{u}_1^{(b)}$.

$\beta_2 = 0$ is the angle between $\vec{u}_3^{(1)}$ and $\vec{u}_3^{(2)}$ about $\vec{u}_1^{(1)}$.

3.1.1.2. Joint Angles

$\theta_1 + \frac{3\pi}{2}$ is the angle between $\vec{u}_1^{(b)}$ and $\vec{u}_1^{(1)}$ about $\vec{u}_3^{(1)}$.

θ_2 is the angle between $\vec{u}_1^{(1)}$ and $\vec{u}_1^{(2)}$ about $\vec{u}_3^{(2)}$

3.1.1.3. Offsets

b_0 is the offset from O_b to O_1 .

b_1 is the offset from O_1 to O_2 .

b_2 is the offset from O_2 to O_e .

Denavit-Hartenberg Parameters for the robotic arm can be further written as a table form as follow,

Table 3.1. *Denavit-Hartenberg Parameters*

	$k = 1$	$k = 2$
β_k	$\frac{-\pi}{2}$	0
θ_k	$\theta_1 + \frac{3\pi}{2}$	θ_2
b_k	b_1	b_2

3.1.2. Transformation Matrices

Transformation matrices are used to transform the components from one reference frame to the other. Transformation matrices between the reference frames are represented in terms of basic rotation matrices. A basic rotation can be defined as the rotation about one of the unit direction vector of a corresponding reference frame [34]. Vectors are rotated by using the basic rotation matrices about one of the unit direction of the corresponding reference frame by a certain angle [34]. In Figure 3.2, the basic rotation matrices are shown. Transformation matrices are derived by using the basic rotation matrices.

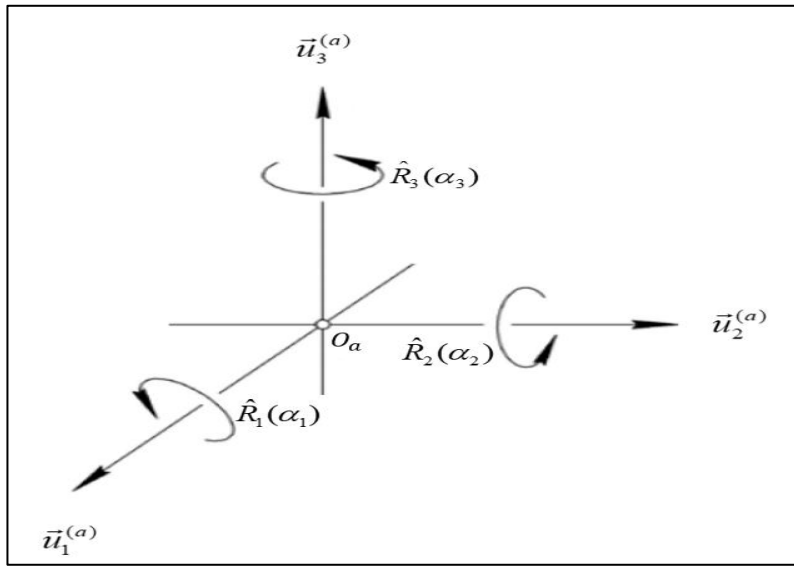


Figure 3.2. Basic Rotation Matrices

Basic rotation matrices can be written in terms of basis vector directions and rotation angles. To come up with following expressions, Rodrigues' formula, and Taylor series expansions are used [34]. Then, the basic rotation matrices in exponential and matrix forms are as follows:

$$\hat{R}_1(\alpha_1) = e^{\tilde{u}_1 \alpha_1} = \begin{bmatrix} 1 & 0 & 0 \\ 0 & \cos(\alpha_1) & -\sin(\alpha_1) \\ 0 & \sin(\alpha_1) & \cos(\alpha_1) \end{bmatrix} \quad (3.1)$$

$$\hat{R}_2(\alpha_2) = e^{\tilde{u}_2 \alpha_2} = \begin{bmatrix} \cos(\alpha_2) & 0 & \sin(\alpha_2) \\ 0 & 1 & 0 \\ -\sin(\alpha_2) & 0 & \cos(\alpha_2) \end{bmatrix} \quad (3.2)$$

$$\hat{R}_3(\alpha_3) = e^{\tilde{u}_3 \alpha_3} = \begin{bmatrix} \cos(\alpha_3) & -\sin(\alpha_3) & 0 \\ \sin(\alpha_3) & \cos(\alpha_3) & 0 \\ 0 & 0 & 1 \end{bmatrix} \quad (3.3)$$

Then, the transformation matrices between the reference frames can be given in terms of the exponential forms of the basic rotation matrices [35].

$$\hat{C}^{(b,1)} = e^{\tilde{\theta}_1 \beta_1} e^{\tilde{\theta}_3(\theta_1 + \frac{3\pi}{2})} = e^{\tilde{\theta}_1(-\frac{\pi}{2})} e^{\tilde{\theta}_3(\theta_1 + \frac{3\pi}{2})} = e^{\tilde{\theta}_2 \theta_1} e^{\tilde{\theta}_1(-\frac{\pi}{2})} e^{\tilde{\theta}_3(\frac{3\pi}{2})} \quad (3.4)$$

$$\hat{C}^{(1,2)} = e^{\tilde{\theta}_1 \beta_2} e^{\tilde{\theta}_3 \theta_2} = e^{\tilde{\theta}_1 0} e^{\tilde{\theta}_3 \theta_2} = e^{\tilde{\theta}_3 \theta_2} \quad (3.5)$$

$$\hat{C}^{(b,2)} = \hat{C}^{(b,1)} \hat{C}^{(1,2)} = e^{\tilde{\theta}_2 \theta_1} e^{\tilde{\theta}_1(-\frac{\pi}{2})} e^{\tilde{\theta}_3(\frac{3\pi}{2})} e^{\tilde{\theta}_3 \theta_2} = e^{\tilde{\theta}_2(\theta_1 + \theta_2 + \frac{3\pi}{2})} e^{\tilde{\theta}_1(-\frac{\pi}{2})} \quad (3.6)$$

Also, the transformation matrix between the quadrotor's body-fixed reference frame and the inertial fixed reference frame can be given as,

$$\begin{aligned} \hat{C}^{(i,b)} &= e^{\tilde{\theta}_3 \psi} e^{\tilde{\theta}_2 \theta} e^{\tilde{\theta}_1 \phi} \\ &= \begin{bmatrix} c(\psi) c(\theta) & c(\psi) s(\theta) s(\phi) - s(\psi) c(\phi) & c(\psi) s(\theta) c(\phi) + s(\psi) s(\phi) \\ s(\psi) c(\theta) & s(\psi) s(\theta) s(\phi) + c(\psi) c(\phi) & s(\psi) s(\theta) c(\phi) - c(\psi) s(\phi) \\ -s(\theta) & c(\theta) s(\phi) & c(\theta) c(\phi) \end{bmatrix} \end{aligned} \quad (3.7)$$

In above equation, c stands for cosine and s stands for sine. Where $\bar{\Omega} = [\theta_1 \ \theta_2]^T$ are the joint angles of the serial manipulator and $\bar{\Upsilon} = [\phi \ \theta \ \psi]^T$ are Euler roll, pitch and yaw angles, or phi, theta and psi.

3.1.3. Position Analysis

Firstly, values of the basic column matrices are defined since they are used in position and velocity analysis. These are:

$$\bar{u}_1 = \begin{bmatrix} 1 \\ 0 \\ 0 \end{bmatrix} \quad \bar{u}_2 = \begin{bmatrix} 0 \\ 1 \\ 0 \end{bmatrix} \quad \bar{u}_3 = \begin{bmatrix} 0 \\ 0 \\ 1 \end{bmatrix} \quad (3.8)$$

The position of the quadrotor in the vector representation is defined as:

$$\vec{p}_q = \overrightarrow{O_i O_b}$$

Then, in the column matrix form:

$$\bar{p}_q^{(i)} = [x \ y \ z]^T \quad (3.9)$$

Then, the position of link-1 of the robotic arm in quadrotor's body-fixed and inertial fixed reference frames can be written as

$$\vec{p}_1^{(b)} = b_0 \vec{u}_3^{(b)} + \frac{b_1}{2} \vec{u}_1^{(1)} \quad (3.10)$$

$$\bar{p}_1^{(b)} = b_0 u_3^{(b/b)} + \frac{b_1}{2} \hat{C}^{(b,1)} u_1^{(1/1)} = \frac{b_1}{2} \sin(\theta_1) \bar{u}_1 + (b_0 + \frac{b_1}{2} \cos(\theta_1)) \bar{u}_3 \quad (3.11)$$

Let's define that:

$$\vec{p}_1 = \overrightarrow{O_i C_1}, \quad C_1 : \text{center of the link 1}$$

$$\bar{p}_1^{(i)} = \bar{p}_q^{(i)} + \hat{C}^{(i,b)} \bar{p}_1^{(b)} \quad (3.12)$$

Similarly, the position of link-2 in different reference frames is obtained as:

$$\vec{p}_2^{(b)} = b_0 \vec{u}_3^{(b)} + b_1 \vec{u}_1^{(1)} + \frac{b_2}{2} \vec{u}_1^{(2)} \quad (3.13)$$

$$\bar{p}_2^{(b)} = b_0 \bar{u}_3^{(b/b)} + b_1 \bar{u}_1^{(1/b)} + \frac{b_2}{2} \bar{u}_1^{(2/b)} = b_0 \bar{u}_3 + b_1 \hat{C}^{(b,1)} \bar{u}_1 + \frac{b_2}{2} \hat{C}^{(b,2)} \bar{u}_1 \quad (3.14)$$

$$\bar{p}_2^{(b)} = (\frac{b_2}{2} \sin(\theta_1 + \theta_2) + b_1 \sin(\theta_1)) \bar{u}_1 + (b_0 + \frac{b_2}{2} \cos(\theta_1 + \theta_2) + b_1 \cos(\theta_1)) \bar{u}_3 \quad (3.15)$$

Let's define that:

$$\vec{p}_2 = \overrightarrow{O_i C_2}, \quad C_2 : \text{center of the link 2}$$

$$\bar{p}_2^{(i)} = \bar{p}_q^{(i)} + \hat{C}^{(i,b)} \bar{p}_2^{(b)} \quad (3.16)$$

Moreover, the position of the end-effector in similar reference frames is explained as,

$$\vec{p}_e^{(b)} = b_0 \vec{u}_3^{(b)} + b_1 \vec{u}_1^{(1)} + b_2 \vec{u}_1^{(2)} \quad (3.17)$$

$$\bar{p}_e^{(b)} = b_0 \bar{u}_3^{(b/b)} + b_1 \bar{u}_1^{(1/b)} + b_2 \bar{u}_1^{(2/b)} = b_0 \bar{u}_3 + b_1 \hat{C}^{(b,1)} \bar{u}_1 + b_2 \hat{C}^{(b,2)} \bar{u}_1 \quad (3.18)$$

$$\bar{p}_e^{(b)} = (\mathbf{b}_2 \sin(\theta_1 + \theta_2) + \mathbf{b}_1 \sin(\theta_1)) \bar{u}_1 + (\mathbf{b}_0 + \mathbf{b}_2 \cos(\theta_1 + \theta_2) + \mathbf{b}_1 \cos(\theta_1)) \bar{u}_3 \quad (3.19)$$

Let's define that:

$$\vec{p}_e = \overrightarrow{O_i O_e}, \quad O_e : \text{center of the link 1}$$

$$\bar{p}_e^{(i)} = \bar{p}_q^{(i)} + \hat{C}^{(i,b)} \bar{p}_e^{(b)} \quad (3.20)$$

3.1.4. Velocity Analysis

3.1.4.1. Linear Velocity Analysis

Linear velocity analysis is made based on the position analysis. An overhead dot ('.') is used for the time derivative of the corresponding variable. The linear velocity of the quadrotor body is as follows.

$$\dot{\bar{p}}_q^{(i)} = [\dot{x} \ \dot{y} \ \dot{z}]^T \quad (3.21)$$

The linear velocity of link-1 is expressed with respect to both quadrotor's body-fixed reference frame and the inertial fixed reference frame. Also, Jacobian matrices are obtained. Linear velocity with respect to quadrotor frame is:

$$\bar{v}_1^{(b)} = \dot{\bar{p}}_1^{(b)} = \left(\frac{b_1}{2} \dot{\theta}_1 \cos(\theta_1) \right) \bar{u}_1 + \left(-\frac{b_1}{2} \dot{\theta}_1 \sin(\theta_1) \right) \bar{u}_3 \quad (3.22)$$

Eq. (3.22) can be written further as,

$$\bar{v}_1^{(b)} = \bar{v}_{11}^{(b)} \dot{\theta}_1 + \bar{v}_{12}^{(b)} \dot{\theta}_2 \quad (3.23)$$

$$\hat{J}_{1v} = \begin{bmatrix} \bar{v}_{11}^{(b)} & \bar{v}_{12}^{(b)} \end{bmatrix} \quad (3.24)$$

where,

$$\begin{aligned}\bar{v}_{11}^{(b)} &= \left(\frac{b_1}{2} \cos(\theta_1)\right) \bar{u}_1 + \left(-\frac{b_1}{2} \sin(\theta_1)\right) \bar{u}_3 \\ \bar{v}_{12}^{(b)} &= 0 \bar{u}\end{aligned}\quad (3.25)$$

Then,

$$\dot{\bar{p}}_1^{(b)} = \hat{J}_{1v} \dot{\bar{\Omega}} \quad (3.26)$$

Linear velocity wrt the inertial frame is as follows,

$$\dot{\bar{p}}_1^{(i)} = \dot{\bar{p}}_q^{(i)} + \dot{\hat{C}}^{(i,b)} \bar{p}_1^{(b)} + \hat{C}^{(i,b)} \dot{\bar{p}}_1^{(b)} \quad (3.27)$$

$$\dot{\bar{p}}_1^{(i)} = \dot{\bar{p}}_q^{(i)} + \hat{C}^{(i,b)} SSM(\bar{w}_q^{(b)}) \bar{p}_1^{(b)} + \hat{C}^{(i,b)} \hat{J}_{1v} \dot{\bar{\Omega}} \quad (3.28)$$

The same procedure is applied to link-2,

$$\begin{aligned}\bar{v}_2^{(b)} &= \dot{\bar{p}}_2^{(b)} = \left(\frac{b_2}{2} (\dot{\theta}_2 + \dot{\theta}_1)\right) \cos(\theta_1 + \theta_2) + b_1 \dot{\theta}_1 \cos(\theta_1) \bar{u}_1 \\ &\quad + \left(-\frac{b_2}{2} (\dot{\theta}_2 + \dot{\theta}_1)\right) \sin(\theta_1 + \theta_2) - b_1 \dot{\theta}_1 \sin(\theta_1) \bar{u}_3\end{aligned}\quad (3.29)$$

$$\bar{v}_2^{(b)} = \bar{v}_{21}^{(b)} \dot{\theta}_1 + \bar{v}_{22}^{(b)} \dot{\theta}_2 \quad (3.30)$$

$$\hat{J}_{2v} = \begin{bmatrix} \bar{v}_{21}^{(b)} & \bar{v}_{22}^{(b)} \end{bmatrix} \quad (3.31)$$

where,

$$\begin{aligned}\bar{v}_{21}^{(b)} &= \left(\frac{b_2}{2} \cos(\theta_1 + \theta_2) + b_1 \cos(\theta_1)\right) \bar{u}_1 + \left(-\frac{b_2}{2} \sin(\theta_1 + \theta_2) - b_1 \sin(\theta_1)\right) \bar{u}_3 \\ \bar{v}_{22}^{(b)} &= \left(\frac{b_2}{2} \cos(\theta_1 + \theta_2)\right) \bar{u}_1 + \left(-\frac{b_2}{2} \sin(\theta_1 + \theta_2)\right) \bar{u}_3\end{aligned}\quad (3.32)$$

Then,

$$\dot{\bar{p}}_2^{(b)} = \hat{J}_{2v} \dot{\bar{\Omega}} \quad (3.33)$$

Linear velocity in inertial frame is calculated as follows:

$$\dot{\bar{p}}_2^{(i)} = \dot{\bar{p}}_q^{(i)} + \hat{C}^{(i,b)} \bar{p}_2^{(b)} + \hat{C}^{(i,b)} \dot{\bar{p}}_2^{(b)} \quad (3.34)$$

$$\dot{\bar{p}}_2^{(i)} = \dot{\bar{p}}_q^{(i)} + \hat{C}^{(i,b)} SSM(\bar{w}_q^{(b)}) \bar{p}_2^{(b)} + \hat{C}^{(i,b)} \hat{J}_{ev} \dot{\bar{\Omega}} \quad (3.35)$$

Similarly, the end-effector linear velocity analysis is found as:

$$\begin{aligned} \bar{v}_e^{(b)} &= \dot{\bar{p}}_e^{(b)} = (b_2 (\dot{\theta}_2 + \dot{\theta}_1) \cos(\theta_1 + \theta_2) + b_1 \dot{\theta}_1 \cos(\theta_1)) \bar{u}_1 \\ &\quad + (-b_2 (\dot{\theta}_2 + \dot{\theta}_1) \sin(\theta_1 + \theta_2) - b_1 \dot{\theta}_1 \sin(\theta_1)) \bar{u}_3 \end{aligned} \quad (3.36)$$

$$\bar{v}_e^{(b)} = \bar{v}_{e1}^{(b)} \dot{\theta}_1 + \bar{v}_{e2}^{(b)} \dot{\theta}_2 \quad (3.37)$$

$$\hat{J}_{ev} = \begin{bmatrix} \bar{v}_{e1}^{(b)} & \bar{v}_{e2}^{(b)} \end{bmatrix} \quad (3.38)$$

where,

$$\begin{aligned} \bar{v}_{e1}^{(b)} &= (b_2 \cos(\theta_1 + \theta_2) + b_1 \cos(\theta_1)) \bar{u}_1 + (-b_2 \sin(\theta_1 + \theta_2) - b_1 \sin(\theta_1)) \bar{u}_3 \\ \bar{v}_{e2}^{(b)} &= (b_2 \cos(\theta_1 + \theta_2)) \bar{u}_1 + (-b_2 \sin(\theta_1 + \theta_2)) \bar{u}_3 \end{aligned} \quad (3.39)$$

Linear velocity in inertial frame is calculated as follows:

$$\dot{\bar{p}}_e^{(i)} = \dot{\bar{p}}_q^{(i)} + \hat{C}^{(i,b)} \bar{p}_e^{(b)} + \hat{C}^{(i,b)} \dot{\bar{p}}_e^{(b)} \quad (3.40)$$

$$\dot{\bar{p}}_e^{(i)} = \dot{\bar{p}}_q^{(i)} + \hat{C}^{(i,b)} SSM(\bar{w}_q^{(b)}) \bar{p}_e^{(b)} + \hat{C}^{(i,b)} \hat{J}_{ev} \dot{\bar{\Omega}} \quad (3.41)$$

3.1.4.2. Angular Velocity Analysis

Let the angular velocity of the quadrotor in the body-fixed reference frame is written as:

$$\bar{\omega}_q^{(b)} = [p \ q \ r]^T \quad (3.42)$$

Eq. (3.42) can be further written in terms of the derivative of the Euler angles [34].

$$\bar{\omega}_q^{(b)} = \hat{L} \dot{\bar{Y}} \quad (3.43)$$

Where \hat{L} is the mapping matrix which is given as [34],

$$\hat{L} = \begin{bmatrix} 1 & 0 & -\sin(\theta) \\ 0 & \cos(\phi) & \cos(\theta)\sin(\phi) \\ 0 & -\sin(\phi) & \cos(\theta)\cos(\phi) \end{bmatrix} \quad (3.44)$$

Then, the angular velocity in the inertial fixed reference frame can be derived as,

$$\bar{\omega}_q^{(i)} = \hat{C}^{(i,b)} \bar{\omega}_q^{(b)} \quad (3.45)$$

$$\bar{\omega}_q^{(i)} = \hat{C}^{(i,b)} \hat{L} \dot{\bar{Y}} = \hat{T} \dot{\bar{Y}} \quad (3.46)$$

Here, \hat{T} maps the derivative of the Euler angles to the quadrotor's angular velocity in the inertial reference frame.

The angular velocities of the links and the end-effector can be obtained from the transformation matrices [35]. For example,

$$\hat{C} = \hat{C}^{(a,b)} = e^{\tilde{n}_1 \theta_1} e^{\tilde{n}_2 \theta_2} e^{\tilde{n}_3 \theta_3} \dots \quad (3.47)$$

Then, the angular velocity of b with respect a in the reference frame a can be computed as follow,

$$\bar{\omega} = \bar{\omega}_{b/a}^{(a)} = \dot{\theta}_1 \bar{n}_1 + \dot{\theta}_2 e^{\tilde{n}_1 \theta_1} \bar{n}_2 + \dot{\theta}_3 e^{\tilde{n}_1 \theta_1} e^{\tilde{n}_2 \theta_2} \bar{n}_3 + \dots \quad (3.48)$$

Therefore, the angular velocity of link-1 is obtained by using Eq. (3.4).

$$\bar{\omega}_1^{(b)} = \dot{\theta}_1 \bar{n}_2 = \bar{\omega}_{11}^{(b)} \dot{\theta}_1 + \bar{\omega}_{12}^{(b)} \dot{\theta}_2 \quad (3.49)$$

$$\hat{J}_{1\omega} = \begin{bmatrix} \bar{\omega}_{11}^{(b)} & \bar{\omega}_{12}^{(b)} \end{bmatrix} \quad (3.50)$$

where,

$$\begin{aligned}\bar{\omega}_{11}^{(b)} &= \bar{u}_2 \\ \bar{\omega}_{12}^{(b)} &= 0\bar{u}\end{aligned}\tag{3.51}$$

Then,

$$\bar{\omega}_1^{(b)} = \hat{J}_{1w} \dot{\bar{\Omega}} \tag{3.52}$$

The angular velocity in the inertial frame as follows,

$$\bar{\omega}_1^{(i)} = \bar{\omega}_q^{(i)} + \hat{C}^{(i,b)} \bar{\omega}_1^{(b)} = \bar{\omega}_q^{(i)} + \hat{C}^{(i,b)} \hat{J}_{1w} \dot{\bar{\Omega}} \tag{3.53}$$

Similarly, from Eq. (3.6), the angular velocity of link-2 is carried out as,

$$\bar{\omega}_2^{(b)} = (\dot{\theta}_2 + \dot{\theta}_1) \bar{u}_2 = \bar{\omega}_{21}^{(b)} \dot{\theta}_1 + \bar{\omega}_{22}^{(b)} \dot{\theta}_2 \tag{3.54}$$

$$\hat{J}_{2\omega} = \begin{bmatrix} \bar{\omega}_{21}^{(b)} & \bar{\omega}_{22}^{(b)} \end{bmatrix} \tag{3.55}$$

where,

$$\begin{aligned}\bar{\omega}_{21}^{(b)} &= \bar{u}_2 \\ \bar{\omega}_{22}^{(b)} &= \bar{u}_2\end{aligned}\tag{3.56}$$

Then,

$$\bar{\omega}_2^{(b)} = \hat{J}_{2w} \dot{\bar{\Omega}} \tag{3.57}$$

The angular velocity in the inertial frame as follows,

$$\bar{\omega}_2^{(i)} = \bar{\omega}_q^{(i)} + \hat{C}^{(i,b)} \bar{\omega}_2^{(b)} = \bar{\omega}_q^{(i)} + \hat{C}^{(i,b)} \hat{J}_{2w} \dot{\bar{\Omega}} \tag{3.58}$$

Similarly, the end-effector's angular velocity is:

$$\bar{\omega}_e^{(b)} = (\dot{\theta}_2 + \dot{\theta}_1) \bar{u}_2 = \bar{\omega}_{e1}^{(b)} \dot{\theta}_1 + \bar{\omega}_{e2}^{(b)} \dot{\theta}_2 \tag{3.59}$$

$$\hat{J}_{e\omega} = \begin{bmatrix} \bar{\omega}_{e1}^{(b)} & \bar{\omega}_{e2}^{(b)} \end{bmatrix} \tag{3.60}$$

where,

$$\begin{aligned}\bar{\omega}_{e1}^{(b)} &= \bar{u}_2 \\ \bar{\omega}_{e2}^{(b)} &= \bar{u}_2\end{aligned}\tag{3.61}$$

The angular velocity in the inertial frame as follows,

$$\bar{\omega}_e^{(i)} = \bar{\omega}_q^{(i)} + \hat{C}^{(i,b)} \bar{\omega}_e^{(b)} = \bar{\omega}_q^{(i)} + \hat{C}^{(i,b)} \hat{J}_{ew} \dot{\Omega}\tag{3.62}$$

After obtaining the linear and angular velocities, let's define the generalized coordinates and the generalized velocities of the combined system.

$$\begin{aligned}\bar{q} &= [x \ y \ z \ \phi \ \theta \ \psi \ \theta_1 \ \theta_2]^T \\ \dot{\bar{q}} &= [\dot{x} \ \dot{y} \ \dot{z} \ \dot{\phi} \ \dot{\theta} \ \dot{\psi} \ \dot{\theta}_1 \ \dot{\theta}_2]^T\end{aligned}\tag{3.63}$$

The linear and angular velocities can be expressed in terms of the generalized velocities in the following form [35],

$$\begin{aligned}\bar{v} &= \sum_{k=1}^8 \bar{V}_k \dot{\bar{q}}(k) \\ \bar{w} &= \sum_{k=1}^8 \bar{W}_k \dot{\bar{q}}(k)\end{aligned}\tag{3.64}$$

In Eq. (3.64), \bar{V} and \bar{W} are the linear and angular velocity influence coefficients, respectively. Therefore, the velocities of the quadrotor, link-1 and link-2 can be written in terms of the velocity influence coefficients and the generalized velocities further as,

$$\dot{\bar{p}}_q^{(i)} = \begin{bmatrix} \hat{I}_{3x3} & \hat{0}_{3x5} \end{bmatrix} \dot{\bar{q}} = \hat{V}_q \dot{\bar{q}}\tag{3.65}$$

$$\bar{w}_q^{(i)} = \begin{bmatrix} \hat{0}_{3x3} & \hat{T} & \hat{0}_{3x2} \end{bmatrix} \dot{\bar{q}} = \hat{W}_q \dot{\bar{q}}\tag{3.66}$$

$$\dot{\bar{p}}_1^{(i)} = \begin{bmatrix} \hat{I}_{3x3} & -\hat{C}^{(i,b)} SSM(\bar{p}_1^{(b)}) \hat{L} & \hat{C}^{(i,b)} \hat{J}_{1v} \end{bmatrix} \dot{\bar{q}} = \hat{V}_1 \dot{\bar{q}}\tag{3.67}$$

$$\bar{w}_1^{(i)} = \begin{bmatrix} \hat{0}_{3 \times 3} & \hat{T} & \hat{C}^{(i,b)} \hat{J}_{1w} \end{bmatrix} \dot{\bar{q}} = \hat{W}_1 \dot{\bar{q}} \quad (3.68)$$

$$\dot{\bar{p}}_2^{(i)} = \begin{bmatrix} \hat{I}_{3 \times 3} & -\hat{C}^{(i,b)} SSM(\bar{p}_2^{(b)}) \hat{L} & \hat{C}^{(i,b)} \hat{J}_{2v} \end{bmatrix} \dot{\bar{q}} = \hat{V}_2 \dot{\bar{q}} \quad (3.69)$$

$$\bar{w}_2^{(i)} = \begin{bmatrix} \hat{0}_{3 \times 3} & \hat{T} & \hat{C}^{(i,b)} \hat{J}_{2w} \end{bmatrix} \dot{\bar{q}} = \hat{W}_2 \dot{\bar{q}} \quad (3.70)$$

The subscript *x* is for the size of the corresponding matrix.

3.2. Dynamics

The equation of motion of the unified system is obtained by benefiting from the Lagrange-D'Alembert formulation. The form of the equation is given in Eq. (3.71).

$$\frac{d}{dt} \left(\frac{\partial L}{\partial \dot{\bar{q}}} \right) - \frac{\partial L}{\partial \bar{q}} = \bar{u} + \bar{u}_{ext} \quad (3.71)$$

$$L = K - U$$

Firstly, the kinetic and potential energies of the combined system are computed, then the equation of motion of the system is constructed.

3.2.1. The Kinetic and Potential Energies

The total kinetic energy of the combined system is the sum of the kinetic energies of each individual mass elements. For this combined system, the quadrotor body, link-1 and link-2 are the mass elements. The kinetic energies are calculated as:

$$K = K_b + K_1 + K_2 \quad (3.72)$$

$$K_b = \frac{1}{2} \dot{\bar{p}}_q^{(i)T} m_b \dot{\bar{p}}_q^{(i)} + \frac{1}{2} \bar{\omega}_q^{(i)T} \hat{C}^{(i,b)} \hat{I}_b \hat{C}^{(i,b)T} \bar{\omega}_q^{(i)} \quad (3.73)$$

$$K_1 = \frac{1}{2} \dot{\bar{p}}_1^{(i)T} m_1 \dot{\bar{p}}_1^{(i)} + \frac{1}{2} \bar{\omega}_1^{(i)T} \hat{C}^{(i,b)} \hat{C}^{(b,1)} \hat{I}_1 \hat{C}^{(b,1)T} \hat{C}^{(i,b)T} \bar{\omega}_1^{(i)} \quad (3.74)$$

$$K_2 = \frac{1}{2} \dot{\bar{p}}_2^{(i)T} m_2 \dot{\bar{p}}_2^{(i)} + \frac{1}{2} \bar{\omega}_2^{(i)T} \hat{C}^{(i,b)} \hat{C}^{(b,2)} \hat{I}_2 \hat{C}^{(b,2)T} \hat{C}^{(i,b)T} \bar{\omega}_2^{(i)} \quad (3.75)$$

In Eq. from (3.73) to (3.75), I is the constant inertia matrix in the body-fixed reference frames of each elements.

Similarly, the potential energies of each elements are obtained as,

$$U = U_b + U_1 + U_2 \quad (3.76)$$

$$U_b = m_b g \bar{u}_3^t \bar{p}_q^{(i)} \quad (3.77)$$

$$U_1 = m_1 g \bar{u}_3^t \bar{p}_1^{(i)} \quad (3.78)$$

$$U_2 = m_2 g \bar{u}_3^t \bar{p}_2^{(i)} \quad (3.79)$$

3.2.2. The Equation of Motion

After Eq. (3.72) and Eq. (3.76) are put into Eq. (3.71), the equation of motion of the overall system is obtained.

$$\hat{M}(\bar{q}) \ddot{\bar{q}} + \hat{C}(\bar{q}, \dot{\bar{q}}) \dot{\bar{q}} + \hat{G}(\bar{q}) = \bar{u} + \bar{u}_{ext} \quad (3.80)$$

Where, $\hat{M}(\bar{q}) \in R^{8x8}$ is the positive definite inertia matrix. $\hat{C}(\bar{q}, \dot{\bar{q}}) \in R^{8x8}$ consists of centripetal, Coriolis and gyroscopic terms. $\hat{G}(\bar{q})$ includes gravity terms.

The inertia matrix can be calculated by using the following kinetic energy formulation [36].

$$K = \frac{1}{2} \dot{\bar{q}}^T \hat{M}(\bar{q}) \dot{\bar{q}} \quad (3.81)$$

The inertia matrix can be further written by using the velocity influenced coefficients obtained in from Eq. (3.65) to Eq. (3.70).

$$\begin{aligned} \hat{M}(\bar{q}) &= \hat{V}_q^T m_b \hat{V}_q + \hat{W}_q^T \hat{C}^{(i,b)} \hat{I}_b \hat{C}^{(i,b)T} \hat{W}_q \\ &+ \sum_{k=1}^2 \hat{V}_k^T m_k \hat{V}_k + \hat{W}_k^T (\hat{C}^{(i,b)} \hat{C}^{(b,k)}) \hat{I}_k (\hat{C}^{(i,b)} \hat{C}^{(b,k)})^T \hat{W}_k \end{aligned} \quad (3.82)$$

The elements of the Coriolis matrix can be calculated by using the following formulation [36].

$$c_{a,b} = \sum_{j=1}^8 \frac{1}{2} \left\{ \frac{\partial m_{a,b}}{\partial q_j} + \frac{\partial m_{a,j}}{\partial q_b} - \frac{\partial m_{j,b}}{\partial q_a} \right\} \quad (3.83)$$

$c_{x,y}$ and $m_{x,y}$ are the elements of the Coriolis and inertia matrices.

Finally, gravity matrix is computed by using the formulation,

$$\hat{G}(\bar{q}) = \frac{\partial U}{\partial \bar{q}} \quad (3.84)$$

3.2.3. Actuating Forces and Torques

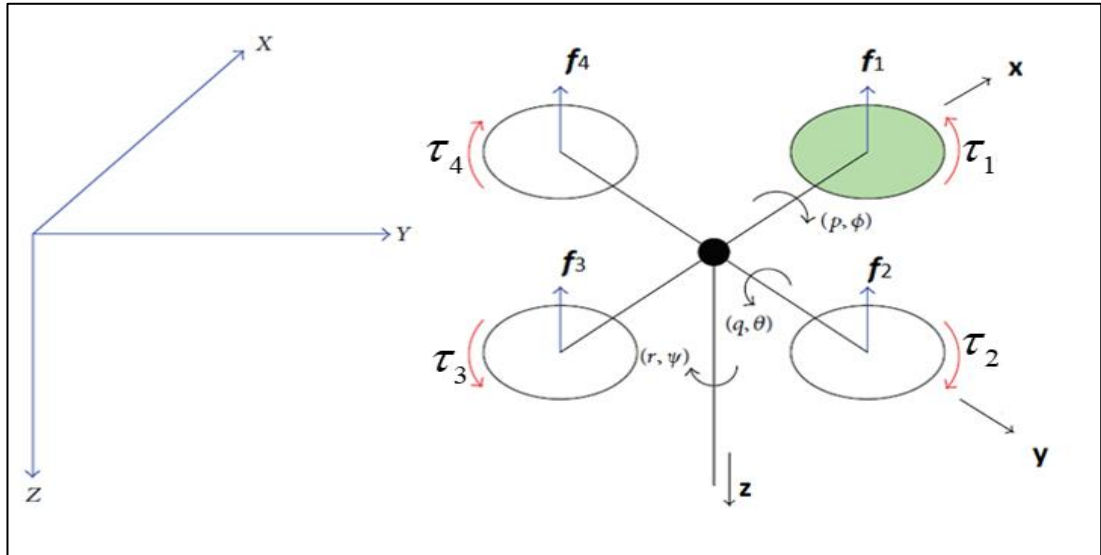


Figure 3.3. Actuating Forces and Torques Generated by the Quadrotor's Motors [51]

Each rotor generates a thrust force, f_j and a torque, τ_j . These forces and torques are computed with following relations. It is assumed that the generated forces and torques are proportional to the square of the rotational speeds of the rotors [1].

$$\begin{aligned} f_j &= c_T \varpi_j^2 \\ \tau_j &= c_Q \varpi_j^2 \end{aligned} \tag{3.85}$$

Where, $j = 1, 2, 3, 4$

Then, the total thrust in the quadrotor's body-fixed reference frame can be written as,

$$\bar{f}_q^{(b)} = \begin{bmatrix} 0 \\ 0 \\ f_z \end{bmatrix} \tag{3.86}$$

Where,

$$f_z = -f_1 - f_2 - f_3 - f_4 \tag{3.87}$$

The total torque applied on the quadrotor's body can be expressed in the body-fixed reference frame as,

$$\bar{\tau}_q^{(b)} = \begin{bmatrix} \tau_{q1} \\ \tau_{q2} \\ \tau_{q3} \end{bmatrix} = \begin{bmatrix} d(f_4 - f_2) \\ d(f_1 - f_3) \\ -\tau_1 + \tau_2 - \tau_3 + \tau_4 \end{bmatrix} = \begin{bmatrix} dc_T(\varpi_4^2 - \varpi_2^2) \\ dc_T(\varpi_1^2 - \varpi_3^2) \\ c_Q(-\varpi_1^2 + \varpi_2^2 - \varpi_3^2 + \varpi_4^2) \end{bmatrix} \tag{3.88}$$

Where d is the distance between the quadrotor's center of mass and one of the rotors.

Therefore, the rotor torques, and forces are associated with the rotational speeds of the propellers with the following relation:

$$\begin{bmatrix} f_z \\ \tau_{q1} \\ \tau_{q2} \\ \tau_{q3} \end{bmatrix} = \begin{bmatrix} -c_T & -c_T & -c_T & -c_T \\ 0 & -dc_T & 0 & dc_T \\ dc_T & 0 & -dc_T & 0 \\ -c_Q & c_Q & -c_Q & c_Q \end{bmatrix} \begin{bmatrix} \varpi_1^2 \\ \varpi_2^2 \\ \varpi_3^2 \\ \varpi_4^2 \end{bmatrix} \tag{3.89}$$

3.2.4. Generalized Input and Interaction Forces

For the quadrotor, to obtain generalized force, \bar{u} , the virtual work principle is used. In the body-fixed reference frame \vec{f}_q and $\vec{\tau}_q$ are the applied forces and moments, respectively. The virtual work done by these forces can be expressed as follows [34]:

$$\delta W = \vec{f}_q \cdot \delta \vec{p}_q + \vec{\tau}_q \cdot \delta \vec{\Psi} \quad (3.90)$$

In Eq. (3.90), $\delta \vec{p}_q = \delta(\vec{p}_q)_{o_b/o_i}$ and $\delta \vec{\Psi} = \delta \vec{\Psi}_{F_b/F_i}$. F_b and F_i represent reference frames body and inertial.

By using the column matrix representations of all the vectors in body-fixed reference frame, Eq. (3.90) can also be written as

$$\delta W = \vec{f}_q^{(b)T} \cdot \hat{C}^{(i,b)T} \delta \vec{p}_q^{(i)} + \vec{\tau}_q^{(b)T} \cdot \delta \vec{\Psi}^{(b)} \quad (3.91)$$

In Eq. (3.91), $\delta \vec{\Psi}^{(b)}$ is usually expressed in terms of suitable set of Euler angles,

$$\delta \Psi^{(b)} = \hat{L} \delta \bar{\Upsilon} \quad (3.92)$$

Hence, Eq. (3.91) can be written further as,

$$\delta W = \vec{f}_q^{(b)T} \cdot \hat{C}^{(i,b)T} \delta \vec{p}_q^{(i)} + \vec{\tau}_q^{(b)T} \cdot \hat{L} \delta \bar{\Upsilon} = [\hat{C}^{(i,b)} \vec{f}_q^{(b)}] \delta \vec{p}_q^{(i)} + [\hat{L}^T \vec{\tau}_q^{(b)}] \delta \bar{\Upsilon} \quad (3.93)$$

Let \bar{Q}_x and \bar{Q}_y be defined as the generalized forces associated with $\delta \vec{p}_q^{(i)}$ and $\delta \bar{\Upsilon}$.

Then, Eq. (3.93) can be written as,

$$\delta W = \bar{Q}_x^t \delta \vec{p}_q^{(i)} + \bar{Q}_y^t \delta \bar{\Upsilon} \quad (3.94)$$

For the manipulator, the virtual work can be obtained further as,

$$\delta W = \vec{\tau}_{12} \cdot \delta \bar{\theta}_{12} \quad (3.95)$$

$$\delta W = \tau_1 \cdot \delta \theta_1 + \tau_2 \cdot \delta \theta_2 \quad (3.96)$$

Therefore, for the overall system, the generalized force input can be written as,

$$\bar{u} = \hat{S} \begin{bmatrix} \bar{f}_q^{(b)} \\ \bar{\tau}_q^{(b)} \\ \bar{\tau}_{12} \end{bmatrix} \quad (3.97)$$

$$\bar{u} = \begin{bmatrix} \hat{C}^{(i,b)} & \hat{0}_{3x3} & \hat{0}_{3x2} \\ \hat{0}_{3x3} & \hat{L}' & \hat{0}_{3x2} \\ \hat{0}_{2x3} & \hat{0}_{2x3} & \hat{I}_{2x2} \end{bmatrix} \begin{bmatrix} \bar{f}_q^{(b)} \\ \bar{\tau}_q^{(b)} \\ \bar{\tau}_{12} \end{bmatrix} \quad (3.98)$$

Where,

$$\bar{u} = [u_1 \ u_2 \ u_3 \ u_4 \ u_5 \ u_6 \ u_7 \ u_8]^T \quad (3.99)$$

In Eq. (3.97),

$$\det(\hat{S}) = \cos(\theta) \quad (3.100)$$

Therefore, if $\theta \neq \pi n - \frac{\pi}{2}$, $n \in Z$ then, \hat{S} is an invertible matrix. In this thesis,

the range of values of theta satisfies this condition. Where, $\tau_{12} = [\tau_1 \ \tau_2]^T$ is the vector of manipulator joint torques.

Analysis of the external forces applied on the end-effector at the vehicle and joint level as follow. Let \bar{F} be the applied force and \bar{M} be the applied moments on the end-effector.

$$\bar{F} = [F_1 \ F_2 \ F_3]^T \quad \text{and} \quad \bar{M} = [M_1 \ M_2 \ M_3]^T \quad (3.101)$$

Then, the applied forces and moments can be written as an augmented column matrix form.

$$\bar{P} = [\bar{F}; \bar{M}] = [F_1 \ F_2 \ F_3 \ M_1 \ M_2 \ M_3]^T \quad (3.102)$$

Therefore, the applied forces and moments can be written in the generalized coordinates level as,

$$\bar{u}_{ext} = \hat{H}\bar{P} \quad (3.103)$$

Where, $\hat{H} \in R^{8 \times 6}$ is the conversion matrix. Its elements are computed step by step as:

For the generalized coordinates $[x \ y \ z]$,

$$\begin{bmatrix} u_{ext1} \\ u_{ext2} \\ u_{ext3} \end{bmatrix} = \begin{bmatrix} 1 & 0 & 0 \\ 0 & 1 & 0 \\ 0 & 0 & 1 \end{bmatrix} \begin{bmatrix} F_1 \\ F_2 \\ F_3 \end{bmatrix} \quad (3.104)$$

For the generalized coordinates $[\phi \ \theta \ \psi]$,

$$\begin{bmatrix} u_{ext4} \\ u_{ext5} \\ u_{ext6} \end{bmatrix} = \vec{p}_e^{(b)} x \vec{F} + \begin{bmatrix} 1 & 0 & 0 \\ 0 & 1 & 0 \\ 0 & 0 & 1 \end{bmatrix} \begin{bmatrix} M_1 \\ M_2 \\ M_3 \end{bmatrix} = SSM(\vec{p}_e^{(b)}) \vec{F} + \begin{bmatrix} 1 & 0 & 0 \\ 0 & 1 & 0 \\ 0 & 0 & 1 \end{bmatrix} \begin{bmatrix} M_1 \\ M_2 \\ M_3 \end{bmatrix} \quad (3.105)$$

Eq. (3.105) can be further written as,

$$\begin{bmatrix} u_{ext4} \\ u_{ext5} \\ u_{ext6} \end{bmatrix} = \begin{bmatrix} 0 & -p_{e3} & p_{e2} \\ p_{e3} & 0 & -p_{e1} \\ p_{e2} & p_{e1} & 0 \end{bmatrix} \begin{bmatrix} F_1 \\ F_2 \\ F_3 \end{bmatrix} + \begin{bmatrix} 1 & 0 & 0 \\ 0 & 1 & 0 \\ 0 & 0 & 1 \end{bmatrix} \begin{bmatrix} M_1 \\ M_2 \\ M_3 \end{bmatrix} \quad (3.106)$$

For the generalized coordinates $[\theta_1 \ \theta_2]$,

The joint actuators reaction torques can be written in terms of the end effector Jacobian and the applied forces and the moments [35].

$$\begin{bmatrix} u_{ext7} \\ u_{ext8} \end{bmatrix} = \hat{J}_e^{(b)} \bar{P} \quad (3.107)$$

Where,

$$\hat{J}_e^{(b)} = [\hat{J}_{ev}^T : \hat{J}_{e\omega}^T] \quad (3.108)$$

$$\begin{bmatrix} u_{ext7} \\ u_{ext8} \end{bmatrix} = \begin{bmatrix} v_{e11} & v_{e12} & v_{e13} & \omega_{e11} & \omega_{e12} & \omega_{e13} \\ v_{e21} & v_{e22} & v_{e23} & \omega_{e21} & \omega_{e22} & \omega_{e23} \end{bmatrix} \begin{bmatrix} F_1 \\ F_2 \\ F_3 \\ M_1 \\ M_2 \\ M_3 \end{bmatrix} \quad (3.109)$$

Finally, by using Eq. (3.104), Eq. (3.106), and Eq. (3.109), following relation is obtained.

$$\bar{u}_{ext} = \begin{bmatrix} 1 & 0 & 0 & 0 & 0 & 0 \\ 0 & 1 & 0 & 0 & 0 & 0 \\ 0 & 0 & 1 & 0 & 0 & 0 \\ 0 & -p_{e3} & p_{e2} & 1 & 0 & 0 \\ p_{e3} & 0 & -p_{e1} & 0 & 1 & 0 \\ -p_{e2} & p_{e1} & 0 & 0 & 0 & 1 \\ v_{e11} & v_{e12} & v_{e13} & \omega_{e11} & \omega_{e12} & \omega_{e13} \\ v_{e21} & v_{e22} & v_{e23} & \omega_{e21} & \omega_{e22} & \omega_{e23} \end{bmatrix} \begin{bmatrix} F_1 \\ F_2 \\ F_3 \\ M_1 \\ M_2 \\ M_3 \end{bmatrix} \quad (3.110)$$

Eq. (3.110) can be expressed more compactly as,

$$\bar{u}_{ext} = \begin{bmatrix} \hat{I}_{3x3} & \hat{0}_{3x3} \\ SSM(\bar{p}_e^{(b)}) & \hat{I}_{3x3} \\ \hat{J}_{ev}^T & \hat{J}_{e\omega}^T \end{bmatrix} \bar{P} \quad (3.111)$$

3.2.5. The Moments of Inertia Analysis

The values of the diagonal elements of the moments of inertias of the quadrotor are taken from the quadrotor whose moments of inertias are experimentally identified by Yıldız [37]. Off-diagonal elements are assumed to zero since the quadrotor is a symmetric vehicle.

$$\hat{I}_b = \begin{bmatrix} I_{xx} & 0 & 0 \\ 0 & I_{yy} & 0 \\ 0 & 0 & I_{zz} \end{bmatrix} \quad (3.112)$$

For the links of robotic arm following formulations are used to calculate the moments of inertias of the links. Links are considered as the rectangular prism.

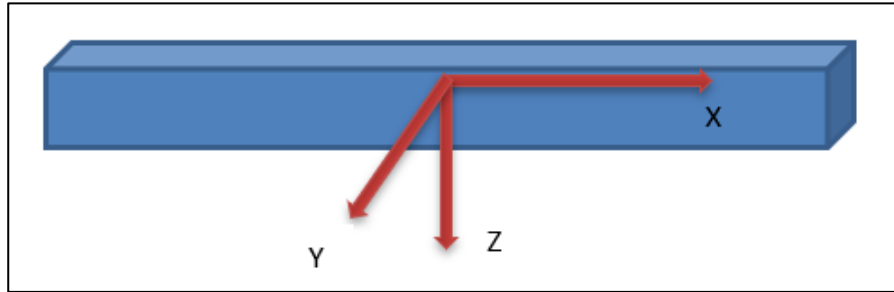


Figure 3.4. Approximate 3-D Link Element

For the link-1,

$$\begin{aligned}
 I_{xx1} &= \iiint (y^2 + z^2) dm = \iiint_{x=\frac{\pm b_1}{2}, y=\frac{\pm c_1}{2}, z=\frac{\pm d_1}{2}} (y^2 + z^2) \rho dz dy dx = \frac{1}{12} m_1 (c_1^2 + d_1^2) \\
 I_{yy1} &= \iiint (x^2 + z^2) dm = \iiint_{x=\frac{\pm b_1}{2}, y=\frac{\pm c_1}{2}, z=\frac{\pm d_1}{2}} (x^2 + z^2) \rho dz dy dx = \frac{1}{12} m_1 (b_1^2 + d_1^2) \\
 I_{zz1} &= \iiint (x^2 + y^2) dm = \iiint_{x=\frac{\pm b_1}{2}, y=\frac{\pm c_1}{2}, z=\frac{\pm d_1}{2}} (x^2 + y^2) \rho dz dy dx = \frac{1}{12} m_1 (b_1^2 + c_1^2)
 \end{aligned} \quad (3.113)$$

Similarly, for the link-2,

$$\begin{aligned}
I_{xx2} &= \frac{1}{12} m_2 (c_2^2 + d_2^2) \\
I_{yy2} &= \frac{1}{12} m_2 (b_2^2 + d_2^2) \\
I_{zz2} &= \frac{1}{12} m_2 (b_2^2 + c_2^2)
\end{aligned} \tag{3.114}$$

Since the beam is a symmetric element, off-diagonal elements are all zero.

Then,

$$\hat{I}_1 = \begin{bmatrix} I_{xx1} & 0 & 0 \\ 0 & I_{yy1} & 0 \\ 0 & 0 & I_{zz1} \end{bmatrix}, \quad \hat{I}_2 = \begin{bmatrix} I_{xx2} & 0 & 0 \\ 0 & I_{yy2} & 0 \\ 0 & 0 & I_{zz2} \end{bmatrix} \tag{3.115}$$

3.2.6. DC and Servo Motors Transfer Functions

To create a more realistic simulation environment, transfer functions of the quadrotor's dc motor and robotic arm joint servos are implemented. For the dc motor, the transfer function that is identified for a thesis study is used [37]. The transfer function between the commanded propeller speed and the achieved propeller speed is as follows,

$$G(s) = \frac{\omega_{achieved}}{\omega_{commanded}} = \frac{0.98}{0.062s + 1} \tag{3.116}$$

For the joint servos, it is assumed that the inputs of the servos are torques. To reflect the dynamics of the servo motors, a second order transfer function is used with $\zeta = 0.707$ and $w_n = 20$ Hz.

$$G(s) = \frac{\tau_{achieved}}{\tau_{commanded}} = \frac{w_n^2}{s^2 + 2\zeta w_n s + w_n^2} \tag{3.117}$$

CHAPTER 4

CONTROLLER DESIGN

After the equations of motion of the combined system are obtained, control algorithms are developed based on these equations. Three different control structures are built, and their performances are observed in a simulation environment. The first controller is the cascaded PID controller that is obtained by using the linearized equations of motion of the system. The second controller is the feedback linearizing controller. It is developed based on the Eq. (3.80). Finally, the last controller is the feedback linearizing controller which is combined with an extended state observer to estimate the parametric uncertainties and the external disturbances. Moreover, the control inputs of the quadrotor are the rotational speeds of the propellers. For the joint arms servos, the control inputs are the torques of the joint servo motors.

4.1. Cascaded PID Controller

This controller is designed by considering the linear and decoupled equations of motion of the unified system. Since quadrotor is an underactuated UAV, in order to move the quadrotor in the inertial x-direction, the vehicle should tilt in the pitch plane, and to move in the inertial y-direction, the vehicle should tilt in the roll plane while yaw angle is kept at zero degree. Therefore, state x is coupled with state θ , and state y is coupled with state ϕ . Hence, a controller structure that has two stages is designed. In the outer loop, the desired pitch and roll angles are computed for the desired translations in x and y directions. Then, all the desired states are fed into the inner loop of the controller to compute control input, \bar{u} . The overall control architecture is given in Figure 4.1.

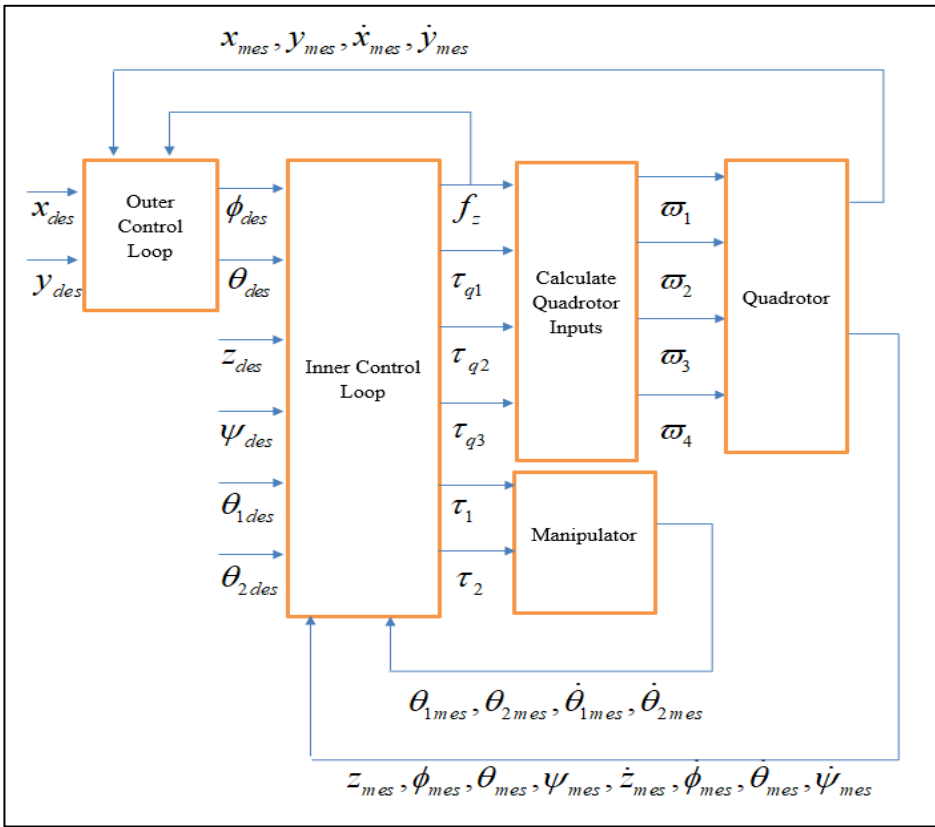


Figure 4.1. The Control Architecture of the Cascaded PID Controller

4.1.1. Outer Loop Controller Design

4.1.1.1. Translational x&y Controller

This controller generates intermediate control inputs θ_{des} and ϕ_{des} for the reference inputs x and y , respectively. The controller is designed by using Eq's. (3.98) and (3.99). From these equations, following relations can be written,

$$\begin{aligned} u_1 &= f_z(\cos(\psi)\sin(\theta)\cos(\phi) + \sin(\psi)\sin(\phi)) \\ u_2 &= f_z(\sin(\psi)\sin(\theta)\cos(\phi) - \cos(\psi)\sin(\phi)) \end{aligned} \quad (4.1)$$

Then, by small angle assumptions for ϕ and θ , and by assuming $\psi = 0$, Eq. (4.1) can be further written as,

$$\begin{aligned} u_1 &= m_t \ddot{x} = f_z \theta \\ u_2 &= m_t \ddot{y} = -f_z \phi \end{aligned} \quad (4.2)$$

By using Eq. (4.2), the following PID control laws are obtained by using feedback linearizing logic for both θ_{des} and ϕ_{des}

$$\theta_{des} = \frac{m_t}{f_z} (\ddot{x}_{des} + K_{px} e_x(t) + K_{ix} \int_0^t e_x(\tau) d\tau + K_{dx} \frac{de_x(t)}{dt}) \quad (4.3)$$

$$\phi_{des} = -\frac{m_t}{f_z} (\ddot{y}_{des} + K_{py} e_y(t) + K_{iy} \int_0^t e_y(\tau) d\tau + K_{dy} \frac{de_y(t)}{dt}) \quad (4.4)$$

Where,

$$\begin{aligned} e_x &= x_{des} - x_{mes} \\ e_y &= y_{des} - y_{mes} \end{aligned} \quad (4.5)$$

Feedforward terms \ddot{x}_{des} and \ddot{y}_{des} are the desired accelerations. These values are not available at this stage, but they can be calculated by numerical differentiation. However, since it can be very noisy, a noise filter should be used, or these desired accelerations can be fed from the outside to the simulation. In this thesis, they are taken to be zero in the control law.

4.1.2. Inner Loop Controller Design

This control loop consists of altitude, and attitude controllers of the quadrotor and joint controllers of the serial manipulator.

4.1.2.1. Altitude Controller

This is also a PID controller that ensures the quadrotor to track reference altitude. It is developed by using Eq's. (3.98) and (3.99). The following expression is written based on these equations.

$$u_3 = m_t \ddot{z} = f_z + m_t g \quad (4.6)$$

Then, the control law can be written down,

$$f_z = m_t (\ddot{z}_{des} + K_{pz} e_z(t) + K_{iz} \int_0^t e_z(\tau) d\tau + K_{dz} \frac{de_z(t)}{dt}) - m_t g \quad (4.7)$$

Again, \ddot{z}_{des} is taken as zero.

4.1.2.2. Attitude Controller

From Eq's. (3.98) and (3.99), the following expressions are written for roll, pitch and yaw dynamics.

$$u_4 = I_{xx} \dot{\phi} = \tau_{q1} \quad (4.8)$$

$$u_5 = I_{yy} \dot{\theta} = \tau_{q2} \quad (4.9)$$

$$u_6 = I_{zz} \dot{\psi} = \tau_{q3} \quad (4.10)$$

Then, cascaded type attitude controllers are developed. This control structure is more robust to the oscillations. There is an inner loop which stabilizes the angular velocity and outer loop which controls the attitudes of the vehicle. A PI controller is used for the inner loop and a P controller is used for the outer loop. The control scheme can be seen in Figure 4.2.

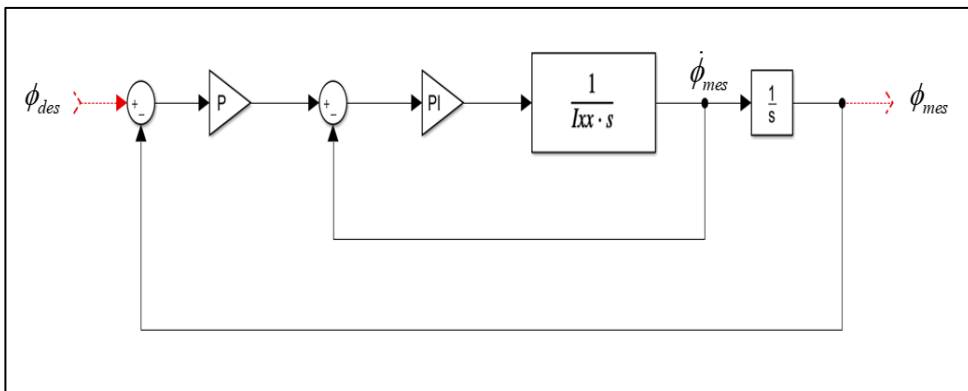


Figure 4.2. Roll Controller Structure

The cascaded control laws for the attitude are as follows,

$$\tau_{q1} = (K_{p2\phi}e_\phi(t) - \dot{\phi})[K_{p\dot{\phi}}e_{\dot{\phi}}(t) + K_{i\dot{\phi}} \int_0^t e_{\dot{\phi}}(\tau)d\tau] \quad (4.11)$$

$$\tau_{q2} = (K_{p2\theta}e_\theta(t) - \dot{\theta})[K_{p\dot{\theta}}e_{\dot{\theta}}(t) + K_{i\dot{\theta}} \int_0^t e_{\dot{\theta}}(\tau)d\tau] \quad (4.12)$$

$$\tau_{q3} = (K_{p2\psi}e_\psi(t) - \dot{\psi})[K_{p\dot{\psi}}e_{\dot{\psi}}(t) + K_{i\dot{\psi}} \int_0^t e_{\dot{\psi}}(\tau)d\tau] \quad (4.13)$$

Where,

$$\begin{aligned} e_\phi &= \phi_{des} - \phi_{mes} & e_\theta &= \theta_{des} - \theta_{mes} & e_\psi &= \psi_{des} - \psi_{mes} \\ e_{\dot{\phi}} &= \dot{\phi}_{des} - \dot{\phi}_{mes} & e_{\dot{\theta}} &= \dot{\theta}_{des} - \dot{\theta}_{mes} & e_{\dot{\psi}} &= \dot{\psi}_{des} - \dot{\psi}_{mes} \end{aligned} \quad (4.14)$$

4.1.2.3. Robotic Arm Joints Controller

To develop the PID joint controllers for the robotic arm, following relations are used.

$$I_{yy12}\ddot{\theta}_1 = \tau_1 - m_{12}g \sin(\theta_1)(\frac{b_1+b_2}{2}) \quad (4.15)$$

$$I_{yy2}\ddot{\theta}_2 = \tau_2 - m_2g \sin(\theta_2)(\frac{b_2}{2}) \quad (4.16)$$

In Eq. (4.15), I_{yy12} is the total moments of inertia of link-1 and link-2. The control law can be written by using feedback linearizing logic as:

$$\begin{aligned} \tau_1 &= I_{12}(\ddot{\theta}_{1des} + \tau_{\theta1}) + m_{12}g \sin(\theta_1)(\frac{b_1+b_2}{2}) \\ \tau_{\theta1} &= K_{p\theta1}e_{\theta1}(t) + K_{i\theta1} \int_0^t e_{\theta1}(\tau)d\tau + K_{d\theta1} \frac{de_{\theta1}(t)}{dt} \end{aligned} \quad (4.17)$$

$$\begin{aligned}\tau_2 &= I_2(\ddot{\theta}_{2des} + \tau_{\theta2}) + m_2 g \sin(\theta_2) \left(\frac{b_2}{2}\right) \\ \tau_{\theta2} &= K_{p\theta2} e_{\theta2}(t) + K_{i\theta2} \int_0^t e_{\theta2}(\tau) d\tau + K_{d\theta2} \frac{de_{\theta2}(t)}{dt}\end{aligned}\quad (4.18)$$

Where,

$$\begin{aligned}e_{\theta1} &= \theta_{1des} - \theta_{1mes} \\ e_{\theta2} &= \theta_{2des} - \theta_{2mes}\end{aligned}\quad (4.19)$$

After obtaining control laws, quadrotors inputs that are rotational speeds of the rotors can be expressed by using Eq's (3.89), (4.7), (4.11), (4.12), and (4.13).

$$\begin{bmatrix} \varpi_1^2 \\ \varpi_2^2 \\ \varpi_3^2 \\ \varpi_4^2 \end{bmatrix} = \begin{bmatrix} -c_T & -c_T & -c_T & -c_T \\ 0 & -dc_T & 0 & dc_T \\ dc_T & 0 & -dc_T & 0 \\ -c_Q & c_Q & -c_Q & c_Q \end{bmatrix}^{-1} \begin{bmatrix} f_z \\ \tau_{q1} \\ \tau_{q2} \\ \tau_{q3} \end{bmatrix} \quad (4.20)$$

For the serial manipulator, Eq's (4.17), and (4.18) define the control inputs.

Finally, the gains of the controllers are determined by using the root locus method and shown in Table 4.1. The Gains of the PID Controllers

Table 4.1. *The Gains of the PID Controllers*

	x	y	z	ϕ	θ	ψ	θ_1	θ_2
K_p	24.790	24.790	39.430	1.959	1.959	1.269	1325	4669
K_i	12.360	12.360	27.880	20.880	20.880	4.390	6169	40370
K_d	9.407	9.407	12.170	-	-	-	70.450	129.800
K_{p2}	-	-	-	9.172	9.172	3.339	-	-

4.2. Feedback Linearizing Controller

A hybrid system that is consisting of an underactuated aerial vehicle and a 2-DOF serial robotic arm is studied. The combined system is still underactuated, as well. The nonlinear equation of motion of the system is obtained in a standard form that is common in conventional robotics applications. Then, feedback linearizing control law is developed for the tracking control of the combined system. The basic idea behind the feedback linearization is that constructing a transformation which exactly linearizes the nonlinear equations of motion of the system.

4.2.1. Background

If we have a fully actuated robotic system, then to directly linearize the Eq. (3.80) with $\bar{u}_{ext} = 0$, the following control law can be written [38].

$$\bar{u} = \hat{M}(\bar{q})\bar{v} + \hat{C}(\bar{q}, \dot{\bar{q}})\dot{\bar{q}} + \bar{G}(\bar{q}) \quad (4.21)$$

Here, \bar{v} is an auxiliary control input.

Then, this control law is put into Eq. (3.80), the next expression is obtained.

$$\ddot{\bar{q}} = \bar{v} \quad (4.22)$$

Then, the complicated and nonlinear controller design problem takes the shape of a simpler linear controller design task. By using the feedback linearizing logic, \bar{v} can be chosen as,

$$\bar{v} = \ddot{\bar{q}}_{des} + \hat{K}_p \bar{e} + \hat{K}_d \dot{\bar{e}} + \hat{K}_i \int_0^t \bar{e}(\tau) d\tau \quad (4.23)$$

The feedforward term $\ddot{\bar{q}}_{des}$ can be calculated numerically or it can be fed from the outside to the system. However, it is taken as zero in the analysis.

Where

$$\bar{e} = \bar{q}_{des} - \bar{q}_{mes} \quad (4.24)$$

After Eq. (4.23) is plugged into Eq.(4.21), the following control input is obtained.

$$\bar{u} = \hat{M}(\bar{q})(\ddot{\bar{q}}_d + \hat{K}_p \bar{e} + \hat{K}_d \dot{\bar{e}} + \hat{K}_i \int_0^t \bar{e}(\tau) d\tau) + \hat{C}(\bar{q}, \dot{\bar{q}}) \dot{\bar{q}} + \bar{G}(\bar{q}) \quad (4.25)$$

From Eq's. (3.80) and (4.25), the error dynamics can be written as,

$$\ddot{\bar{e}} + \hat{K}_p \bar{e} + \hat{K}_d \dot{\bar{e}} + K_i \int_0^t \bar{e}(\tau) d\tau = 0 \quad (4.26)$$

According to linear system theory, convergence of the Eq. (4.26) to zero is guaranteed with the suitable selection of the gain parameters [38].

While implementing the controller into the simulation environment, Eq. (3.116) is used for the dynamics of the dc motors, and Eq. (3.117) is used for the dynamics of the servo motors of the manipulator.

4.2.2. Problem Formulation

However, the aerial manipulator in this thesis is an underactuated system. Positions x and y are coupled with the attitudes pitch and roll angles. In this cascaded controller architecture, there is an outer loop that computes the motion references of the attitudes pitch and roll angles for the motion references of the x and y positions, and tracks the motion reference of the position z. Also, there is an inner loop that tracks the motion references of quadrotor attitudes, and joint angles of the robotic arm. Therefore, the problem is formulated in a slightly different way. Due to the underactuated nature of the system, the feedback linearization technique is partially applicable. So as to extend the f/b linearization approach to the control of the aerial manipulator, the couplings between the roll/pitch dynamics and the x/y dynamics are utilized together with the manipulations in the relevant inertia matrices as expressed in Section 4.2.3.

The general controller architecture is given in Figure 4.3.

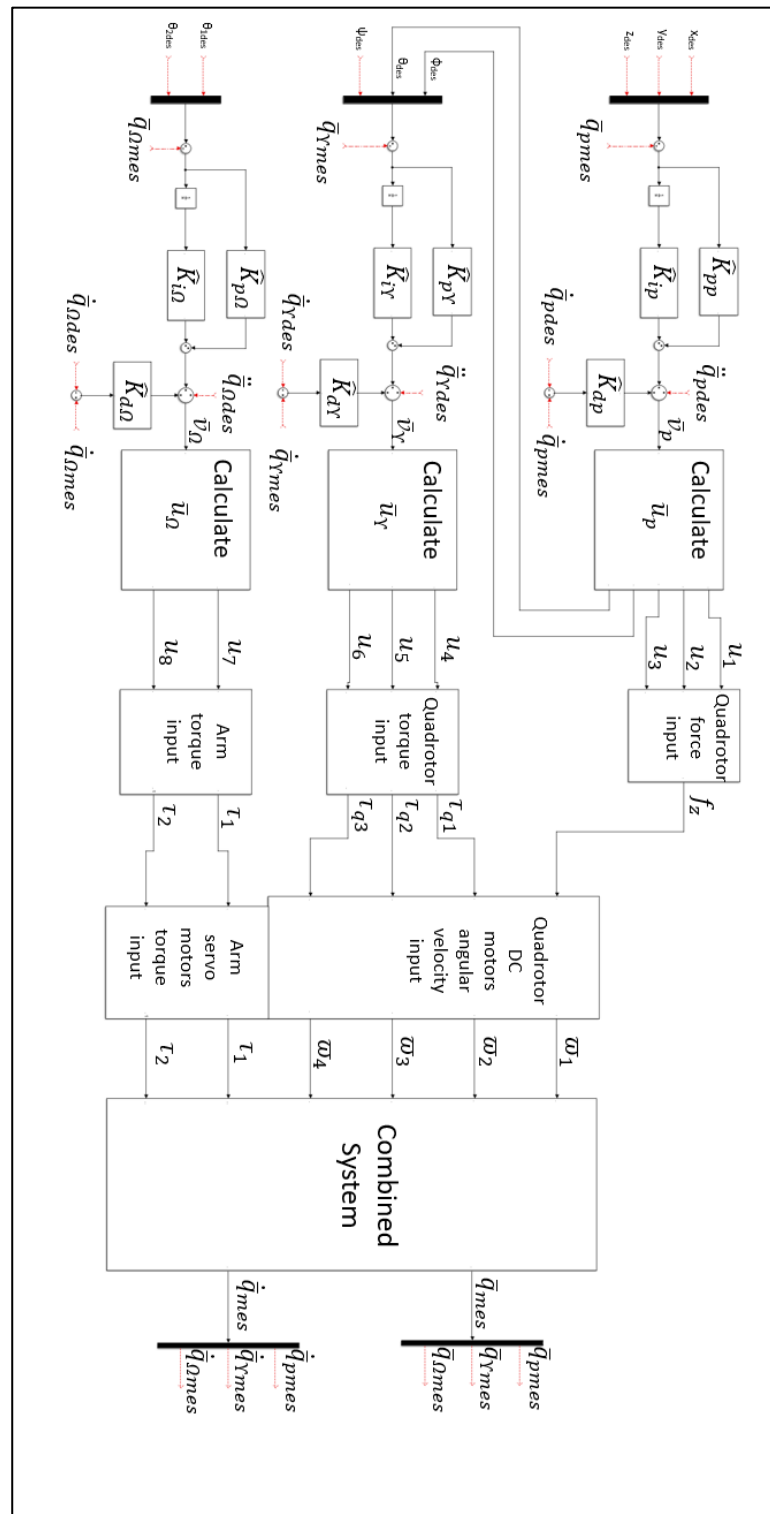


Figure 4.3. Feedback Linearizing Controller Architecture

Hence, the elements of the Eq. (4.21) are partitioned as [13]:

$$\hat{M} = \begin{bmatrix} \hat{M}_{pp} & \hat{M}_{p\gamma} & \hat{M}_{p\Omega} \\ \hat{M}_{p\gamma}^T & \hat{M}_{\gamma\gamma} & \hat{M}_{\gamma\Omega} \\ \hat{M}_{p\Omega}^T & \hat{M}_{\gamma\Omega}^T & \hat{M}_{\Omega\Omega} \end{bmatrix}, \hat{C} = \begin{bmatrix} \hat{C}_{pp} & \hat{C}_{p\gamma} & \hat{C}_{p\Omega} \\ \hat{C}_{p\gamma}^T & \hat{C}_{\gamma\gamma} & \hat{C}_{\gamma\Omega} \\ \hat{C}_{p\Omega}^T & \hat{C}_{\gamma\Omega}^T & \hat{C}_{\Omega\Omega} \end{bmatrix}$$

$$\bar{G} = \begin{bmatrix} \bar{G}_p \\ \bar{G}_\gamma \\ \bar{G}_\Omega \end{bmatrix}, \bar{u} = \begin{bmatrix} \bar{u}_p \\ \bar{u}_\gamma \\ \bar{u}_\Omega \end{bmatrix}, \bar{v} = \begin{bmatrix} \bar{v}_p \\ \bar{v}_\gamma \\ \bar{v}_\Omega \end{bmatrix}, \bar{q} = \begin{bmatrix} \bar{q}_p \\ \bar{q}_\gamma \\ \bar{q}_\Omega \end{bmatrix}$$
(4.27)

$$\hat{M}_{pp} \in R^{3x3}, \hat{M}_{p\gamma} \in R^{3x3}, \hat{M}_{p\Omega} \in R^{3x2}, \hat{M}_{\gamma\gamma} \in R^{3x3}, \hat{M}_{\gamma\Omega} \in R^{3x2}, \hat{M}_{\Omega\Omega} \in R^{2x2}$$

$$\text{Here, } \hat{C}_{pp} \in R^{3x3}, \hat{C}_{p\gamma} \in R^{3x3}, \hat{C}_{p\Omega} \in R^{3x2}, \hat{C}_{\gamma\gamma} \in R^{3x3}, \hat{C}_{\gamma\Omega} \in R^{3x2}, \hat{C}_{\Omega\Omega} \in R^{2x2}$$

$$\bar{G}_p, \bar{u}_p, \bar{v}_p, \bar{q}_p \in R^{3x1}, \bar{G}_\gamma, \bar{u}_\gamma, \bar{v}_\gamma, \bar{q}_\gamma \in R^{3x1}, \bar{G}_\Omega, \bar{u}_\Omega, \bar{v}_\Omega, \bar{q}_\Omega \in R^{2x1}$$

Then, the linearized dynamics can be written as:

$$\begin{aligned} \ddot{\bar{q}}_p &= \bar{v}_p \\ \ddot{\bar{q}}_\gamma &= \bar{v}_\gamma \\ \dot{\bar{q}}_\Omega &= \bar{v}_\Omega \end{aligned}$$
(4.28)

From Eq. (4.23), the auxiliary control inputs are written as:

$$\begin{aligned} \bar{v}_p &= \ddot{\bar{q}}_{pdes} + \hat{K}_{pp}\bar{e}_p + \hat{K}_{dp}\dot{\bar{e}}_p + \hat{K}_{ip}\int_0^t \bar{e}_p(\tau)d\tau \\ \bar{v}_\gamma &= \ddot{\bar{q}}_{\gamma des} + \hat{K}_{p\gamma}\bar{e}_\gamma + \hat{K}_{d\gamma}\dot{\bar{e}}_\gamma + \hat{K}_{i\gamma}\int_0^t \bar{e}_\gamma(\tau)d\tau \\ \bar{v}_\Omega &= \ddot{\bar{q}}_{\Omega des} + \hat{K}_{p\Omega}\bar{e}_\Omega + \hat{K}_{d\Omega}\dot{\bar{e}}_\Omega + \hat{K}_{i\Omega}\int_0^t \bar{e}_\Omega(\tau)d\tau \end{aligned}$$
(4.29)

4.2.3. Position Control of the Quadrotor

For the position control, the following feedback linearizing control law can be written.

$$\bar{u}_p = \begin{bmatrix} u_1 \\ u_2 \\ u_3 \end{bmatrix} = \hat{M}_{pp}\bar{v}_p + \hat{M}_{p\gamma}^*\bar{v}_\gamma + \hat{M}_{p\Omega}\bar{v}_\Omega + \hat{C}_{pp}\dot{\bar{q}}_p + \hat{C}_{p\gamma}\dot{\bar{q}}_\gamma + \hat{C}_{p\Omega}\dot{\bar{q}}_\Omega + \bar{G}_p \quad (4.30)$$

In Eq.(4.30), to evaluate the control inputs for the position control, desired roll and pitch angles are required. However, in this stage, they are not available due to the underactuated nature of the quadrotor. To deal with this problem, the control input \bar{u}_p is obtained by using a slightly different way. First and second columns of the matrix $\hat{M}_{p\gamma}$ are taken as zero and modified $\hat{M}_{p\gamma}^*$ matrix is obtained. By this way, the roll and pitch multipliers of the inertia matrix is replaced by zero so that requirement of the knowledge of the desired roll and pitch angles are removed. This assumption is made because these elements of the inertia matrix are generally negligible since manipulator's links are much lighter than the mass of the UAV [13]. To validate this assumption, 2-norms of the original and modified inertia matrix throughout the simulation are given in following figures. As it is seen, the norms are very close to each other. Therefore, for controller design, using modified inertia matrix is an acceptable assumption [13].

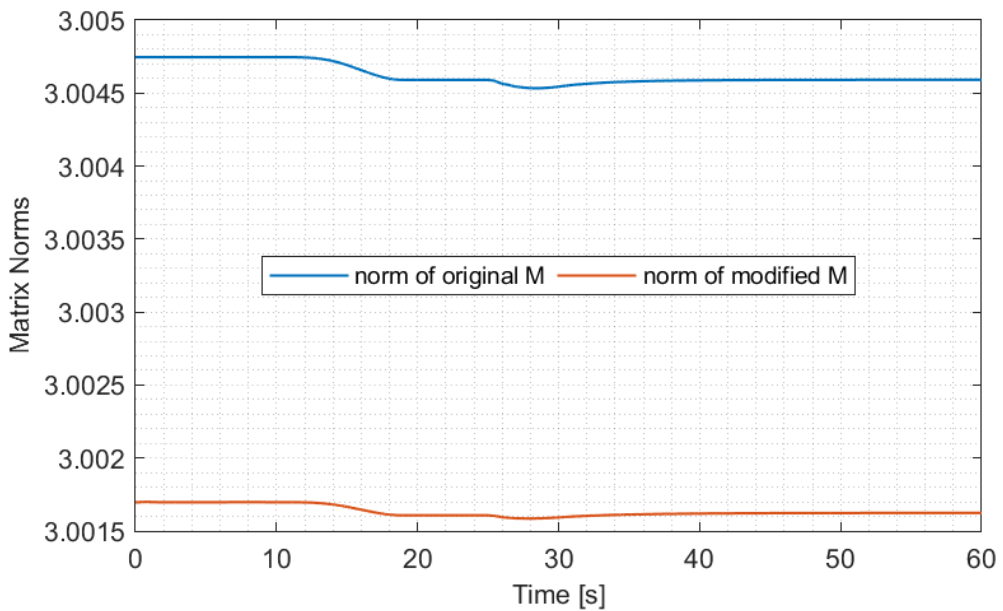


Figure 4.4. Norms of the Original and Modified Inertia Matrices

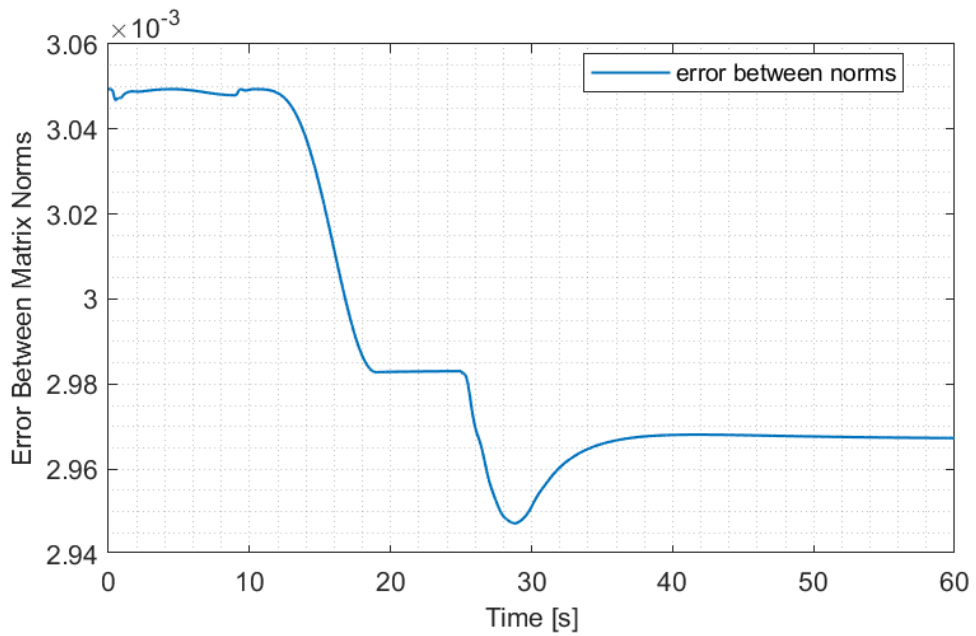


Figure 4.5. The Error Between the Norms of the Original and Modified Inertia Matrices

Now, \bar{u}_p can be computed.

Therefore, reference values of the roll and pitch angles can be calculated by using Eq's. (3.86), and (3.98).

$$\bar{u}_p = \begin{bmatrix} u_1 \\ u_2 \\ u_3 \end{bmatrix} = \begin{bmatrix} (c\psi s\theta c\phi + s\psi s\phi) f_z \\ (s\psi s\theta c\phi - c\psi s\phi) f_z \\ (c\theta c\phi) f_z \end{bmatrix} \quad (4.31)$$

From Eq. (4.31),

$$f_z = \sqrt{\bar{u}_p^T \bar{u}_p} \quad (4.32)$$

$$\theta_{des} = \arctan\left(\frac{u_1 \cos(\psi) + u_2 \sin(\psi)}{u_3}\right) \quad (4.33)$$

$$\phi_{des} = \arcsin\left(\frac{u_1 \sin(\psi) - u_2 \cos(\psi)}{f_z}\right) \quad (4.34)$$

4.2.4. Attitude Control of the Quadrotor

After obtaining reference values of the roll and pitch angles, the following feedback linearizing control law can be written for the attitude control.

$$\bar{u}_r = \begin{bmatrix} u_4 \\ u_5 \\ u_6 \end{bmatrix} = \hat{M}_{p\gamma}^T \bar{v}_p + \hat{M}_{\gamma\gamma} \bar{v}_\gamma + \hat{M}_{\gamma\Omega} \bar{v}_\Omega + \hat{C}_{p\gamma}^T \dot{\bar{q}}_p + \hat{C}_{\gamma\gamma} \dot{\bar{q}}_\gamma + \hat{C}_{\gamma\Omega} \dot{\bar{q}}_\Omega + \bar{G}_\gamma \quad (4.35)$$

From the Eq. (3.98), and (4.35), the torques that are generated by the propellers are calculated as,

$$\bar{\tau}_q^{(b)} = (\hat{L}')^{-1} \bar{u}_r \quad (4.36)$$

Thus, the quadrotor's propellers rotational speed inputs can be calculated by using Eq's (3.89), (4.32), and (4.36) as:

$$\begin{bmatrix} \varpi_1^2 \\ \varpi_2^2 \\ \varpi_3^2 \\ \varpi_4^2 \end{bmatrix} = \begin{bmatrix} -c_T & -c_T & -c_T & -c_T \\ 0 & -dc_T & 0 & dc_T \\ dc_T & 0 & -dc_T & 0 \\ -c_Q & c_Q & -c_Q & c_Q \end{bmatrix}^{-1} \begin{bmatrix} f_z \\ \tau_{q1} \\ \tau_{q2} \\ \tau_{q3} \end{bmatrix} \quad (4.37)$$

4.2.5. Joints Angle Control of the Manipulator

The following feedback linearizing control law can be written for the attitude control.

$$\bar{u}_\Omega = \begin{bmatrix} u_7 \\ u_8 \end{bmatrix} = \hat{M}_{p\Omega}^T \bar{v}_p + \hat{M}_{r\Omega}^T \bar{v}_r + \hat{M}_{\Omega\Omega}^T \bar{v}_\Omega + \hat{C}_{p\Omega}^T \dot{\bar{q}}_p + \hat{C}_{r\Omega}^T \dot{\bar{q}}_r + \hat{C}_{\Omega\Omega}^T \dot{\bar{q}}_\Omega + \bar{G}_\Omega \quad (4.38)$$

From Eq. (3.98), and Eq. (4.38), joint torques are obtained as,

$$\bar{\tau}_{12} = \bar{u}_\Omega \quad (4.39)$$

The gains of the CTC are determined by solving a multi-objective optimization problem. The method is that the simulation model is converted into executable model to faster the optimization process. By using the MATLAB Optimization Toolbox, and using ITAE as a cost function, the multi-objective problem is solved. The cost function is as follows:

$$ITAE = \int_0^t t |e(t)| dt$$

Here, “e” is the error between the reference and achieved trajectories. Optimization problem is solved to minimize the error. Nonlinear least-squares solver of the MATLAB is used for optimization purposes.

The obtained gain values calculated as:

$$\begin{aligned} K_p &= \begin{bmatrix} \hat{K}_{pp} & \hat{K}_{pr} & \hat{K}_{p\Omega} \end{bmatrix} \\ K_d &= \begin{bmatrix} \hat{K}_{dp} & \hat{K}_{dr} & \hat{K}_{d\Omega} \end{bmatrix} \\ K_i &= \begin{bmatrix} \hat{K}_{ip} & \hat{K}_{ir} & \hat{K}_{i\Omega} \end{bmatrix} \end{aligned} \quad (4.40)$$

$$\begin{aligned}
K_p &= \text{diag}([7.20 \ 10.23 \ 28.83] \ [100.25 \ 40.95 \ 14.33] \ [171.69 \ 1197.65]) \\
K_i &= \text{diag}([2.63 \ 0.69 \ 5.76] \ [37.73 \ 6.86 \ 2.76] \ [57.18 \ 254.40]) \\
K_d &= \text{diag}([3.33 \ 4.17 \ 16.19] \ [19.73 \ 10.55 \ 17.01] \ [23.22 \ 34.35])
\end{aligned} \tag{4.41}$$

Where, $\text{diag}[\dots]$ is the diagonal elements of the corresponding matrices.

4.3. Feedback Linearizing Control with Extended State Observer

While designing the feedback linearizing controller, it is assumed that perfect knowledge of the dynamic system is available, and the effects of the uncertainties are not considered. However, this is not the case in reality since there are unmodeled dynamics and disturbances acting on the UAV. To eliminate these effects, an extended state observer is added to the FLC (Feedback Linearizing Controller) to make the controller more robust.

A state observer is used to estimate the unmeasured state variables by using the measured state variables and control input signals [46]. The system uncertainties such as unmodeled dynamics, mass variations, and externally applied forces can be added as a state to an observer, then an extended state observer is obtained [47].

The inertia, Coriolis and gravity matrices can be rewritten by considering the uncertain parts of them as [45],

$$\begin{aligned}
\hat{M}(\bar{q}) &= \hat{M}'(\bar{q}) - \Delta\hat{M}(\bar{q}) \\
\hat{C}(\bar{q}, \dot{\bar{q}}) &= \hat{C}'(\bar{q}, \dot{\bar{q}}) - \Delta\hat{C}(\bar{q}, \dot{\bar{q}}) \\
\hat{G}(\bar{q}) &= \hat{G}'(\bar{q}) - \Delta\hat{G}(\bar{q})
\end{aligned} \tag{4.42}$$

Then, the Eq. (4.21) can be further written as,

$$\bar{u} = \hat{M}'(\bar{q})\bar{v} + \hat{C}'(\bar{q}, \dot{\bar{q}})\dot{\bar{q}} + \bar{G}'(\bar{q}) \tag{4.43}$$

Later, the Eq. (4.43) is plugged into Eq. (3.80), the following error dynamics is obtained.

$$\ddot{\bar{e}} + \hat{K}_p \bar{e} + \hat{K}_d \dot{\bar{e}} + K_i \int_0^t \bar{e}(\tau) d\tau = \bar{f} \quad (4.44)$$

Where,

$$\bar{f} = \hat{M}'^{-1}(\bar{q}) \left[\Delta \hat{M}(\bar{q}) \ddot{\bar{q}} + \Delta \hat{C}(\bar{q}, \dot{\bar{q}}) \dot{\bar{q}} + \Delta \hat{G}(\bar{q}) + \bar{u}_{ext} \right] \quad (4.45)$$

The conventional FLC might cause an unstable system performance for nonzero uncertainties, f . Therefore, a control law is proposed including the estimate of f .

The estimation is made by using an ESO.

$$\bar{u} = \hat{M}'(\bar{q})(\ddot{\bar{q}}_d + \hat{K}_p \bar{e} + \hat{K}_d \dot{\bar{e}} + \hat{K}_i \int_0^t \bar{e}(\tau) d\tau) + \hat{C}'(\bar{q}, \dot{\bar{q}}) \dot{\bar{q}} + \bar{G}'(\bar{q}) - \hat{M}'(\bar{q}) \tilde{f} \quad (4.46)$$

For further use, f is partitioned as:

$$\bar{f} = \begin{bmatrix} \bar{f}_p \\ \bar{f}_r \\ \bar{f}_\Omega \end{bmatrix} \quad \text{where } \bar{f}_p \in R^{3x1}, \bar{f}_r \in R^{3x1}, \bar{f}_\Omega \in R^{2x1} \quad (4.47)$$

4.3.1. Position Control of the Quadrotor

From Eq. (4.46), the following control law is written by including the estimate of the f .

$$\begin{aligned} \bar{u}_p &= \hat{M}_{pp} \bar{v}_p + \hat{M}_{pr}^* \bar{v}_r + \hat{M}_{p\Omega} \bar{v}_\Omega + \hat{C}_{pp} \dot{\bar{q}}_p + \hat{C}_{pr} \dot{\bar{q}}_r + \hat{C}_{p\Omega} \dot{\bar{q}}_\Omega + \bar{G}_p \\ &\quad - \hat{M}_{pp} \bar{f}_p - \hat{M}_{pr} \bar{f}_r - \hat{M}_{p\Omega} \bar{f}_\Omega \end{aligned} \quad (4.48)$$

Then, the quadrotor input f_z is calculated like in the Eq. (4.32).

4.3.2. Attitude Control of the Quadrotor

From Eq. (4.46), the following control law is written by including the estimate of the f .

$$\begin{aligned}\bar{u}_r = & \hat{M}_{pr}^T \bar{v}_p + \hat{M}_{rr} \bar{v}_r + \hat{M}_{r\Omega} \bar{v}_\Omega + \hat{C}_{pr}^T \dot{\bar{q}}_p + \hat{C}_{rr} \dot{\bar{q}}_r + \hat{C}_{r\Omega} \dot{\bar{q}}_\Omega + \bar{G}_r \\ & - \hat{M}_{pr}^T \bar{f}_p - \hat{M}_{rr} \bar{f}_r - \hat{M}_{r\Omega} \bar{f}_\Omega\end{aligned}\quad (4.49)$$

From Eq. (4.36), quadrotor torque inputs can be calculated.

4.3.3. Joints Angle Control of the Manipulator

From Eq. (4.46), the following control law is written by including the estimate of the f .

$$\begin{aligned}\bar{u}_\Omega = & \hat{M}_{p\Omega}^T \bar{v}_p + \hat{M}_{r\Omega}^T \bar{v}_r + \hat{M}_{\Omega\Omega} \bar{v}_\Omega + \hat{C}_{p\Omega}^T \dot{\bar{q}}_p + \hat{C}_{r\Omega}^T \dot{\bar{q}}_r + \hat{C}_{\Omega\Omega}^T \dot{\bar{q}}_\Omega + \bar{G}_\Omega \\ & - \hat{M}_{p\Omega}^T \bar{f}_p - \hat{M}_{r\Omega}^T \bar{f}_r - \hat{M}_{\Omega\Omega}^T \bar{f}_\Omega\end{aligned}\quad (4.50)$$

Then, by using Eq. (4.39), the joint torques are obtained.

Therefore, to apply proposed control laws, the estimation of the uncertainty, f is very crucial. In the next sections, the concept of ESO and the designing an ESO for our system to estimate f are given.

In Figure 4.66, the general architecture of the controller with ESO in Eq. (4.46) that we used in this thesis is given.

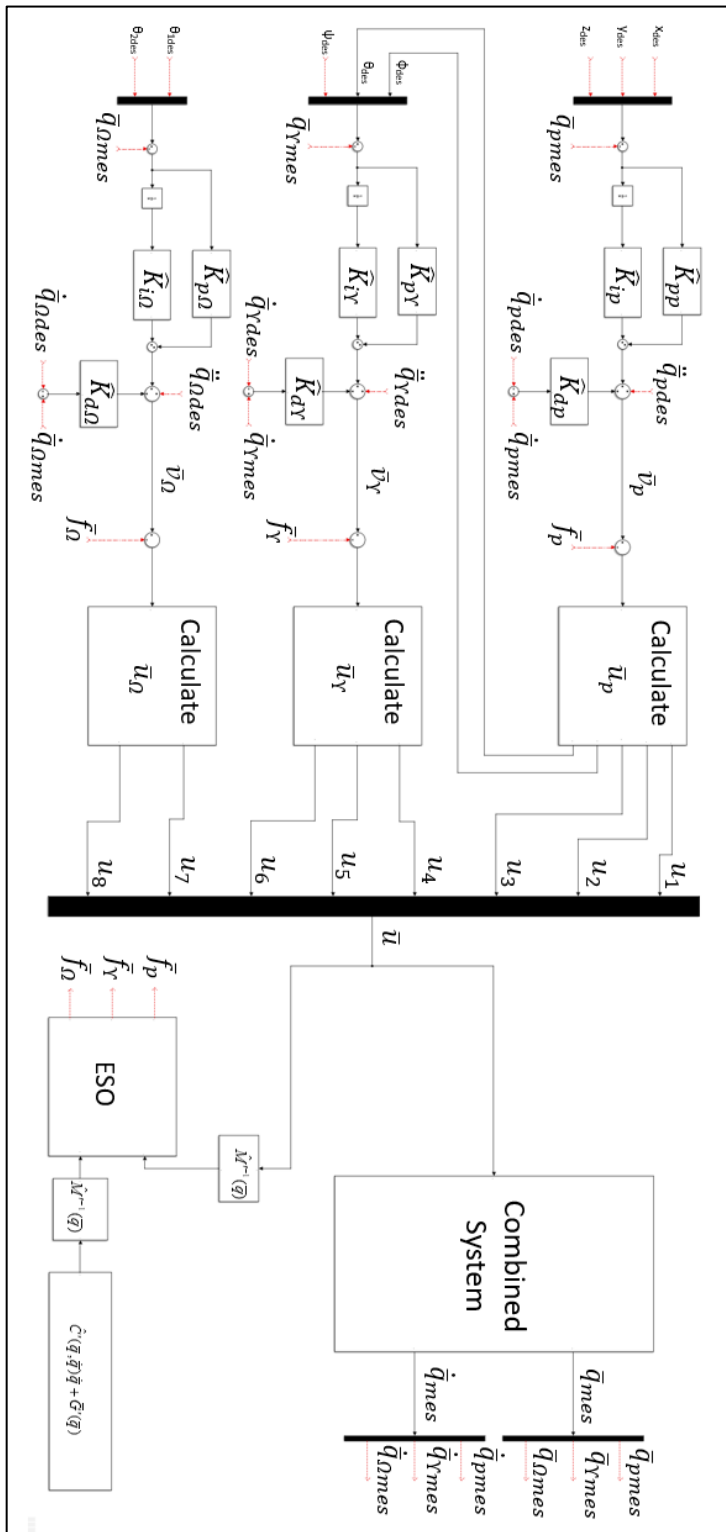


Figure 4.6. FLC – ESO Architecture

4.3.4. Concept of Extended State Observer

To describe the concept of ESO, consider the following integral chain system with uncertainty [48].

$$\begin{cases} \dot{x}_1 = x_2 \\ \dot{x}_2 = x_3 \\ \vdots \\ \dot{x}_n = f(x_1, \dots, x_n, w(t), t) + bu \\ y = x_1 \end{cases} \quad (4.51)$$

Where, x_1, x_2, \dots, x_n are the states of the system. u is the input control signal, b is the system parameter, and y is the measured output. $w(t)$ is the disturbance acting on the system such as external interaction forces and unmodeled dynamics. $f(x_1, \dots, x_n, w(t), t)$ represents the dynamics of uncertainty.

In the scope of ESO, Eq. (4.51) can be further written as,

$$\begin{cases} \dot{x}_1 = x_2 \\ \dot{x}_2 = x_3 \\ \vdots \\ \dot{x}_n = x_{n+1} + bu \\ \dot{x}_{n+1} = h(t) \\ y = x_1 \end{cases} \quad (4.52)$$

Where, $h(t) = \dot{f}(x_1, \dots, x_n, w(t), t)$ which is the rate of change of the uncertainty. x_{n+1} is the extended state to represent the uncertainty. Then, to estimate the states of the system, the following linear ESO can be provided [48].

$$\begin{cases} \dot{z}_1 = z_2 + \beta_1(y - z_1) \\ \dot{z}_2 = z_3 + \beta_2(y - z_1) \\ \vdots \\ \dot{z}_n = z_{n+1} + \beta_n(y - z_1) + bu \\ \dot{z}_{n+1} = \beta_{n+1}(y - z_1) \end{cases} \quad (4.53)$$

In Eq. (4.53), $z_1, z_2, \dots, z_n, z_{n+1}$ are the estimates of the states. $\beta_1, \beta_2, \dots, \beta_n, \beta_{n+1}$ are the gains of the linear ESO.

4.3.5. Problem Formulation

Let $x_1 = q$ and $x_2 = \dot{q}$, and from Eq's. (3.80) and (4.42), the following relation can be written.

$$\ddot{\bar{q}} = \hat{M}'^{-1}(\bar{q}) \left[\bar{u} - \hat{C}'(\bar{q}, \dot{\bar{q}}) \dot{\bar{q}} - \bar{G}'(\bar{q}) \right] + \bar{f} \quad (4.54)$$

Then, Eq. (4.54) can be further written as a subsystem for each joint(generalized coordinates) space parameters $i = 1, 2, \dots, 8$.

$$\begin{cases} \dot{x}_{1i} = x_{2i} \\ \dot{x}_{2i} = U_i + f_i \\ y_i = x_{1i} \end{cases} \quad (4.55)$$

Where, $U_i = \left[\hat{M}'^{-1}(\bar{q}) \left[\bar{u} - \hat{C}'(\bar{q}, \dot{\bar{q}}) \dot{\bar{q}} - \bar{G}'(\bar{q}) \right] \right]_i$. Then, for the continuous and differentiable f_i , an extended state $x_{3i} = f_i$ is added. Afterwards, Eq. (4.55) is expressed as,

$$\begin{cases} \dot{x}_{1i} = x_{2i} \\ \dot{x}_{2i} = U_i + x_{3i} \\ \dot{x}_{3i} = h_i(t) \\ y_i = x_{1i} \end{cases} \quad (4.56)$$

Here, $h_i(t) = \dot{f}_i$ is assumed to be an unknown and bounded function [49]. It is the rate of change of the uncertainty for each generalized coordinates.

Eq. (4.56) can be rewritten in state space form for each generalized coordinates as,

$$\begin{aligned}
\dot{\bar{x}}_i &= \begin{bmatrix} 0 & 1 & 0 \\ 0 & 0 & 1 \\ 0 & 0 & 0 \end{bmatrix} \begin{bmatrix} x_{1i} \\ x_{2i} \\ x_{3i} \end{bmatrix} + \begin{bmatrix} 0 \\ 1 \\ 0 \end{bmatrix} U_i + \begin{bmatrix} 0 \\ 0 \\ h_i(t) \end{bmatrix} \\
y_i &= [1 \ 0 \ 0] \bar{x}_i \\
&\text{OR} \\
\dot{\bar{x}}_i &= \hat{A}_i \bar{x}_i + \bar{B}_i U_i + \bar{E} h_i(t) \\
y_i &= \hat{C}_i \bar{x}_i
\end{aligned} \tag{4.57}$$

Based on Eq. (4.57), the following ESO is designed for disturbance rejection.

$$\begin{aligned}
\dot{\bar{z}}_i &= \begin{bmatrix} 0 & 1 & 0 \\ 0 & 0 & 1 \\ 0 & 0 & 0 \end{bmatrix} \begin{bmatrix} z_{1i} \\ z_{2i} \\ z_{3i} \end{bmatrix} + \begin{bmatrix} 0 \\ 1 \\ 0 \end{bmatrix} U_i + \bar{L}_i (y_i - \tilde{y}_i) \\
\tilde{y}_i &= [1 \ 0 \ 0] \bar{z}_i \\
&\text{OR} \\
\dot{\bar{z}}_i &= \hat{A}_i \bar{z}_i + \bar{B}_i U_i + \bar{L}_i (y_i - \tilde{y}_i) \\
\tilde{y}_i &= \hat{C}_i \bar{z}_i
\end{aligned} \tag{4.58}$$

In Eq. (4.58), z_{1i} , z_{2i} , z_{3i} , and \tilde{y}_i are the estimated values of x_{1i} , x_{2i} , x_{3i} , and y_i , respectively. L is the gains of the linear ESO, and it is in the following form.

$$\bar{L} = [\beta_{1i} \ \beta_{2i} \ \beta_{3i}]^T \tag{4.59}$$

These coefficients can be determined by using a proper method like pole placement. For stability analysis, by using Eq's. (4.57) and (4.58), the following error equation can be written.

$$\dot{\bar{e}}_i = \hat{A}_{ei} \bar{e}_i + \bar{E}_i h_i(t) \tag{4.60}$$

Where,

$$\bar{e}_i = \bar{x}_i - \bar{z}_i \quad \text{and} \quad \hat{A}_{ei} = \begin{bmatrix} -\beta_{1i} & 1 & 0 \\ -\beta_{2i} & 0 & 1 \\ -\beta_{3i} & 0 & 0 \end{bmatrix} \tag{4.61}$$

The proposed linear ESO is stable if \hat{A}_{ei} is Hurwitz and $h_i(t)$ is bounded [50]. The characteristic polynomial of \hat{A}_{ei} is written as,

$$\lambda_i(s) = s^3 + \beta_{1i}s^2 + \beta_{2i}s + \beta_{3i} = (s + w_0)^3 \quad (4.62)$$

Let w_0 is the bandwidth of the observer, then the coefficients of the Eq. (4.62) can be selected as [50],

$$\beta_{1i} = 3w_0, \beta_{2i} = 3w_0^2, \text{ and } \beta_{3i} = w_0^3 \quad (4.63)$$

The gains of the FLC is the same as in (4.41). The gains of the ESO is obtained again by solving a multi-objective optimization problem by benefiting from the MATLAB Optimization Toolbox. The gains are shown in Table 4.2.

Table 4.2. *The Gains of the Extended State Observer for the Generalized Coordinates*

	x	y	z	ϕ	θ	ψ	θ_1	θ_2
β_1	4.28	4.28	15.84	17.11	8.11	28.75	24.62	49.51
β_2	6.10	6.10	83.61	97.53	21.90	275.52	202.03	816.97
β_3	2.90	2.90	147.14	185.36	19.72	880.12	552.63	4493.91

Remark 1: A large observer gain w_0 indicates a small estimation error. Furthermore, a large gain increases the speed at which the ESO tracks the total disturbance. However, a high gain leads to an increased noise sensitivity [45].

CHAPTER 5

SIMULATION RESULTS AND DISCUSSION

5.1. Simulation Environment Information

The nonlinear coupled system dynamics and kinematics models are coded in MATLAB/Simulink environment. Also, the proposed control algorithms are implemented in the same environment and tested with these nonlinear unified system model. The ODE2 (Heun) Solver of Simulink with the fixed time step of 0.001 seconds is used to simulate the scenarios.

Moreover, to avoid unrealistic controller commands, saturation blocks are added to the controller outputs. These are the internal control inputs roll and pitch angles, $+/-17$ degree, rotational speeds of the rotors, 2000 rad/sec, and the torque inputs of the servo motors of the robotic arm, $+/-3$ Nm.

Numerical parameters of the unified system are given in Table 5.1. The most of these parameters are taken from thesis written by Yıldız [37].

Table 5.1. *Numerical Parameters of the Combined System*

m_b [kg]	2.6550	d [m]	0.3435
$m_{1,2}$ [kg]	0.1700	b_0 [m]	0.0800
$I_{xx,b}$ [kgm ²]	0.0457	$b_{1,2}$ [m]	0.3000
$I_{yy,b}$ [kgm ²]	0.0457	$c_{1,2}$ [m]	0.0500
$I_{zz,b}$ [kgm ²]	0.0846	$d_{1,2}$ [m]	0.0500
$I_{xx,12}$ [kgm ²]	7.0830e-05	gravity [m/s ²]	9.8100
$I_{yy,12}$ [kgm ²]	0.0013	c_T [N/(rad/s) ²]	2.7400e-05
$I_{zz,12}$ [kgm ²]	0.0013	c_Q [Nm/(rad/s) ²]	0.0470e-05

5.2. Simulation Scenario

For all controller structures, the same scenario is used. However, the performance comparison is made between FLC architecture and FLC-ESO architecture since the cascaded PID controller structure is simulated with ideal motor and sensor models. The FLC and FLC-ESO controller architectures are simulated with nonideal motor models and ideal sensor models. The scenario is presented in Table 5.2 and Figure 5.1.

Reference Trajectories of the Combined System

Table 5.2. *The Simulation Scenario*

Time [s]	0-9	10-19	25-30	30-60
x [m]	0-5	5	5	5
y [m]	0-3	3	3	3
z [m]	0-(-2)	-2	-2	-2
ϕ [deg]	-	-	-	-
θ [deg]	-	-	-	-
ψ [deg]	0-(-5)	-5	-5	-5
θ_1 [deg]	0	0-15	15	15
θ_2 [deg]	0	0-10	10	10
F_1 [N]	0	0	0-5	5
F_2 [N]	0	0	0-2	2
F_3 [N]	0	0	0-6	6

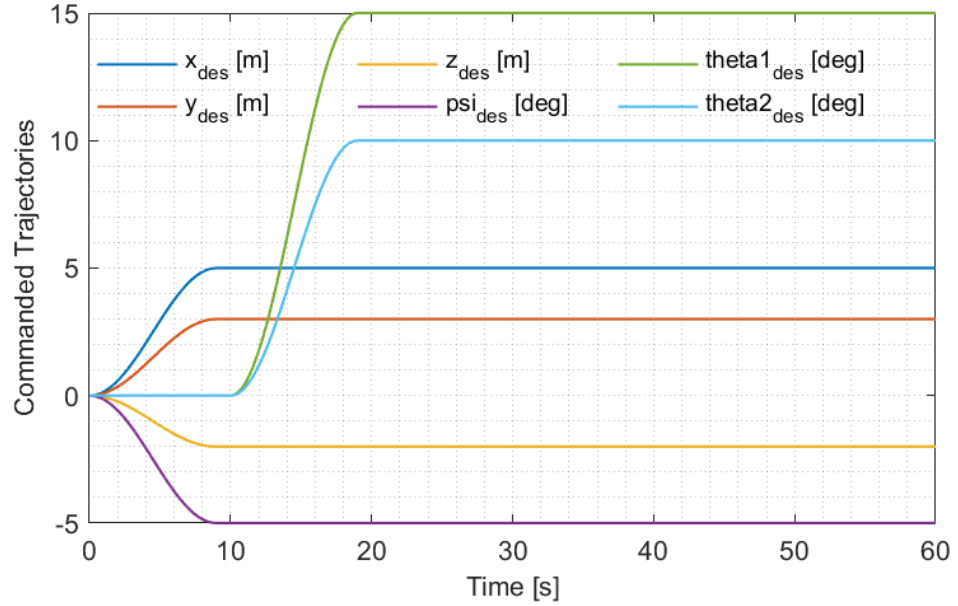


Figure 5.1. Reference Trajectories of the Combined System

In Figure 5.1, the reference trajectories of the combined system are shown. In this figure, the reference roll and pitch angles do not exist since they are internal control inputs that are generated for the reference cartesian coordinates of x and y . However, they are provided in upcoming sections. Here, coupled commands are given to the combined system for performance analysis of the controllers. Performance results are also presented in the proceeding sections.

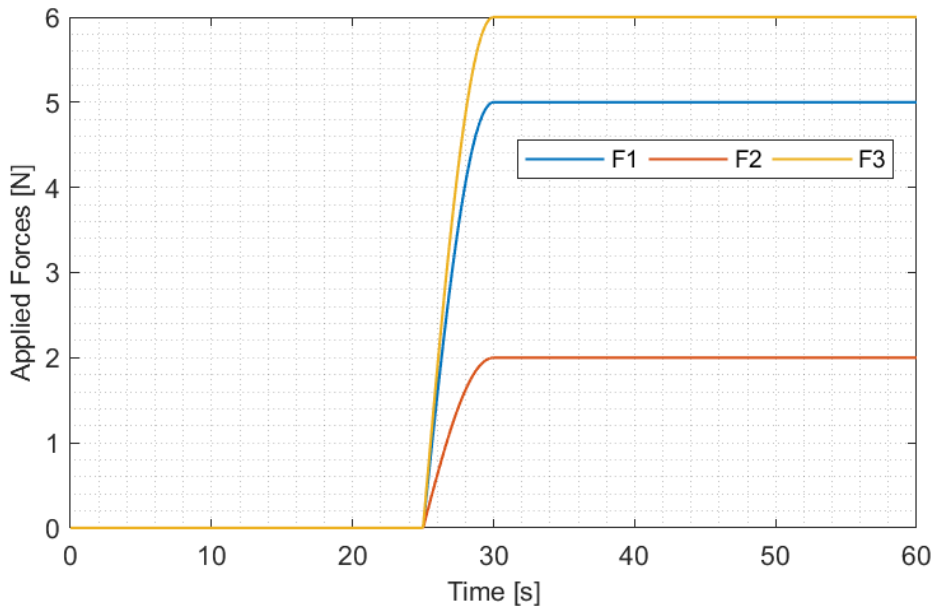


Figure 5.2. Externally Applied Forces on the End-Effector

In Figure 5.2, the applied forces on the tip point of the end-effector of the combined system are illustrated. These applied forces are acting on the system in three directions of the cartesian coordinate system simultaneously.

5.3. Simulation Results

5.3.1. Cascaded PID Controller

This controller architecture, unlike the other two controllers, has been tested with ideal motor models. Results are presented as follows.

5.3.1.1. Position Control of the Quadrotor

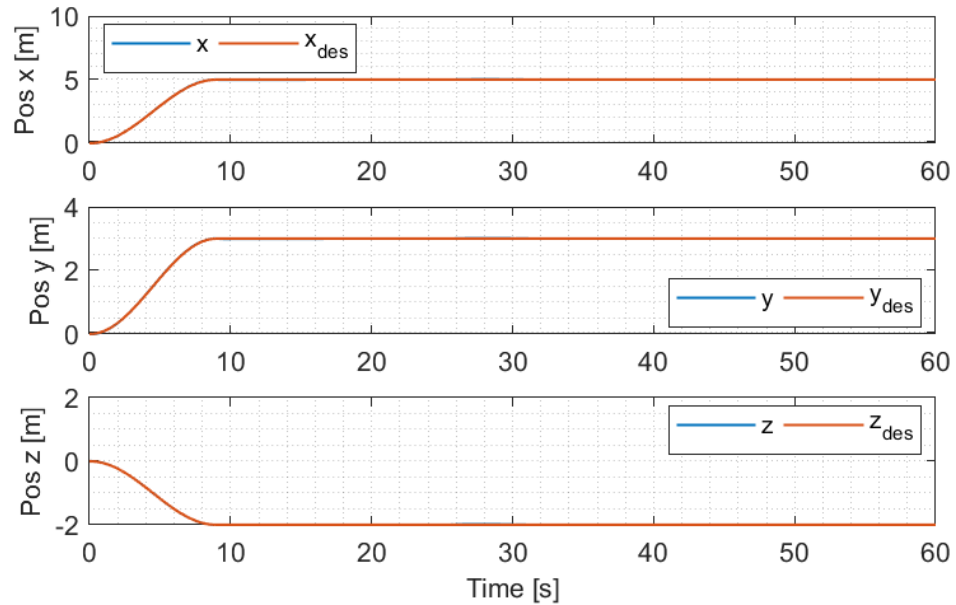


Figure 5.3. Desired and Achieved Inertial Position of the Quadrotor

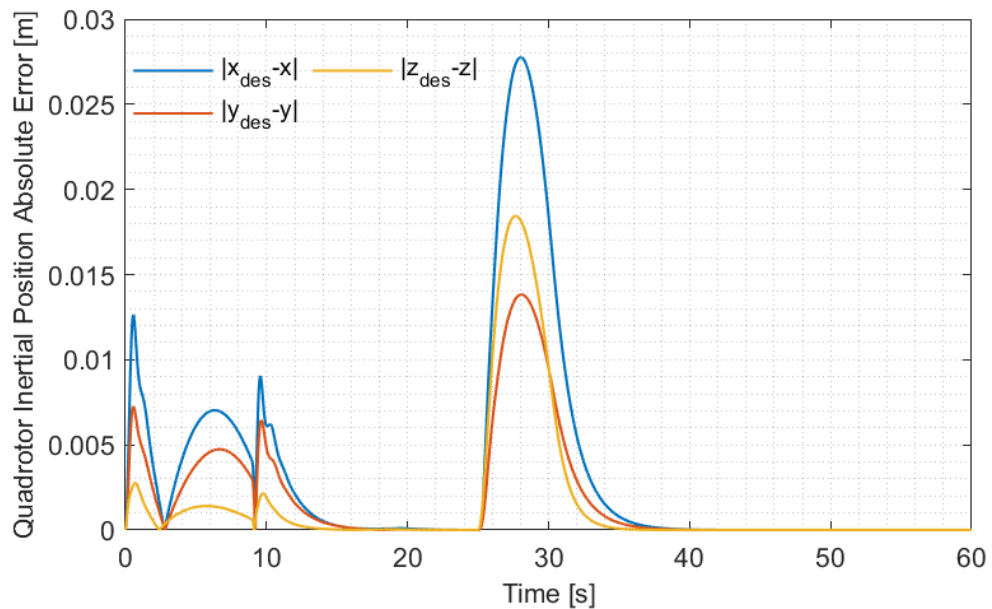


Figure 5.4. The Absolute Error Between the Commanded and the Achieved Quadrotor Position

From Figure 5.3 and Figure 5.4, the commanded position tracking performance of the controllers can be seen. The controllers are tracking the reference trajectories with a very small error at first, and around zero errors throughout the simulation scenario. The initial deviations are due to the transient behavior of the controllers. However, the initial deviation in the x-direction is bigger than other channels (y and z) since the channel x is highly coupled with the manipulator joint arm angles. In other words, the Euler pitch and joint angles are in the same plane, and channel x is directly related to the Euler pitch angle. Therefore, at first, there are some oscillations in joint angles, and this affects the position x of the quadrotor. At time 10 seconds, since the robotic arms are moved, some deviations occur. However, these deviations are suppressed by the controllers. At time 25 seconds, the external forces are started to be applied to the end-effector. This disturbs the quadrotor of its hover position. In a short amount of time, these disturbance forces are balanced by the controllers, and the quadrotor comes to its original position.

5.3.1.2. Orientation Control of the Quadrotor

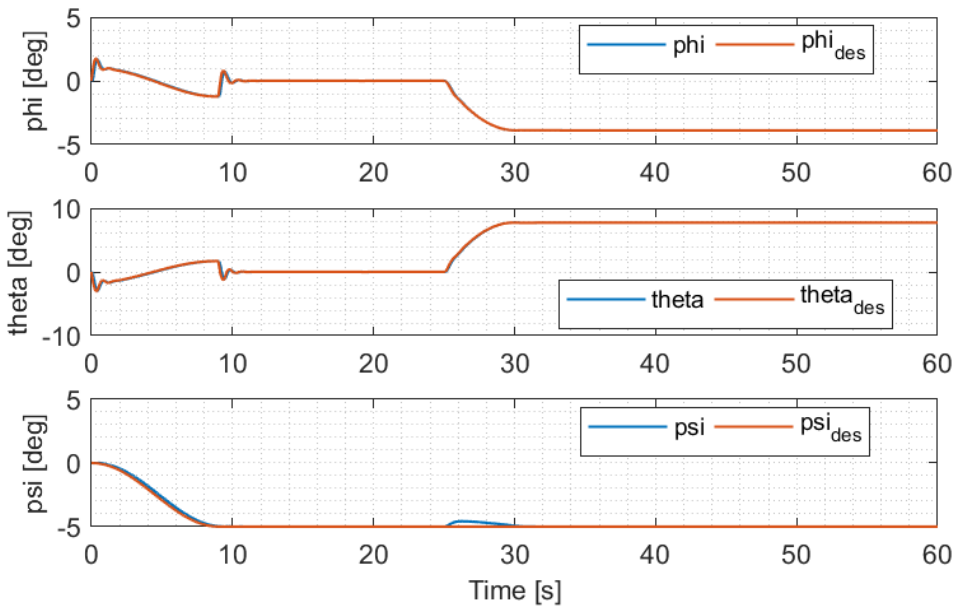


Figure 5.5. The Reference and Achieved Orientation of the Quadrotor

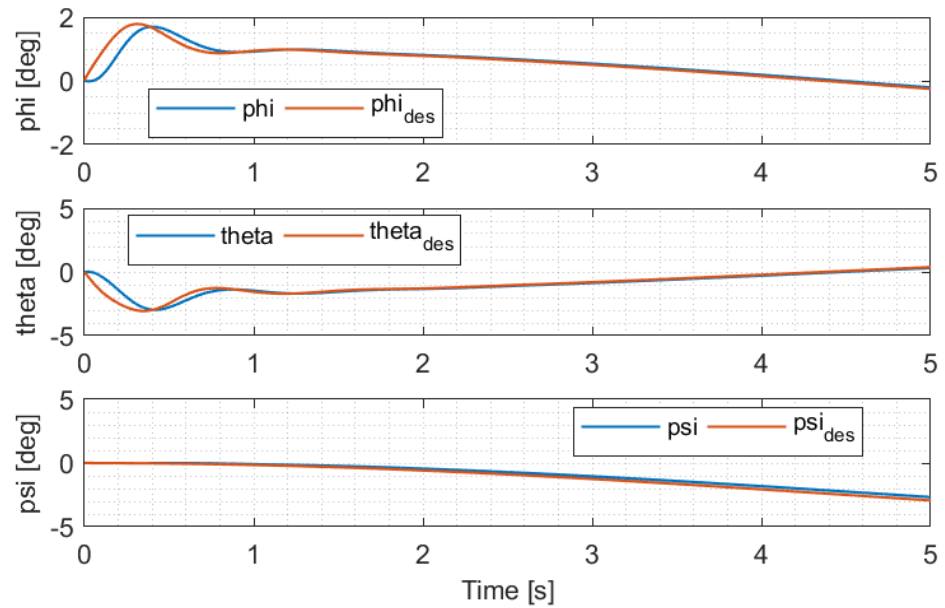


Figure 5.6. The Reference and Achieved Orientation of the Quadrotor Between 0 to 5 Seconds

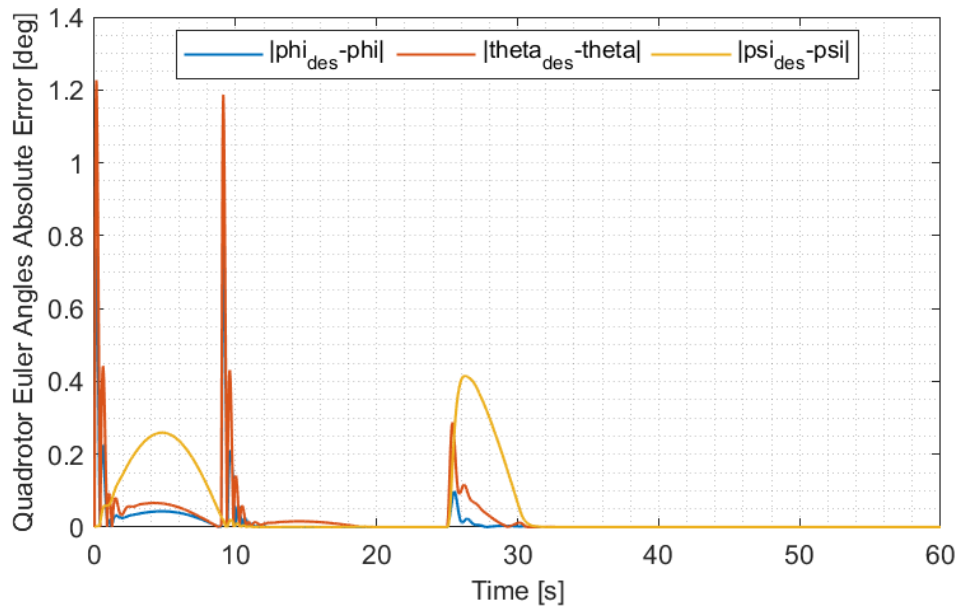


Figure 5.7. The Absolute Error Between the Commanded and the Achieved Quadrotor Orientation

Figure 5.5 and its zoomed version Figure 5.6 illustrate the desired and achieved orientation of the quadrotor. Here, phi and theta are the intermediate control signals

that are generated for reference y and z positions, respectively. To avoid instability due to unrealistic control signals, their maximum values are limited to certain bounds. Also, the controllers command high ϕ and θ angles initially, and system response is slower with respect to this, so the initial errors are high. At 25 seconds, the disturbance forces are applied to the end-effector, and to balance these forces, quadrotor tilts in both roll and pitch planes. As a result, ϕ and θ angles are different from the zero values in the hover position. Further, at 25 seconds, the yaw angle is affected by these disturbances, but the yaw controller brings it to its original position. In general, the attitude controllers track the desired orientations with very small errors throughout the scenario.

5.3.1.3. Joint Angles Control of the Robotic Arm

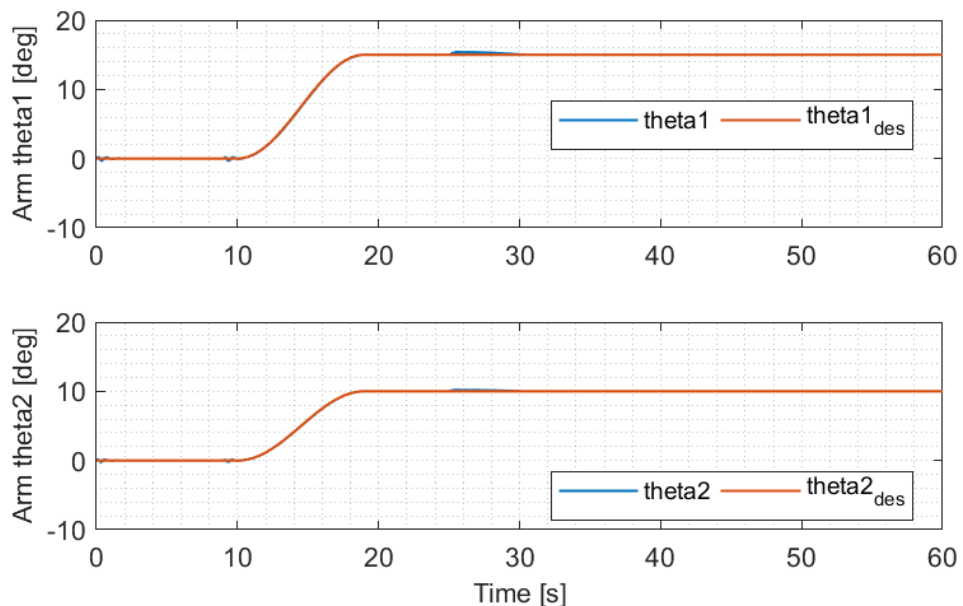


Figure 5.8. The Reference and Achieved Joint Angles of the Robotic Arm

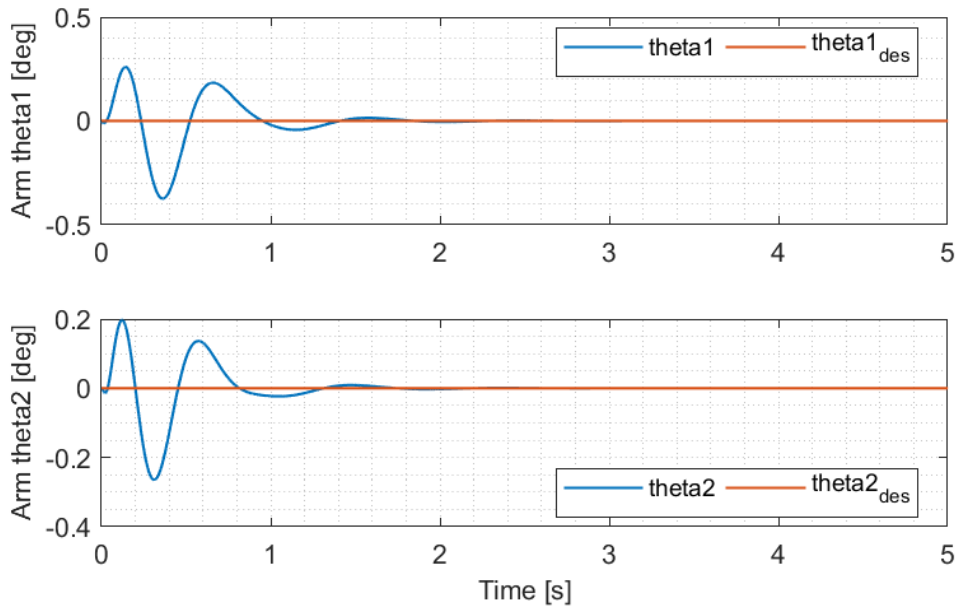


Figure 5.9. The Reference and Achieved Joint Angles of the Robotic Arm Between 0 to 5 Seconds

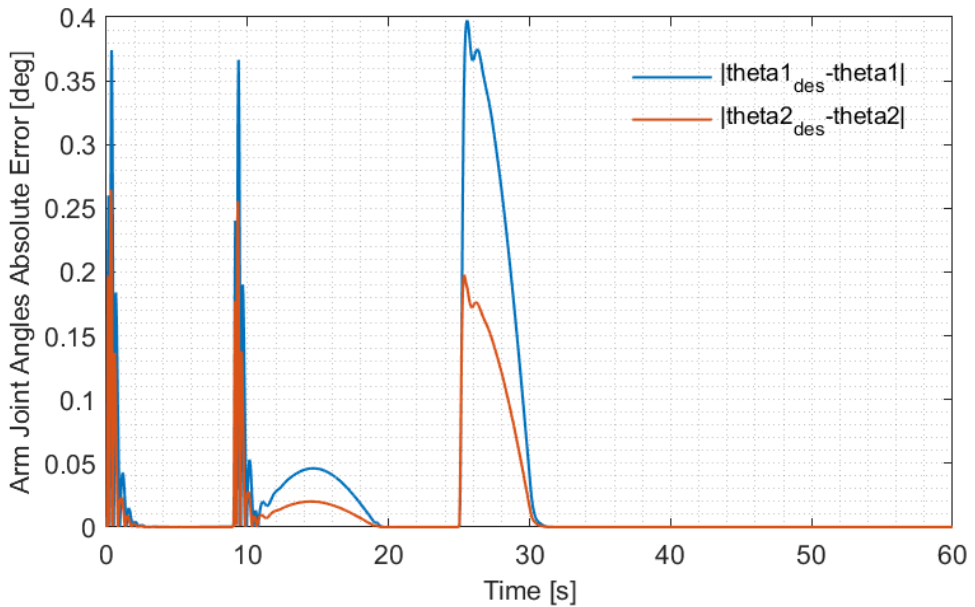


Figure 5.10. The Absolute Error Between the Commanded and the Achieved Joint Angles

Figure 5.8 and its zoomed version Figure 5.9 shows the commanded and obtained manipulator's joint angles, and Figure 5.10 illustrates the error between them. At first,

there are some small oscillations due to the transient characteristics, and quadrotor's movement. In other words, they are affected by the fast pitch dynamics of the quadrotor. The other reason is that joint angles are controlled by the independent joint controllers, so they are influenced by the quadrotor's motion. However, the joint controllers suppress these oscillations in a short amount of time. At time 10 seconds, the joint angles are commanded to come at certain angles, and this is achieved by controllers successfully. At 25 seconds, the effects of the disturbance forces deviate the joint angles from the reference values, but the joint controllers cope with these interruption forces well. These controllers show satisfactory performance.

5.3.2. Feedback Linearizing Controller and Feedback Linearizing Control with Extended State Observer

In this subsection, the performance results of the two controller structures that are FLC and ESO- FLC are presented. Their performances are also compared to each other in terms of some measurement's techniques in the next section. ESO based FLC is the modified version of the FLC. Both controller architectures have the same FLC gains. In order to increase the robustness of the FLC, an ESO is added. With this ESO, the combined system has been gained active disturbance rejection characteristics. Moreover, both controllers are implemented and tested in a simulation environment that has a nonideal dc motor model and a servo motor model to simulate a more realistic scenario.

5.3.2.1. Position Control of the Quadrotor

From Figure 5.11, Figure 5.12, Figure 5.13, and Figure 5.14, the following observations can be made. Both position controllers show stable system performances, and they track the desired trajectories. At first, these two controllers demonstrate similar tracking performances. Also, at 10 seconds, the quadrotor moves away from the desired path due to the movement of the serial manipulator. Then, this is compensated by the controller for both architectures with similar performances.

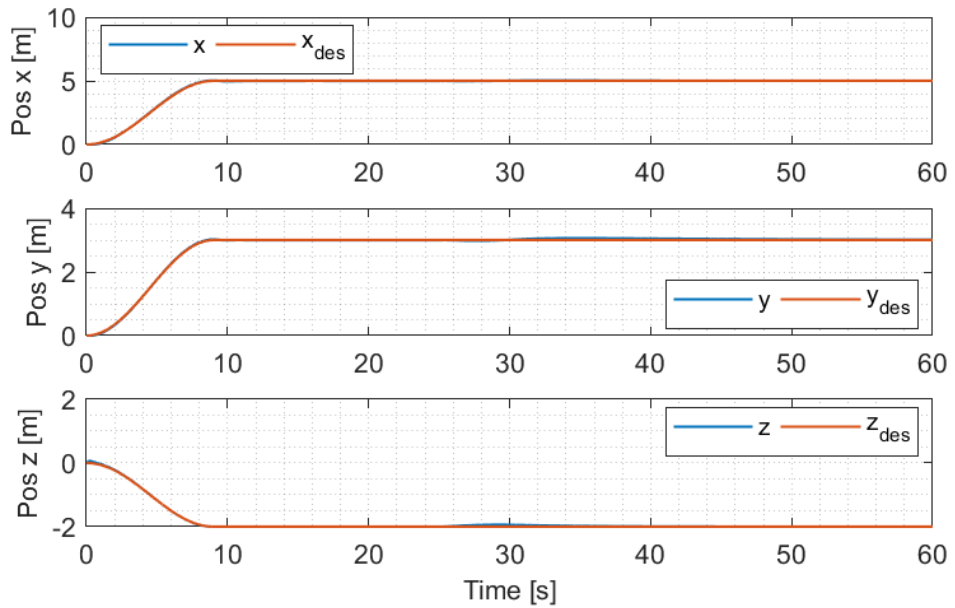


Figure 5.11. Desired and Achieved Inertial Position of the Quadrotor [FLC]

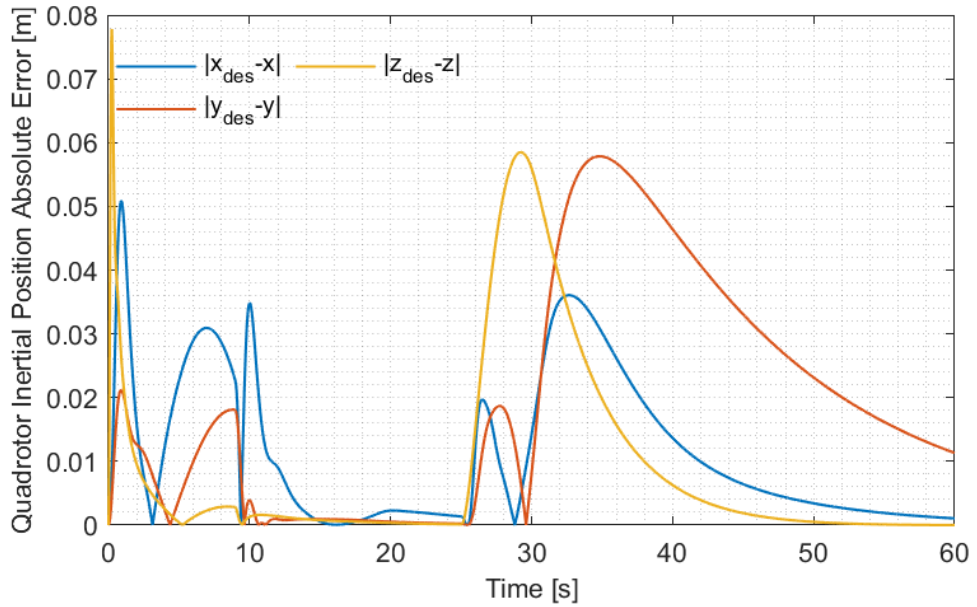


Figure 5.12. The Absolute Error Between the Commanded and the Achieved Quadrotor Position [FLC]

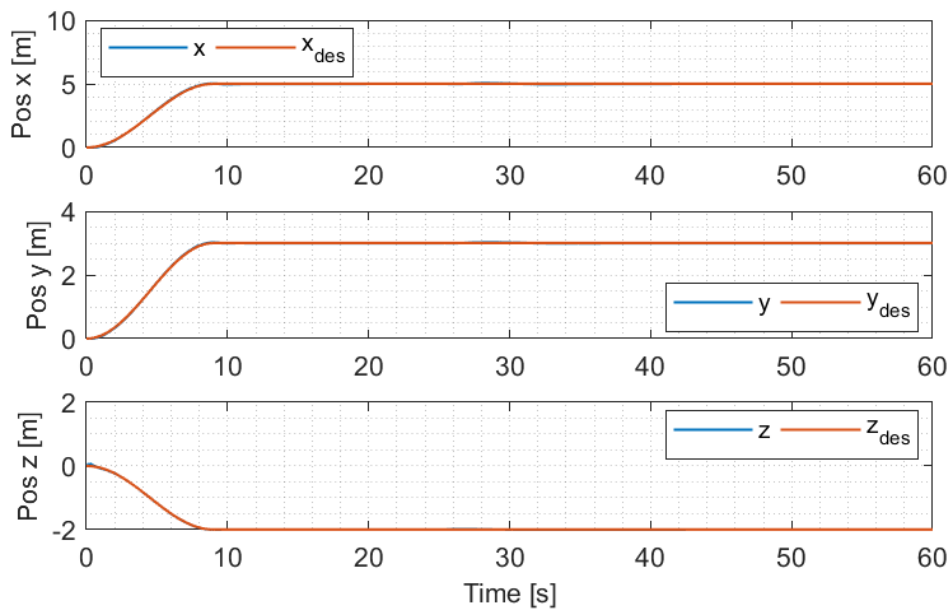


Figure 5.13. Desired and Achieved Inertial Position of the Quadrotor [FLC-ESO]

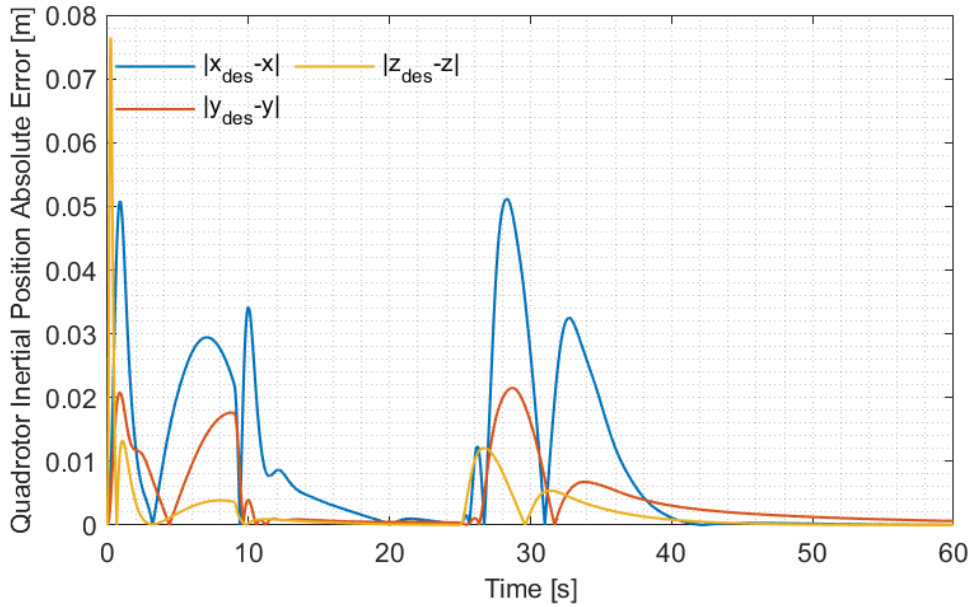


Figure 5.14. The Absolute Error Between the Commanded and the Achieved Quadrrotor Position [FLC-ESO]

However, the performance differences come out when the disturbance forces are applied to the unified system at 25 seconds. As it can be seen from Figure 5.12, and Figure 5.14, the system with the FLC controller more sensitive to the disturbances with respect to the system with ESO-FLC. Due to its active disturbance rejection property, the ESO-FLC suits faster to these interruption forces and enables quadrotor to settle down to the reference trajectory faster.

5.3.2.2. Orientation Control of the Quadrotor

The orientation control has a direct effect on the position control of the quadrotor since it is an underactuated vehicle, and roll and pitch angles are coupled with the cartesian positions y and x , respectively. From the position control section, it is known that ESO-FLC shows better position error minimization characteristics. Therefore, it should be the result of better orientation control of the controllers, and it can be observed from Figure 5.17 and Figure 5.20.

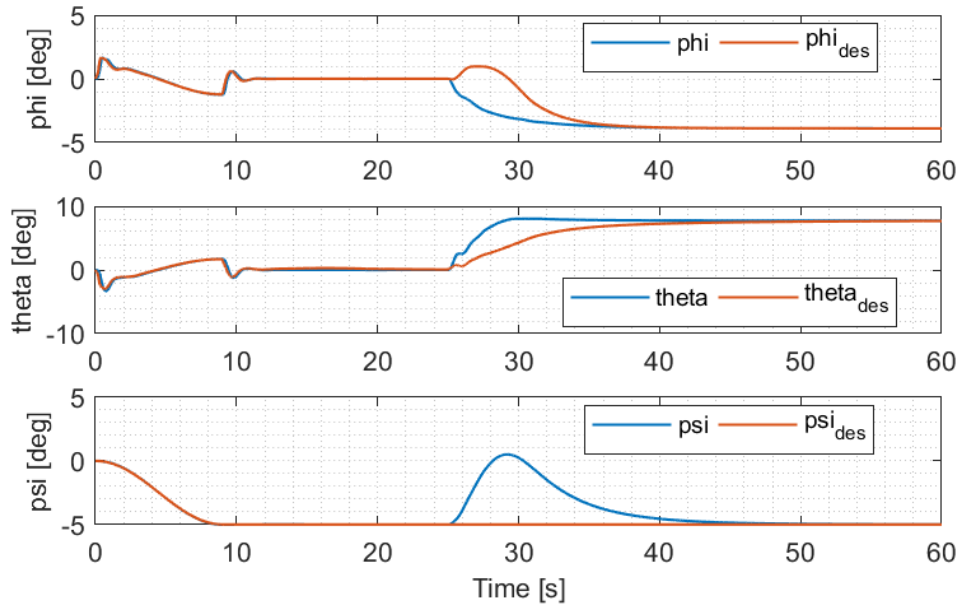


Figure 5.15. The Reference and Achieved Orientation of the Quadrotor [FLC]

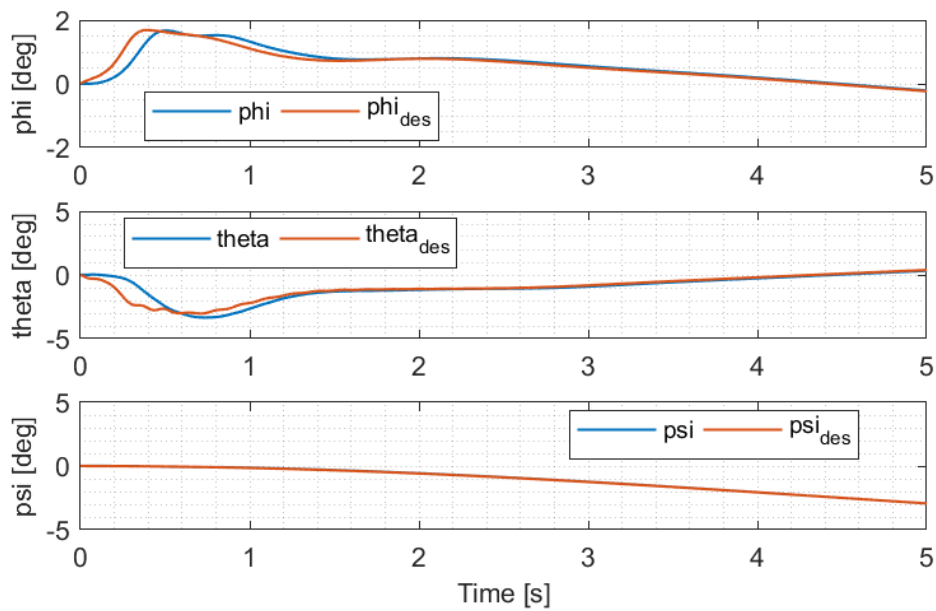


Figure 5.16. The Reference and Achieved Orientation of the Quadrotor Between 0 to 5 Seconds
[FLC]

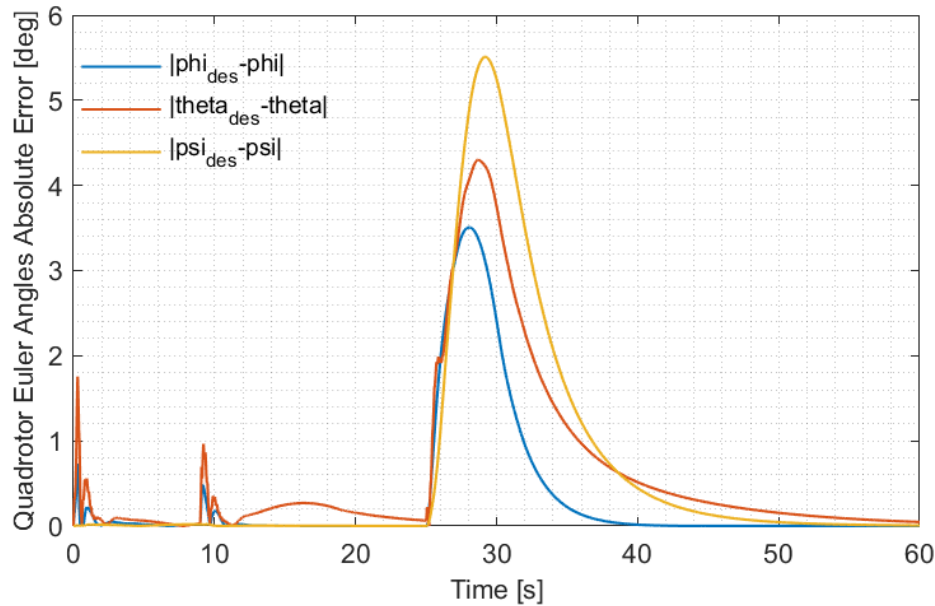


Figure 5.17. The Absolute Error Between the Commanded and the Achieved Quadrotor Orientation
[FLC]

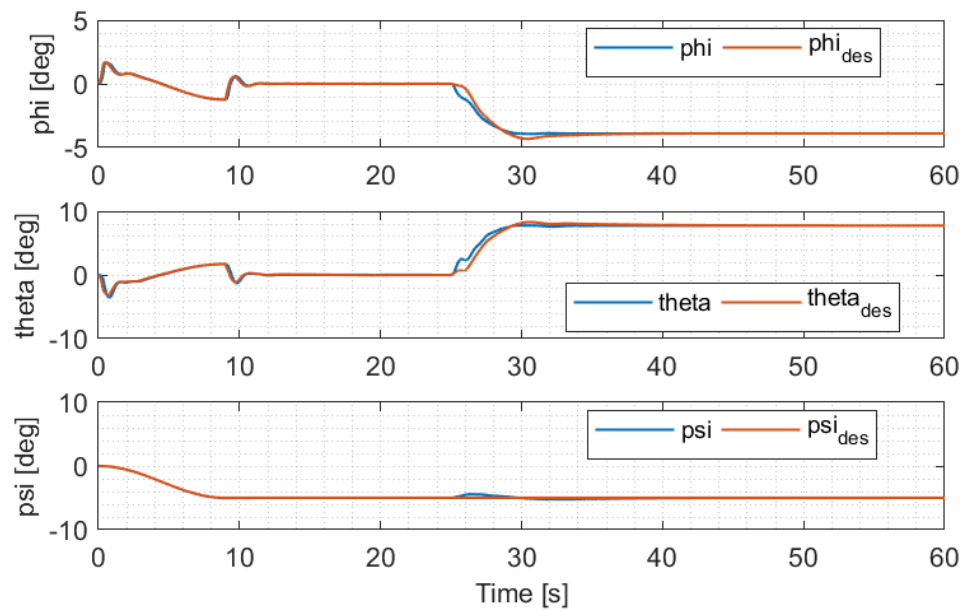


Figure 5.18. The Reference and Achieved Orientation of the Quadrotor [FLC-ESO]

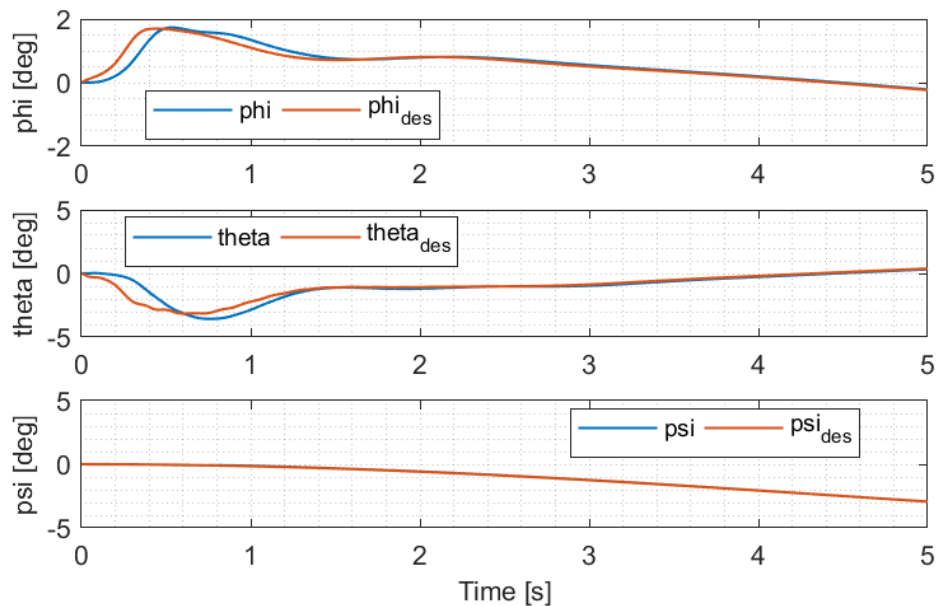


Figure 5.19. The Reference and Achieved Orientation of the Quadrotor Between 0 to 5 Seconds [FLC-ESO]

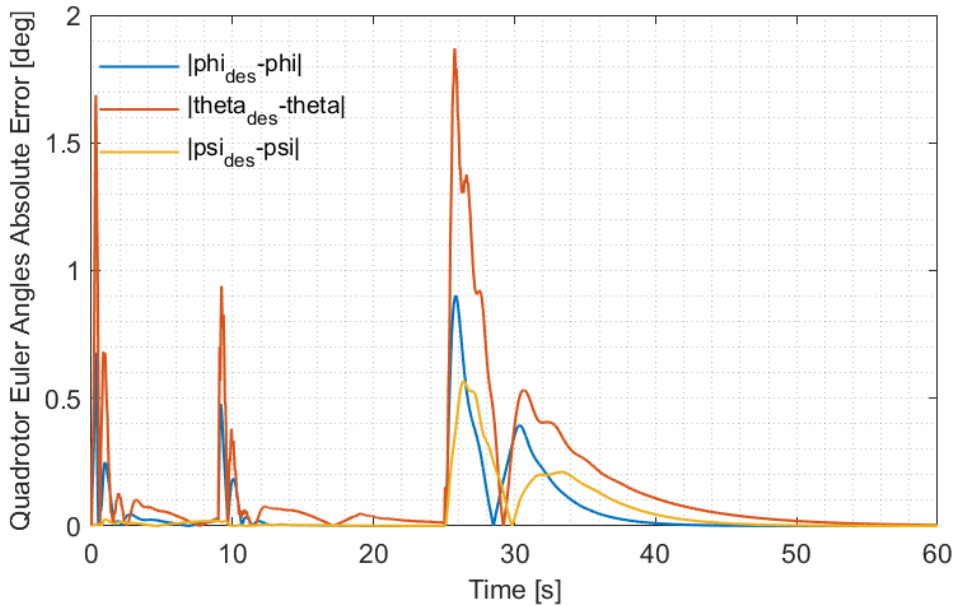


Figure 5.20. The Absolute Error Between the Commanded and the Achieved Quadrotor Orientation [FLC-ESO]

Before the external forces are applied on the system, FLC and ESO-FLC controller structures show similar performances in terms of the orientation control of the quadrotor as seen from Figure 5.15 and Figure 5.18. However, after the exerted disturbance forces, ESO-FLC stands out in terms of its disturbance rejection capability. It compensates these disturbances faster and brings the quadrotor to the desired orientation more quickly.

5.3.2.3. Joint Angles Control of the Robotic Arm

The FLC and ESO-FLC performances are very similar until the interruption forces are applied. At first, there are small oscillations due to the transient dynamics of the controllers and coupling between the pitch orientation. However, these oscillations are suppressed by the controllers in a short amount of time.

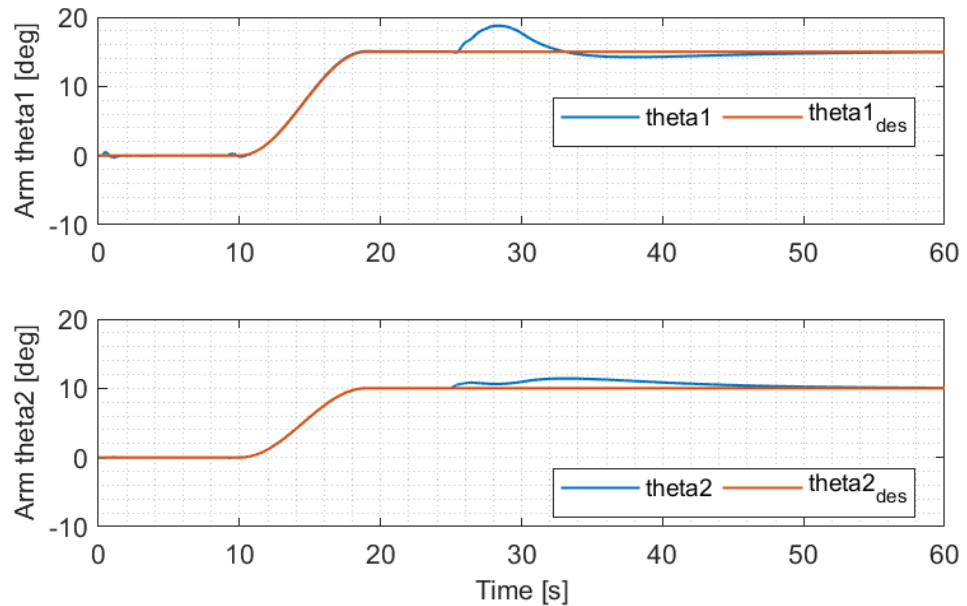


Figure 5.21. The Reference and Achieved Joint Angles of the Robotic Arm [FLC]

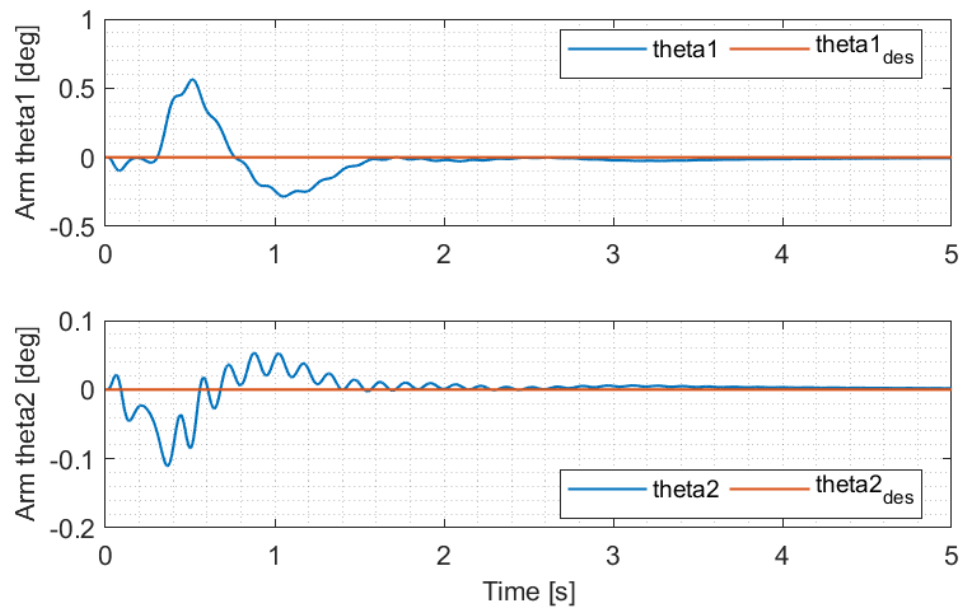


Figure 5.22. The Reference and Achieved Joint Angles of the Robotic Arm Between 0 to 5 Seconds [FLC]

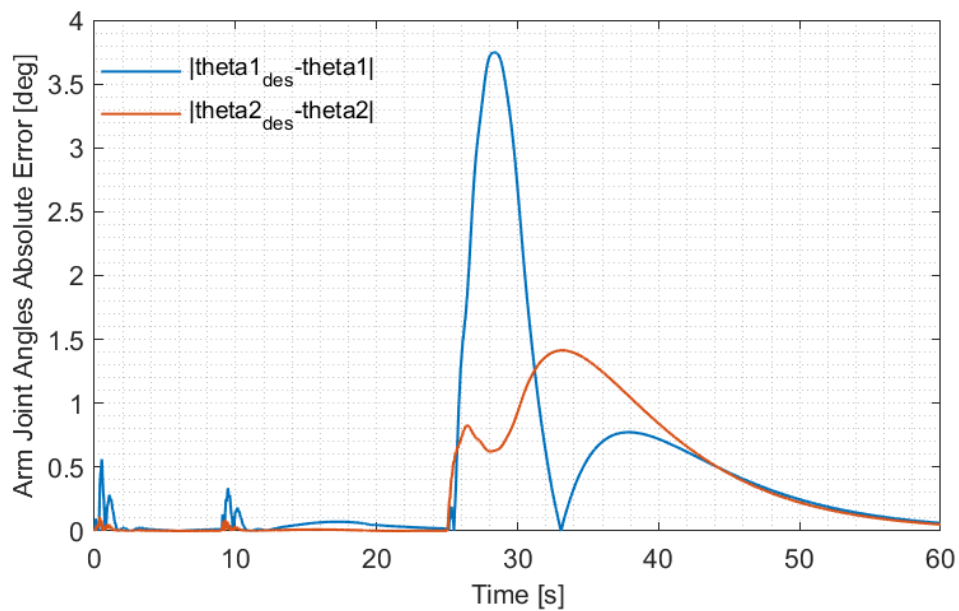


Figure 5.23. The Absolute Error Between the Commanded and the Achieved Joint Angles [FLC]

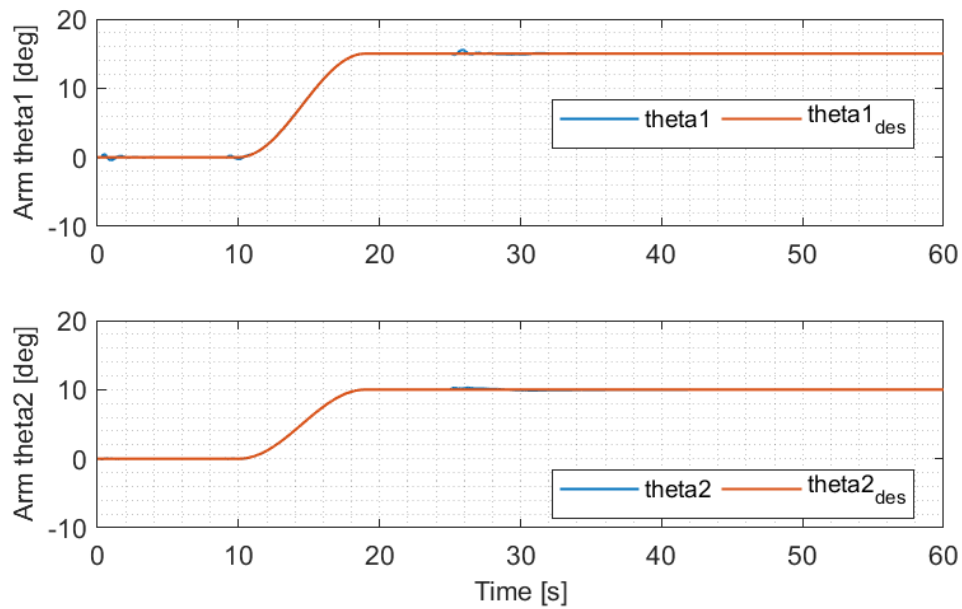


Figure 5.24. The Reference and Achieved Joint Angles of the Robotic Arm [FLC-ESO]

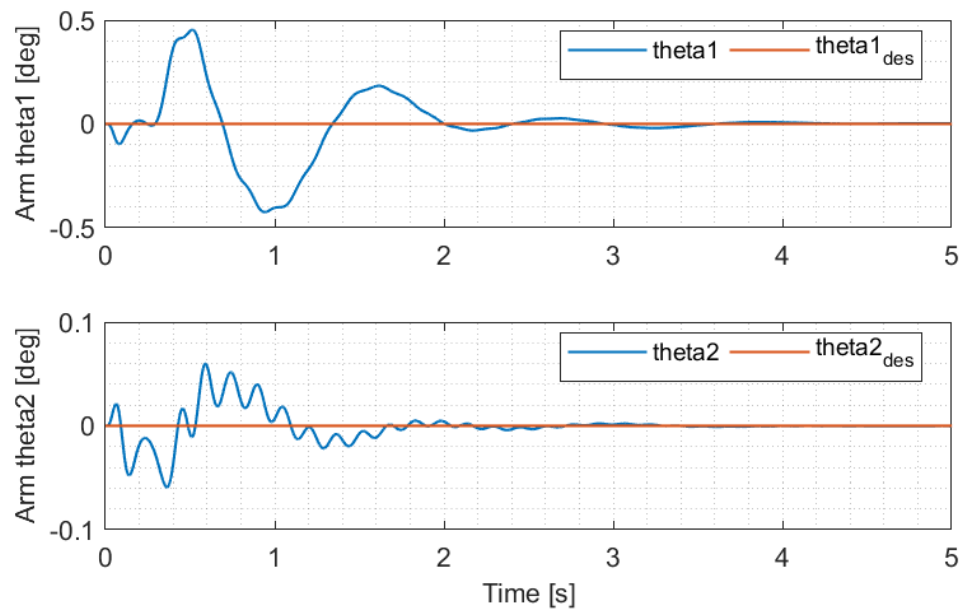


Figure 5.25. The Reference and Achieved Joint Angles of the Robotic Arm Between 0 to 5 Seconds [FLC-ESO]

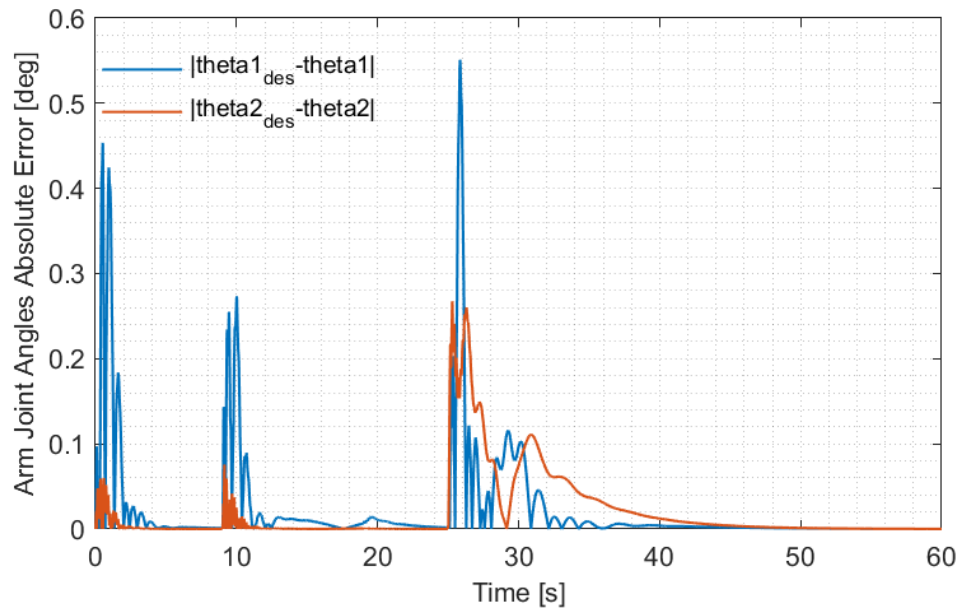


Figure 5.26. The Absolute Error Between the Commanded and the Achieved Joint Angles [FLC-ESO]

It can be understood from Figure 5.23, and Figure 5.26, the joint angles of the FLC controlled system are disturbed more. FLC-ESO minimizes the error faster with respect to the FLC because of its active disturbance rejection capability. In general, both controllers provide reference joint angles tracking, but the FLC-ESO structure is more powerful.

5.3.3. Performance Comparison of the Feedback Linearizing Controller and Feedback Linearizing Controller with Extended State Observer

To investigate and compare the performances of the controllers, there are some measurement methods like calculation of the error terms.

5.3.3.1. Comparison of Error Terms

In literature, there are several measures to compare the performances of the control systems. The most common ones The Integral of Squared Error (ISE), The Integral of Absolute Error (IAE), The Integral of Time Multiply Squared Error (ITSE), and The Integral of Time multiply Absolute Error (ITAE). They are calculated based on the error between the desired and achieved states. They can be formulated as,

$$e(t) = q_{des}(t) - q_{mes}(t) \quad (5.1)$$

$$ISE = \int_0^t (e(t))^2 dt \quad (5.1)$$

$$IAE = \int_0^t |e(t)| dt \quad (5.2)$$

$$ITSE = \int_0^t t(e(t))^2 dt \quad (5.3)$$

$$ITAE = \int_0^t t|e(t)| dt \quad (5.4)$$

The error terms of the commanded generalized coordinates are tabulated in the following table. Since phi and theta are the intermediate control inputs, they are not included into this table.

Table 5.3. The Error Term Values of the Each Generalized Coordinates

Generalized Coordinates	ISE		IAE		ITSE		ITAE	
	FLC	FLC -ESO	FLC	FLC -ESO	FLC	FLC -ESO	FLC	FLC - ESO
x	0.016	0.015	0.681	0.553	0.336	0.294	16.410	10.763
y	0.042	0.003	1.156	0.257	1.587	0.053	43.256	5.622
z	0.020	0.002	0.541	0.124	0.518	0.013	14.678	2.256
ψ	0.043	0.000	0.697	0.055	1.303	0.007	21.905	1.663
θ_1	0.016	0.000	0.481	0.025	0.465	0.001	15.918	0.435
θ_2	0.006	0.000	0.376	0.020	0.212	0.001	13.715	0.589

From Table 5.3, it can be said that tracking performance of the FLC-ESO controller is superior to FLC controller. Estimation of the disturbances significantly increases the robustness of the system.

5.3.3.2. Comparison of Energy Consumption

One of the most common performance comparison techniques of the comparison of the controllers is the energy consumption of the controlled system under the action of the controllers. The total energy consumption of the combined system is the sum of the energy consumptions of the quadrotor's dc motors and robotic arm joint servo motors. The calculations are made by benefiting from the achieved rotational speeds of the dc motors and generated dc motors torques for the quadrotor. For the robotic arm, achieved joint velocities of the servo motors and generated joint servo torques are used for calculations. To find the energy consumptions, first, the power consumptions can be computed for both quadrotor and arm by using the following formulae. Here, the powers are calculated in the unit of Joule/sec.

$$P_{quad} = \sum_{j=1}^4 \tau_j w_j \quad \text{and} \quad P_{arm} = \sum_{j=1}^2 t_j \dot{\theta}_j \quad (5.5)$$

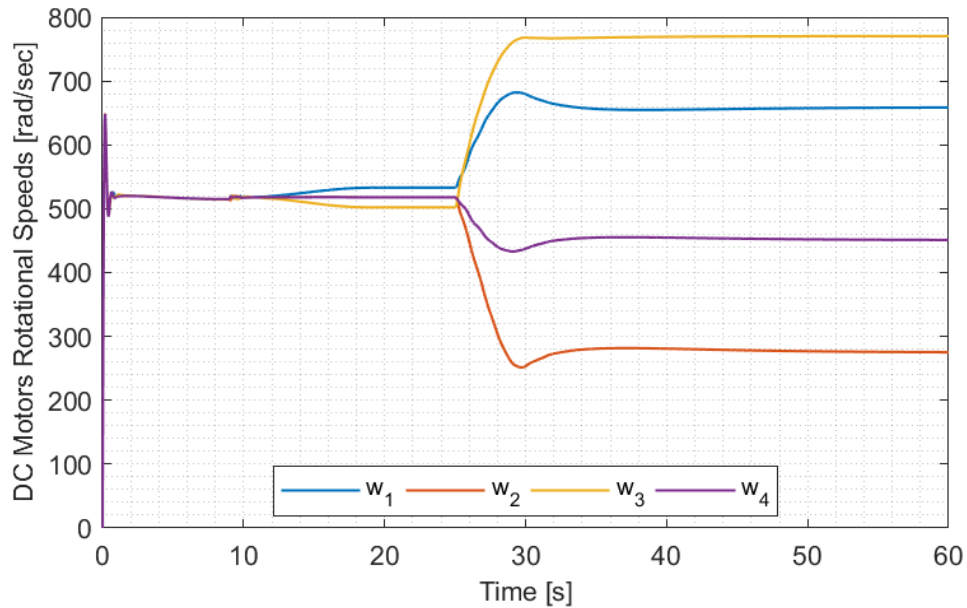


Figure 5.27. Rotational Speeds of the Each DC Motors of the Quadrotor [FLC]

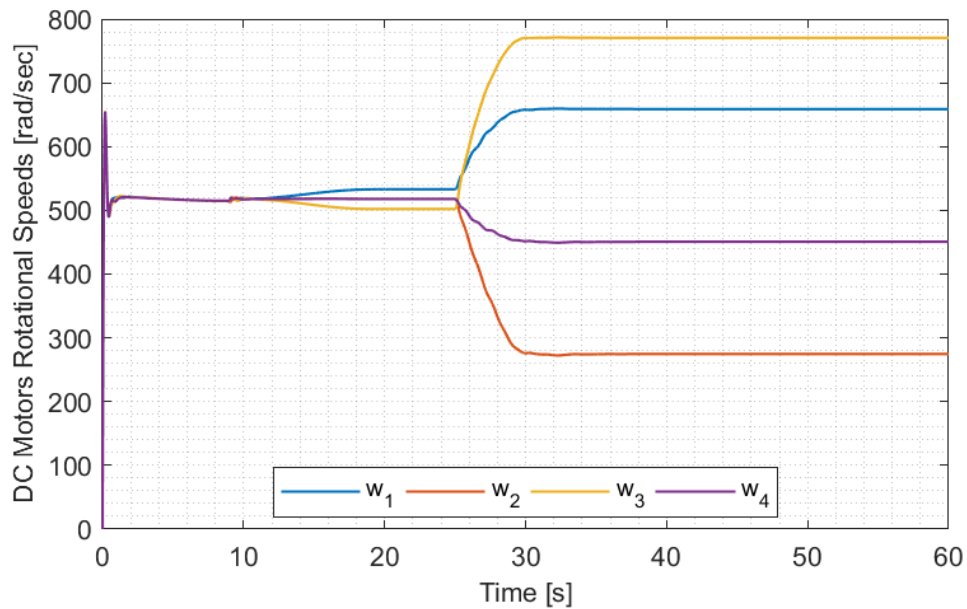


Figure 5.28. Rotational Speeds of the Each DC Motors of the Quadrotor [FLC-ESO]

Then, the integral of the powers with respect to time is gave the energy consumption of the quadrotor and the joints in the unit of Joule. Also, Figure 5.27 and Figure 5.28

are the visualization of the used rotational speeds of the rotors for FLC and ESO- FLC controlled systems. Moreover, Figure 5.29, and Figure 5.30 show the generated joint torques by the joint servo motors. Finally, Figure 5.31, and Figure 5.32 demonstrate the joint velocities of the serial robotic manipulator.

$$FLC \rightarrow \begin{cases} E_{quad} = \int_0^{60} P_{quad} dt = 20313.975 \\ E_{arm} = \int_0^{60} P_{arm} dt = 0.173 \end{cases} \quad (5.6)$$

$$ESO - FLC \rightarrow \begin{cases} E_{quad} = \int_0^{60} P_{quad} dt = 20315.464 \\ E_{arm} = \int_0^{60} P_{arm} dt = 0.073 \end{cases} \quad (5.7)$$

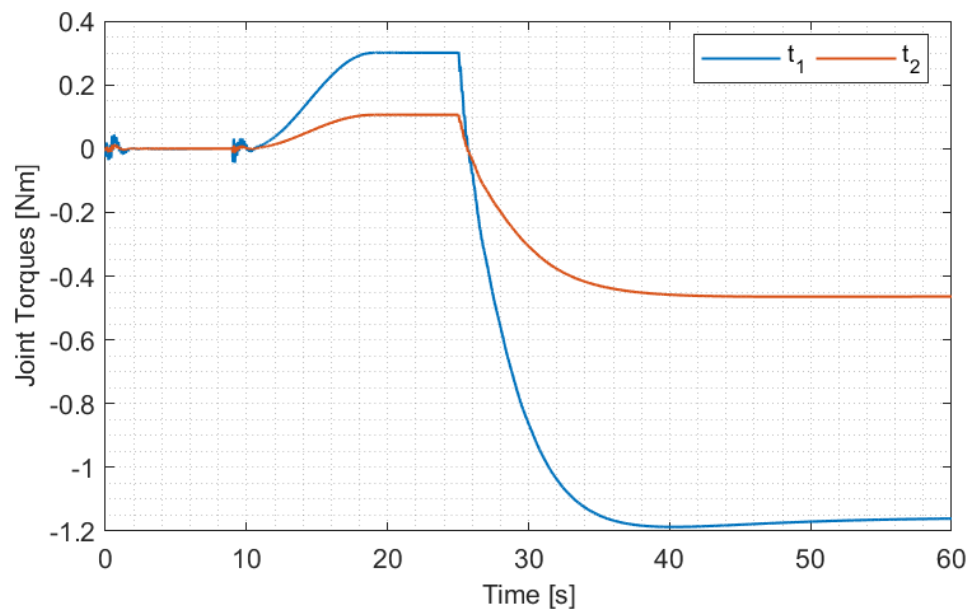


Figure 5.29. Robotic Arm Joint Torques [FLC]

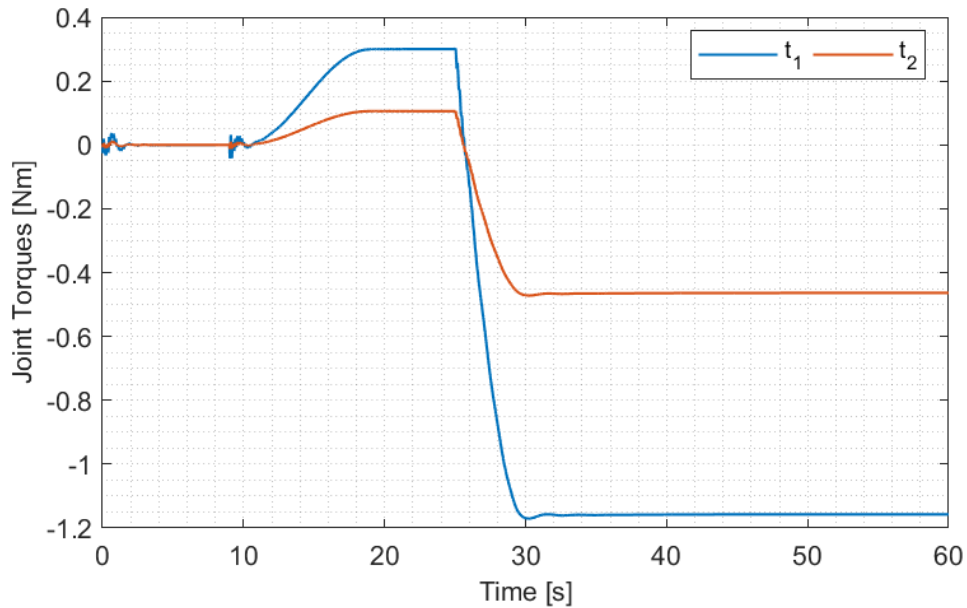


Figure 5.30. Robotic Arm Joint Torques [FLC-ESO]

Base on Eq's. (5.6) and (5.7), the quadrotor energy consumption in the system with FLC controller scheme is less with respect to FLC-ESO architecture, but they are very close to each other. For the robotic arm, FLC-ESO architecture is more energy efficient. Overall, the total energy consumption of the FLC-ESO structure is slightly bigger than the FLC architecture.

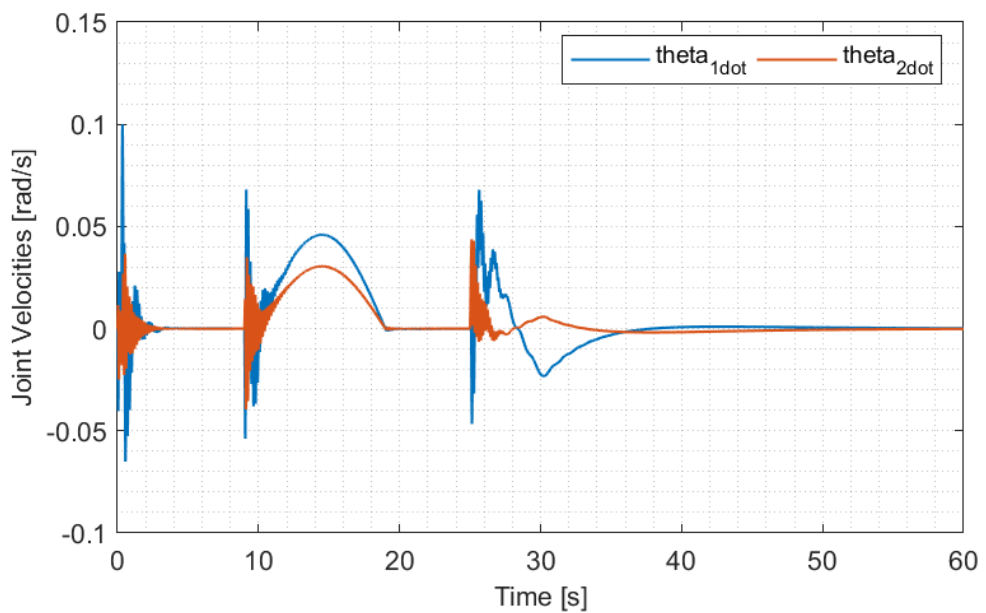


Figure 5.31. The Joint Velocities of the Robotic Arm [FLC]

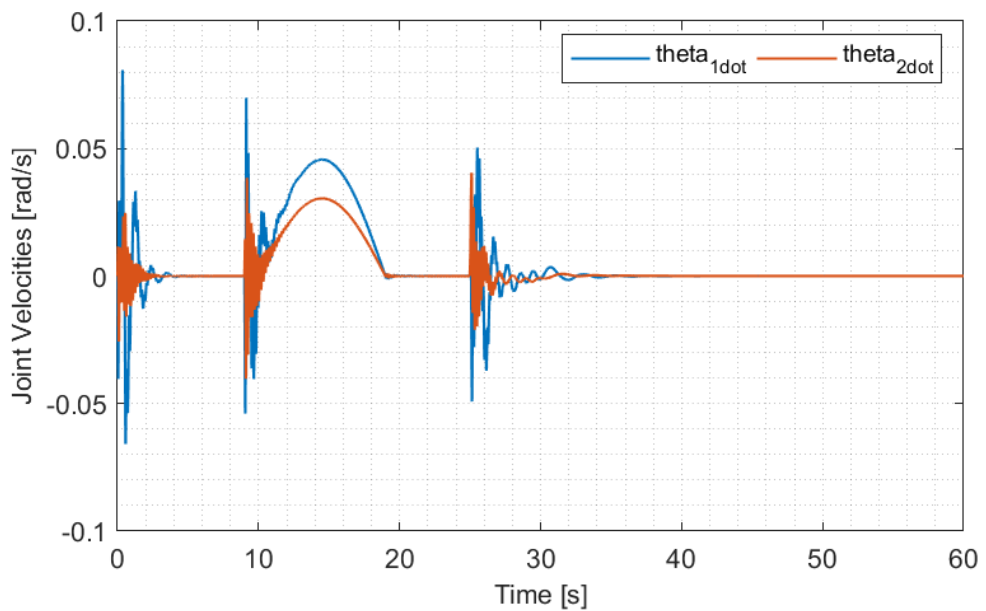


Figure 5.32. The Joint Velocities of the Robotic Arm [FLC-ESO]

CHAPTER 6

CONCLUSION

6.1. General Conclusion

In this thesis, modeling, simulation, and control of an aerial manipulation system consisting of a quadrotor and a 2-DOF robotic serial manipulator are presented. Quadrotor and robotic manipulator are considered as one combined system and modeled accordingly. Firstly, kinematics of the unified system is derived, and Denavit-Hartenberg parameters are obtained for the serial manipulator. Then, by using the kinematics parameters, the dynamics of the unified system are formulated by utilizing the Lagrange-D'Alembert method. Based on the equations of motion of the combined system, the control system algorithms are developed for reference trajectory tracking. Three different control system algorithms are studied. The 3-D position and yaw orientation of the quadrotor, and joint angles of the serial manipulator are directly controlled. The roll and pitch orientation of the quadrotor is not directly controlled since they are coupled with quadrotor positions y and x. Their reference values are generated for desired y and x positions, and they are indirectly controlled as an intermediate generalized coordinate.

The cascaded PID controllers are derived by taking advantage of the linear decoupled equations for each generalized coordinate. Root locus method is used to tune the gain of the controllers. Then, developed control algorithms are tested with the highly nonlinear system model. While testing this controller structure, ideal dc and servo motor models are used. As it can be seen from the simulation results, the decoupled controllers show satisfactory performances. Reference trajectories are tracked as desired. Also, disturbance forces are applied to the end-effector, but the controllers compensate these interruptions and bring the system to the reference paths.

Secondly, by using the nonlinear equations of motion of the unified system, one of the most common controllers in the robotics research area which is a feedback linearizing controller is designed for stable system performance. The gains of this controller are selected to converge the errors to the zero. While tuning the gains, the root locus method is tried. However, the gains could not be optimized by this method satisfactorily. Then, these gains are optimized by using the nonlinear least-squares solver of the MATLAB. Afterward, with optimized gains, the proposed control algorithm is tested in a simulation case study. It is seen that the overall system tracks the reference trajectories and error dynamics converge to zero in time. Also, when the external disturbance forces are applied to the system, the controller deals with these unwanted interactions considerably.

However, the feedback linearizing controller assumes the availability of the exact dynamics model of the system. Unfortunately, this is not the case for real-life applications since there are unmodeled dynamics like friction. Also, there may be external disturbances on the system, load variations, and parameter variations. These uncertainties can cause instability. Therefore, these uncertainties are modeled as an extended state and an extended state observer is designed to eliminate those uncertainties. This ESO is added to the FLC control architecture. In the FLC-ESO control structure, the gains of the FLC are the same as the gains of the predesigned FLC. To determine the ESO gains, the pole placement technique is tried, but the optimized solution could not be found. Thus, the gains of the ESO is tuned by benefiting from the nonlinear least-squares solver of the MATLAB. Then, developed algorithms are implemented in the nonlinear system simulation environment. As it can be seen from the simulation results, the trajectory tracking performance of the FLC is significantly increased with ESO. The performances of the FLC and FLC-ESO control architectures are compared with the calculation of error terms and energy consumption of the controlled systems. In terms of error terms, the performance of the FLC-ESO structure is very ahead of the performance of the FLC architecture. They are close to each other in the aspect of energy consumption.

6.2. Future Work

Nonideal sensor models such as accelerometer/indoor GPS, gyroscope and encoder will be implemented in the simulation environment to reflect a more realistic scenario. Also, the gains of the controllers will be updated. Developed algorithms will be validated with an experiment study.

The designed system is more sensitive to the disturbance forces in yaw plane with respect to the disturbances in roll and pitch planes due to its lower moment of inertia. To overcome this drawback, the design of the robotic arm may be updated. In this thesis, both revolute joints operate in pitch plane. If one of the revolute joints operates in the yaw plane, then the end-effector's position can be controlled more successfully.

REFERENCES

- [1] R. Mahony, V. Kumar, and P. Corke, “Multirotor Aerial Vehicles: Modeling, Estimation, and Control of Quadrotor,” *IEEE Robotics & Automation Magazine*, vol. 19, no. 3, pp. 20–32, 2012.
- [2] A. Das, F. Lewis, and K. Subbarao, “Dynamic inversion with zero-dynamics stabilisation for quadrotor control,” *IET Control Theory & Applications*, vol. 3, no. 3, pp. 303–314, 2009.
- [3] D. Kotarski, Z. Benic, and M. Krznar, “Control Design for Unmanned Aerial Vehicles with Four Rotors,” *Interdisciplinary Description of Complex Systems*, vol. 14, no. 2, pp. 236–245, 2016.
- [4] F. Goodarzi, D. Lee and T. Lee, "Geometric control of a quadrotor UAV transporting a payload connected via flexible cable", *International Journal of Control, Automation and Systems*, vol. 13, no. 6, pp. 1486-1498, 2015.
- [5] K. Sreenath and V. Kumar, “Dynamics, Control and Planning for Cooperative Manipulation of Payloads Suspended by Cables from Multiple Quadrotor Robots,” *Robotics: Science and Systems IX*, 2013.
- [6] Y. Alothman, M. Guo, and D. Gu, “Using iterative LQR to control two quadrotors transporting a cable-suspended load,” *IFAC-PapersOnLine*, vol. 50, no. 1, pp. 4324–4329, 2017.
- [7] S. Kim, S. Choi, and H. J. Kim, “Aerial manipulation using a quadrotor with a two DOF robotic arm,” *2013 IEEE/RSJ International Conference on Intelligent Robots and Systems*, 2013.
- [8] F. Caccavale, G. Giglio, G. Muscio, and F. Pierri, “Adaptive control for UAVs equipped with a robotic arm,” *IFAC Proceedings Volumes*, vol. 47, no. 3, pp. 11049–11054, 2014.
- [9] A. Jimenez-Cano, J. Martin, G. Heredia, A. Ollero, and R. Cano, “Control of an aerial robot with multi-link arm for assembly tasks,” *2013 IEEE International Conference on Robotics and Automation*, 2013.
- [10] T. W. Danko, K. P. Chaney, and P. Y. Oh, “A parallel manipulator for mobile manipulating UAVs,” *2015 IEEE International Conference on Technologies for Practical Robot Applications (TePRA)*, 2015.
- [11] S. Kim, H. Seo, S. Choi, and H. J. Kim, “Vision-Guided Aerial Manipulation Using a Multirotor With a Robotic Arm,” *IEEE/ASME Transactions on Mechatronics*, vol. 21, no. 4, pp. 1912–1923, 2016.

- [12] V. Lippiello and F. Ruggiero, "Cartesian Impedance Control of a UAV with a Robotic Arm," IFAC Proceedings Volumes, vol. 45, no. 22, pp. 704–709, 2012.
- [13] G. Arleo, F. Caccavale, G. Muscio, and F. Pierri, "Control of quadrotor aerial vehicles equipped with a robotic arm," 21st Mediterranean Conference on Control and Automation, 2013.
- [14] G. Giglio and F. Pierri, "Selective compliance control for an unmanned aerial vehicle with a robotic arm," 22nd Mediterranean Conference on Control and Automation, 2014.
- [15] E. Cataldi, G. Muscio, M. A. Trujillo, Y. Rodriguez, F. Pierri, G. Antonelli, F. Caccavale, A. Viguria, S. Chiaverini, and A. Ollero, "Impedance Control of an aerial-manipulator: Preliminary results," IEEE/RSJ International Conference on Intelligent Robots and Systems (IROS), pp. 3848–3853, 2016.
- [16] A. Khalifa, M. Fanni, A. Ramadan, and A. Abo-Ismail, "Modeling and control of a new quadrotor manipulation system," 2012 First International Conference on Innovative Engineering Systems, 2012.
- [17] A. Khalifa, M. Fanni, A. Ramadan, and A. Abo-Ismail, "New Quadrotor Manipulation System: Inverse Kinematics, Identification And Ric-Based Control," International Journal of Recent advances in Mechanical Engineering, vol. 4, no. 3, pp. 39–58, 2015.
- [18] M. Fanni and A. Khalifa, "A New 6-DOF Quadrotor Manipulation System: Design, Kinematics, Dynamics, and Control", IEEE/ASME Transactions on Mechatronics, vol. 22, no. 3, pp. 1315-1326, 2017.
- [19] R. M. Jones, D. Sun, G. B. Haberfeld, A. Lakshmanan, T. Marinho, and N. Hovakimyan, "Design and Control of a Small Aerial Manipulator for Indoor Environments," AIAA Information Systems-AIAA Infotech @ Aerospace, 2017.
- [20] M. Orsag, C. Korpela, S. Bogdan, and P. Oh, "Lyapunov based model reference adaptive control for aerial manipulation," 2013 International Conference on Unmanned Aircraft Systems (ICUAS), 2013.
- [21] V. Sumathy, D. Ghose, and S. N. Omkar, "Analysis of a Quadcopter Manipulator Operating in a Workspace above the Altitude of the Aerial Vehicle," 2018 AIAA Guidance, Navigation, and Control Conference, 2018.
- [22] H. Lee, S. Kim, and H. J. Kim, "Control of an aerial manipulator using on-line parameter estimator for an unknown payload," 2015 IEEE International Conference on Automation Science and Engineering (CASE), 2015.
- [23] D. Lee, C. Nataraj, and T. C. Burg, "Coordinated Control of Flying Robotic Arm," Volume 3: Renewable Energy Systems; Robotics; Robust Control;

Single Track Vehicle Dynamics and Control; Stochastic Models, Control and Algorithms in Robotics; Structure Dynamics and Smart Structures; 2012.

- [24] J. Villagómez, M. Vargas, M. Ortega, and F. Rubio, “Modeling and Control of the tPVTOL**This work was partially supported by the spanish Ministry of Education (MECD) under national research projects DPI2012 — 37580 — C02 — 02 and DPI2013 — 44135 — R.,” IFAC-PapersOnLine, vol. 48, no. 9, pp. 150–155, 2015.
- [25] G. Garimella and M. Kobilarov, “Towards model-predictive control for aerial pick-and-place,” 2015 IEEE International Conference on Robotics and Automation (ICRA), 2015.
- [26] J. U. Álvarez-Muñoz, Nicolas Marchand, Fermi Guerrero-Castellanos, Sylvain Durand, A. E. Lopez-Luna. Improving control of quadrotors carrying a manipulator arm. XVI Congreso Latinoamericano de Control Automático (CLCA 2014), Oct 2014, -, Mexico. 6 p., 2014.
- [27] G. Antonelli and E. Cataldi, “Adaptive control of arm-equipped quadrotors. Theory and simulations,” 22nd Mediterranean Conference on Control and Automation, 2014.
- [28] F. Ruggiero, M. Trujillo, R. Cano, H. Ascorbe, A. Viguria, C. Perez, V. Lippiello, A. Ollero, and B. Siciliano, “A multilayer control for multirotor UAVs equipped with a servo robot arm,” 2015 IEEE International Conference on Robotics and Automation (ICRA), 2015.
- [29] V. Ghadiok, J. Goldin, and W. Ren, “Autonomous indoor aerial gripping using a quadrotor,” 2011 IEEE/RSJ International Conference on Intelligent Robots and Systems, 2011.
- [30] J. Thomas, J. Polin, K. Sreenath, and V. Kumar, “Avian-Inspired Grasping for Quadrotor Micro UAVs,” Volume 6A: 37th Mechanisms and Robotics Conference, 2013.
- [31] G. Heredia, A. Jimenez-Cano, I. Sanchez, D. Llorente, V. Vega, J. Braga, J. Acosta, and A. Ollero, “Control of a multirotor outdoor aerial manipulator,” 2014 IEEE/RSJ International Conference on Intelligent Robots and Systems, 2014.
- [32] P. O. Pereira, R. Zanella, and D. V. Dimarogonas, “Decoupled design of controllers for aerial manipulation with quadrotors,” 2016 IEEE/RSJ International Conference on Intelligent Robots and Systems (IROS), 2016.
- [33] H. Yang and D. Lee, “Dynamics and control of quadrotor with robotic manipulator,” 2014 IEEE International Conference on Robotics and Automation (ICRA), 2014.

- [34] M. K. Ozgoren, "Lecture Notes for ME 502 (Advanced Dynamics)", Department of Mechanical Engineering, METU, 2016.
- [35] M. K. Ozgoren, "Lecture Notes for ME 522 (Principles of Robotics)", Department of Mechanical Engineering, METU, 2017.
- [36] B. Siciliano, "Robotics: Modelling, Planning and Control". 2010.
- [37] M. Yıldız, "Effects of Active Landing Gear On The Attitude Dynamics Of A Quadrotor (thesis)," 2015.
- [38] B. Siciliano and O. Khatib, Springer handbook of robotics. Berlin: Springer, 2008.
- [39] F. L. Lewis, C. T. Abdallah, D. M. Dawson, and F. L. Lewis, Robot manipulator control: theory and practice. Milton Keynes UK: Lightning Source UK Ltd., 2018.
- [40] M. W. Spong, Robot Modeling and Control. John Wiley & Sons, 2012.
- [41] M. F. Khan, R. ul Islam, and J. Iqbal, "Control Strategies for Robotic Manipulators," IEEE International Conference of Robotics and Artificial Intelligence, 2012.
- [42] B. Randal, "Quadrotor Dynamics and Control Rev 0.1". All Faculty Publications. 1325., 2008.
- [43] T. Luukkonen, "Modelling and control of quadcopter," Independent research project in applied mathematics. Aalto University, 2011.
- [44] K. Kondak, K. Krieger, A. Albu-Schaeffer, M. Schwarzbach, M. Laiacker, I. Maza, A. Rodriguez-Castano, and A. Ollero, "Closed-Loop Behavior of an Autonomous Helicopter Equipped with a Robotic Arm for Aerial Manipulation Tasks," International Journal of Advanced Robotic Systems, vol. 10, no. 2, p. 145, 2013.
- [45] C. Chen, C. Zhang, T. Hu, H. Ni, and W. Luo, "Model-assisted extended state observer-based computed torque control for trajectory tracking of uncertain robotic manipulator systems," International Journal of Advanced Robotic Systems, vol. 15, no. 5, p. 172988141880173, 2018.
- [46] K. Ogata, Modern control engineering. Delhi: Pearson, 2016.
- [47] S. Zarovy and M. Costello, "Extended State Observer for Helicopter Mass and Center-of-Gravity Estimation," Journal of Aircraft, vol. 52, no. 6, pp. 1939–1950, 2015.
- [48] S. Li, J. Yang, W.-H. Chen, and X. Chen, "Generalized Extended State Observer Based Control for Systems With Mismatched Uncertainties," IEEE

TRANSACTIONS ON INDUSTRIAL ELECTRONICS, vol. 59, no. 12, pp. 4792–4802, Dec. 2012.

- [49] S. Talole, J. Kolhe, and S. Phadke, “Extended-State-Observer-Based Control of Flexible-Joint System With Experimental Validation,” IEEE Transactions on Industrial Electronics, vol. 57, no. 4, pp. 1411–1419, 2010.
- [50] Z. Gao, “Scaling and bandwidth-parameterization based controller tuning,” Proceedings of the 2003 American Control Conference, 2003.
- [51] M. Chipofya, D. J. Lee, and K. T. Chong, “Trajectory Tracking and Stabilization of a Quadrotor Using Model Predictive Control of Laguerre Functions,” Abstract and Applied Analysis, vol. 2015, pp. 1–11, 2015.